# Design of Aeroelastically Scaled Wind Tunnel Models Using Sensitivity Based Parameter identification

Dissertation

Submitted To

Graduate Engineering & Research

School of Engineering

UNIVERSITY OF DAYTON

In Partial Fulfillment of the Requirements for

The Degree

Doctor of Philosophy in Aerospace Engineering

by

Mark French

University of Dayton

Dayton, Ohio

August 1993

DESIGN OF AEROELASTICALLY SCALED WIND TUNNEL MODELS USING SENSITIVITY BASED PARAMETRIC IDENTIFICATION

Approved By:

Franklin Eastep, Ph.D.
Professor
Aerospace Engineering
Committee Chairman

Robert Brockman, Ph.D.
Associate Professor
Mechanical and Aerospace Engineering
Committee Member

John Kauflin, Ph.D.
Associate Professor
Mathematics
Committee Member

Ronald Tayor, Ph.D.
Associate Professor
Mechanical and Aerospace Engineering
Committee Member

Vipperla Venkayya, Ph.D.
Principal Scientist, Analysis and Optimization Branch
USAF Flight Dynamics Directorate
Committee Member

Donald L. Moon
Interim Associate Dean/Director
Graduate Engineering & Research
School of Engineering

Joseph Lestingi, D.Eng, P.E.
Dean
School of Engineering

## Abstract

Designing aeroelastically scaled wind tunnel models is a common task in flight vehicle development programs. Model design methods, however, often rely heavily on repeated analysis, experience and intuition. This work presents a procedure which uses numerical optimization techniques to automate the model design process.

The proposed method offers many advantages over current ones. The model structure can be made as complex as necessary. Also, no unrealistic structural assumptions are required of the designer; any structure which can be discretized using a finite element approximation may be considered. The method uses readily available flexibility and modal response data from the full scale structure to size elements in the wind tunnel model structure automatically, eliminating repeated analysis.

Several variations on the optimization-based approach are evaluated here using a low-aspect ratio fighter wing as a sample problem. Desired flutter characteristics are compared to those calculated for the final model design. To verify the numerical work, a sample model structure has been fabricated and tested using laser metrology techniques. Results of static and modal tests compare well with numerical predictions.

**Acknowledgements**

I would like to thank the people without whom I would never have finished this work. Mr. Gene Maddux patiently answered innumerable questions, offered many helpful suggestions, introduced me to the world of photomechanics and let me use (and sometimes break) his equipment. The management of the USAF Flight Dynamics Directorate provided the time and resources which made my entire graduate education possible. My hope is that this and future work may return their investment. I thank my co-workers who have helped me so much: Dr. Max Blair, V. James Sallee, Esq, (soon to be Dr.) Mark Hopkins, Terry Harris and Doin. Amy gave me understanding, encouragement and perspective; I'll try to do the same if ever the tables are turned. Keith gave me friendship with three part harmony (and feeling).

Finally, I would like to thank my family: my sister, Anne, for her support and perpetual good humor, my mother, Virginia, for teaching me persistence and determination, and my father, Richard G. French, my first engineering teacher, for teaching me patience and kindness and starting me along this path a long time ago. This work is dedicated to him.

## Table of Contents

## List of Figures

## List of Tables

Chapter I

# Introduction

The design of aeroelastically scaled wind tunnel models is a common problem in aircraft development efforts. The usual purpose of testing such a model is to verify the accuracy of aerodynamic predictions. Since aeroelastic instabilities can result in loss of a vehicle, and uncertainties still exist in many computational aerodynamic predictions, wind tunnel testing is needed. Designers assume that the behavior of a properly scaled wind tunnel model is representative of the behavior of the full scale vehicle. The model need not be a complete vehicle, and may be as little as a single lifting surface.

The desired geometry, stiffness and mass characteristics of the wind tunnel model are scaled from the full size article. A properly designed model will display the same aeroelastic behavior as the full size article, with the flutter velocity and vibrational frequencies varying by known scale factors. Thus, aeroelastic response measured in wind tunnel tests may be considered representative of full scale behavior and used to verify numerical predictions.

Engineers usually divide the aeroelastic response of a vehicle into static and dynamic phenomena. Static phenomena include any deformation in which mass properties of the vehicle have no effect. Typical examples are control surface effectiveness and the flexible lift curve slope of the wing. Dynamic phenomena are those in which the mass properties of the vehicle are not negligible. The most common example is lifting surface flutter. Parameters used to describe the flutter response of a lifting surface are the flutter velocity, the flutter frequency and the modal participation coefficients of the flutter mode. These response parameters are reproduced in a correctly scaled wind tunnel model.

Designing aeroelastically scaled wind tunnel models often involves empirical knowledge and repeated analysis. Sometimes, assumptions are made to simplify the analysis. For instance, high aspect ratio wings can be assumed to have beam-like structural properties; the resulting model structure is then a single beam. An obvious limitation is that low aspect ratio wings do not act much like beams. The introduction of composite structures further complicates the problem by introducing anisotropic material behavior which can make the beam analogy inappropriate.

Another design approach is to scale down the geometry of the full size structure and rely on similarity arguments for proper aeroelastic scaling. Such geometric scaling is impractical for complex structures or ones made with composite materials. For these structures, the parts of small scale models often would be too small to be fabricated accurately.

When a beam model is not adequate and scaling down the structure is not practical, another approach must be used. In the past, intuition and repeated analysis have been used to design and size structural elements. This task is difficult, especially for cases where either the wing behavior is unusual or the model structure is complex. An improvement on the above process is needed to speed the design process and lower the cost of the model.

The design task is to develop a model structure which reproduces a known set of properties from the full scale structure. These properties include deflection due to known loads, mass, natural frequencies and mode shapes. It is reasonable to cast the model design task as a minimization problem. The designer must minimize the difference between desired model properties and calculated (or measured) model properties.

A versatile automated design method would increase the range of options open to the model designer. The designer should be freed from the need to make any simplifying assumptions about the model structure. Flexibility coefficients and modal information scaled from the full size structure, as well as basic geometry for the model structure are required. Automatic by-products from a design which matched those properties would include correct load paths and mass distributions. Solutions not anticipated by the designer could be possible, expanding the range of feasible solutions.

The object of the work presented here is to automate the process of designing aeroelastically scaled wind tunnel models by using an optimization-based parameter identification method. This method is general and can be applied to any type of structure.

The problem addressed in this work falls under the category of parameter identification problems. The most general goal of a parameter identification method is to develop a mathematical representation of a structure using measured structural responses. In the case of the model design problem, the measured structural responses are those scaled from the full size wing. The resulting mathematical representation describes the structure of an aeroelastically scaled wind tunnel model.

Chapter II

## Background and Literature Search

There is little in the literature which deals directly with design of aeroelastically scaled wind tunnel models, although papers which discuss wind tunnel test results sometimes include discussions of the model development process. Discussions of aeroelastic model design are presented as part of a textbook by Bisplinghoff, Ashley and Halfman[1] and as a summary of design and construction experience by Wasserman[2]. Significant discussions of particular model design efforts are presented by Rogers, et. al.[3], and Pendleton, Lee and Wasserman[4].

The model design problem is closely related to parameter identification problems, which are covered extensively in the literature. Another relevant topic is structural optimization - particularly when applied with frequency, displacement or mode shape constraints. The following sections describe relevant work on parameter identification, structural optimization and preliminary work I did on the method developed here.

## 2.1 Model Updating and Parameter Identification Schemes

The most basic mathematical representation of a linear structure is a coupled system of second order ordinary differential equations of the form

$$[M]\{\ddot{x}\} + [C]\{\dot{x}\} + [K]\{x\} = 0 \qquad \textbf{(1)}$$

Many parameter identification schemes seek to generate a system of equations of this form. Some develop the system directly, while others update some initial estimate. Methods which start with some initial estimate are often called model update or model correction schemes. While the focus of this work is on such methods, it is useful to mention a few direct methods.

Keller[5] presents two iterative methods of system matrix identification for which no initial values of the system matrices are required. The first uses response data from a steady state harmonic excitation and the second uses response data from an impulse or some other type of transient excitation. In Ref 6, Keller presents a related method which allows calculation of system eigenvalues and eigenvectors due to harmonic excitations at a single degree of freedom.

The mass of literature on model update and parameter identification methods is very large. The task of absorbing the information available is much easier if the work is organized in some basic categories. Figure 1 presents a simple diagram showing how the various methods are organized here.

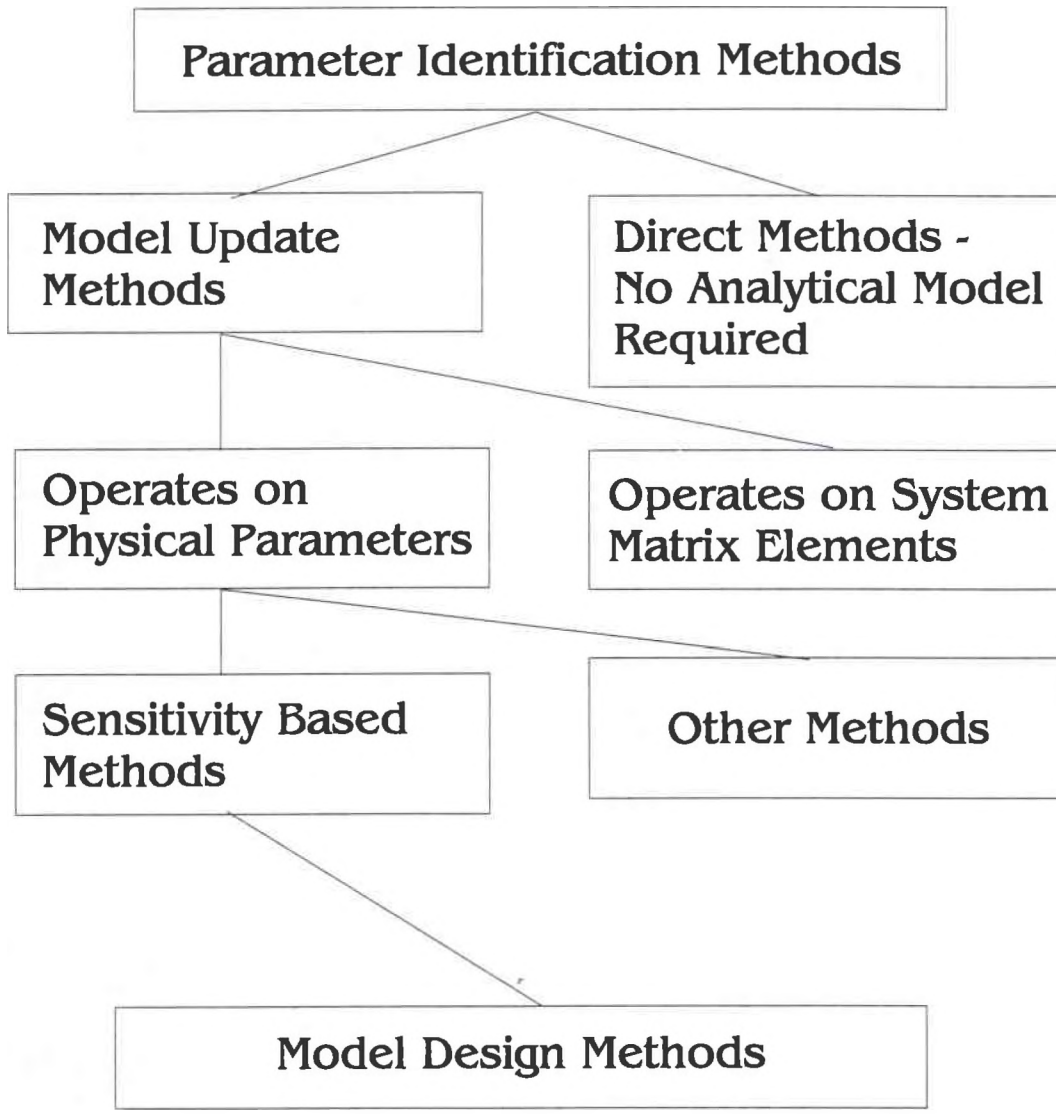


**Figure 1** - A Partial Hierarchy of Parameter Identification Methods

There is a wide range of model update methods. There are issues, however, which are common to all methods. A good introductory discussion is provided by Ibrahim and Saafan[7]. They suggest that inaccuracies in analytical methods limit the quality of correlation between analytical and experimental result. They go on to provide an overview of the role of model update methods and to list issues which a successful method must address. These issues include:

-The number of measured degrees of freedom is almost always less than the number of analytical degrees of freedom

-The measured degrees of freedom are, in the general case, not coincident with analytical degrees of freedom

-Rotation degrees of freedom which may be present in the analytical model are very difficult to measure experimentally

-The number of experimentally identified mode shapes is usually very limited and may contain gaps

-The experimentally identified mode shapes are complex if damping is present (as it almost always is), but analysis results in normal modes

-Measured data always contains some error

Perhaps the most immediate of the problems listed above is the completeness of the dynamic model. A unique solution to the model update problem is possible only when complete response information (flexibility coefficients, eigenvalues and eigenvectors) is

available. This is almost never the case. The problem of uniqueness was addressed in an early work by Berman and Flannely[8]. They point out that when the number of degrees of freedom of the discrete model of a continuous structure exceeds the number of modes for which natural frequencies are available, an infinite number of solutions is possible. Thus, any of the infinite number of analytical models which duplicate the test data could be considered valid.

The model designer must then develop a mathematical representation that's physically realistic as well as mathematically valid. Berman and Flannely state that " A useful model should be able to predict the results of untested loading conditions and the effects of changes in the mass, stiffness, or supports of the structure". They proposed a method of updating a previously existing analytical model consisting of lumped masses interconnected by linear springs with scalar structural damping. The resulting equations of motion are written as

$$\left[ -\omega^2 [M] + (1 + ig)[K] \right] \{y\} = \{f\} \qquad (2)$$

They assume that a 'reasonable' mass matrix has been derived using analytical or intuitive means. They then propose a method to correct that mass matrix with a process based on the pseudo-inverse[9,10] of a system of linear equations which has as variables the unknown elements of the mass matrix. The stiffness matrix is then calculated using modal data and the corrected mass matrix. This method is important to this study since it addresses the problem of incomplete test data with a method that uses an optimization-

like procedure in the form of a pseudo-inverse. The idea of using some type of optimization approach to address the problem of uniqueness of solutions is very powerful and is preset in many successful methods.

### 2.1.1 Parameter Update Methods

All model update methods improve some initial estimate of the desired model. An important distinction is whether they operate directly on system matrices or whether they modify physical system parameters. The update methods of most use in the wind tunnel model design problem operate on physically meaningful parameters.

Methods which operate only on system matrices should not be ignored, since they address many of the problems which are common to all update methods. Early work on structural system identification concentrates on system matrix update methods. Pilkey and Cohen[11] present a good survey of structural identification schemes as of 1972.

If complete modal information were available and contained no errors, updating an analytical model would be trivial. Two of the most basic problems as pointed out by Ibrahim and Saafan are that the measured information is generally incomplete and the

measured eigenvectors are not generally orthogonal. A number of methods have been proposed which attempt to use analytical models to orthogonalize measured modes shapes.

Updating a mathematical model so that the calculated eigenvectors are orthogonal is an important part of the model update problem. One of the earliest attempts to orthogonalize measured mode shapes was proposed by Gravitz[12] in 1958. In this method, he proposed a method of othogonalizing measured modes using an analytical mass matrix. This data is used to calculate a matrix of structural influence coefficients which will, in general be non-symmetric. The matrix is made symmetric by simply averaging the off-diagonal elements. New mode shapes are then computed using the analytical mass matrix, the calculated matrix of influence coefficients and the measured natural frequencies.

The method proposed by Gravitz illustrates the basic goals of model update methods as well as some of the drawbacks. Using a set of measured mode shapes and an analytical mass matrix, it is a simple process to create a complete math model for some structure which will produce orthogonal eigenvectors. If the analytical model is reasonably accurate and testing was done carefully, the updated math model should be a good representation of the test specimen.

The drawbacks are severe, though. The analytical mass matrix needs to be accurate; if a large part of the total mass is nonstructural, calculating an accurate mass matrix may be difficult. While the number of measured modes may be less than the order of the

math model, each measured mode must be complete. That is, each measured mode shape must have an entry for every degree of freedom present in the math model. This requirement is reasonable only for small math models.

Another early method of dealing with nonorthogonal measured modes and also calculating structural influence coefficients (SICs) using measured modal data was presented by Rodden[13] in 1967. The method is noteworthy since it allows calculation of SICs of a structure with free-free boundary conditions. It is common for aircraft to be suspended from soft springs during a ground vibration test in an effort to approximate free-free conditions.

The method allows use of an incomplete set of natural frequencies, but assumes that the mass matrix corresponding to the set of points for which modal deflections are measured is known. Rodden further assumes that all inertial effects are included in the mass matrix and that the vector of measured deflections includes the deflections of all mass points. These assumptions limit the method's applicability.

Using optimization methods to update analytical models is an attractive means of addressing the problem of incomplete data. Baruch and Bar Itzack[14] present an approach which uses an optimization based procedure to orthogonalize measured mode shapes. They then use the results to correct stiffness matrices. As with the previous method, it is assumed that an analytical stiffness matrix is known with enough accuracy that it may

be accepted without correction. The method uses the Lagrange multiplier method to orthogonalize measured eigenvectors while minimizing a weighted Euclidian norm based on the difference between measured and exact mode shapes.

The method has the advantage of producing a closed form solution for the corrected eigenvector matrix. A problem with the approach is that, while a complete set of natural frequencies is not required, a complete eigenvector for each measured natural frequency is required. Another problem is that the eigenvalues and eigenvectors obtained using the corrected stiffness matrix are usually different from those used to obtain the corrected matrix. This deficiency is addressed by Baruch[15]. In another extension of the basic method, Wei[16] proposed a modification which eliminates an assumption made by Baruch and Bar Itzack that an intermediate matrix be symmetric.

In a conceptually related approach, Berman[17] presents a very compact method of correcting analytically derived mass matrices using measured modal data. He suggests that, given the three sets of data common to most update problems: the analytical mass matrix, analytical stiffness matrix and an incomplete set of measured modes, if one set of data is assumed to be correct, the other two may be updated. Accordingly, he assumes the measured mode shapes to be correct and uses them to update the mass matrix.

The procedure minimizes an error function based on the changes in the individual terms of the mass matrix with the constraint that the measured eigenvector must be

orthonormalized with respect to the corrected mass matrix. Since a Lagrange Multiplier approach is used, the expression for the corrected mass matrix is closed form. The resulting corrected mass matrix is optimal in the sense that it represents the matrix closest to the analytical one as measured by the Euclidean norm that still satisfies the orthonormalization constraint. While this method does not require a complete set of mode shapes, Berman still requires that each measured mode shape be complete. Thus, using this method to update large model could be harrowing for the experimentalist.

Berman and Nagy[18] unify Lagrange multiplier-based analytical model update schemes in a method they call Analytical Model Improvement (AMI). Again, experimental data is assumed to be correct and is used to update analytical predictions of the mass and stiffness matrices. The modal information is assumed to consist of an incomplete number of measured modes as well as incompletely measured modes. An approach closely related to Guyan reduction[19] is used to form complete eigenvectors for each measured mode. The process uses the analytical mass and stiffness matrices, so the analytical approximations must be the result of reasonably good approximations to the actual structure. The result is a rectangular matrix of eigenvectors where the number of rows is equal to the number of degrees of freedom of the analytical model and the number of columns is equal to the number of measured modes.

Then, a Lagrange multiplier very similar to the one presented in Reference 17 by Berman is used to update the analytical mass matrix. In the final step, the expanded modal matrix

and corrected mass matrix are used to correct the stiffness matrix. As before, the correction process uses a Lagrange multiplier method to modify the analytical stiffness matrix in a way which minimizes the changes as measured by a Euclidian norm and satisfies a symmetry constraint and two constraints based on the eigenvalue equation.

The AMI method addresses several of the requirements for update methods suggested by Ibrahim and Saafan. It makes no requirement that the number of measurement points be equal to the number of degrees of freedom of the model. It still suffers from the limitation, however, that the update to the stiffness and mass matrices has no physical significance.

An extremely useful idea that of minimizing some measure of the difference between the response of an analytical model and measured data. However, a stronger correlation between the corrected analytical model and the physical system is needed. A step in that direction is made by Kabe[20]. He argues that accuracy increases as the ratio of stiffness coefficients to available equations is reduced. He suggests that connectivity information can be used to supplement measured modal data and describes the Stiffness Matrix Adjustment (KMA) procedure. The additional assumption is made that the connectivity information from the analytical model is correct.

In many ways, KMA resembles other Lagrange multiplier-based approaches. A notable difference between KMA and other methods, though, lies in the error function used as an

objective in the optimization procedure. Kabe makes two compelling arguments. The first is that in many structures, nonstructural mass makes up a significant part of the total vehicle weight. In such cases, it may be inadvisable to use elements of the mass matrix to weight the changes in the stiffness matrix. Second, the form of the error function used in previous references creates a bias that tends to force a greater percentage change in small stiffness coefficients than in large ones. He suggests that an error function measuring change in the stiffness matrix should minimize the percentage change in each stiffness coefficient.

The preceding discussion by no means constitutes a compete list of possible parametric model update schemes. A sample of other methods are those described by Bernd[21], Liping, Kecheng and Zhandi[22] and Coppolino and Stroud[23].

The parametric update schemes discussed so far are not suitable for the model design problem. Some practical problems are:

1. The uncorrected analytical model must be close to the physical model
2. The correction is strictly mathematical (with the exception of KMA) with no corresponding physical significance in both mass and stiffness matrices
3. The corrected matrices are often not useful on their own.

A comparison of mathematical parameter versus physical parameter update methods is offered by Ojalvo[24] in a paper comparing two specific methods[25,26].

### 2.1.2 Physical Parameter Update Methods

The methods presented in the previous section updated the system matrices, usually with no attempt at correlation to a physical model. Berman[27], in a paper on the theoretical and practical bounds of system identification, notes the lack of a unique solution to the model update problem in the face of incomplete test data and concludes:

> The most promising methods select a solution which minimizes changes in a reasonably good analytical model. These methods should include constraints to force physical reality of the solution.

It seems obvious that methods which update models by varying physically meaningful parameters could be more widely useful than methods which are limited to modifying elements of system matrices. It is not surprising then, that a class of parameter identification methods has been developed which operates on physically based parameters, often by modifying a finite element model of the structure in question. These methods are of great interest in the model design problem.

A way of connecting model update results with something more physically meaningful is to use the update results to find errors in a finite element model. A method was proposed by Sidhu and Ewins[28] and further analyzed by Gysin[29], called the Error Matrix Method (EMM), to locate errors in finite element models. The method forms an error matrix from the difference between the stiffness matrices from an analytical model and an experimental model. The analytical stiffness matrix is reduced to the order of the experimental matrix, then a similar procedure is followed for the mass matrix. The method is simple, but has significant problems which would limit its use in a general sense.

One problem is that both experimentally and analytically determined mass and stiffness matrices are required. Since the experimentally determined matrices will be of lower order than the analytical ones for all but the smallest problems, the analytical matrices have to be reduced in order. The reduction process can introduce unacceptable errors.

After a series of numerical experiments, Gysin concludes that the number of modes taken into account is very important and that all modes possible should be measured and included in the correction. Of particular importance are modes greatly influenced by modelling errors. This circular problem further limits the usefulness of the method.

A method with fewer limiting requirements that is still based on physical requirements is desirable. Steinwender and Nordmann[30] proposed a method which was used to vary

the parameters of a finite element model of a pipe and support structure based on experimental data. An optimization procedure based on sensitivity calculations minimizes the squared differences between the measured and calculated natural frequencies of the system. The method does not operate on the finite element model directly, but uses vectors of correction factors to update the model. The correction factors operate on submatrices whose origin is left unexplained by the authors. The reader is left to assume that the submatrices are at least related to the element stiffness matrices. If this is the case, a strong correlation is established between the numerical update procedure and the physics of the problem.

Ojalvo and Pilon[31] examined the use of various identification methods to isolate errors in finite element models with the stated object of avoiding some of the limitations of EMM. They identified two basically different approaches which worked well on the example problems they examined. The first generates a difference function related to the inverses of the analytical and experimental stiffness matrices. The reader is left to use connectivity information to correlate differences in the stiffness matrices with changes in the finite element model.

Their second approach is based on calculating a modal error force. They describe this as the applied harmonic force distribution which would result in an analytical mode shape matching the experimental mode shape for a given natural frequency. Distinguishing differences between stiffness and mass matrix errors, however, requires the assumption

that mass matrix errors appear more prominent for higher modes if more than one mode is used in the analysis. They offer no basis for this assumption.

A slightly more sophisticated approach is to link the model update method directly to a finite element modelling program and use the results of the update algorithm to alter the finite element model. Ojalvo, et al.[32] describe a method developed to correct finite element models and demonstrate its use on a real world structure (many papers in this area use simulated test data for expediency). The method uses results from an earlier work by Ojalvo and Ting[33].

The method uses a one term Taylor series approximation to the difference between the measured modal test results from a structure and the analytical results based on an approximate model. This results in a system of linear equations in which the unknowns are finite element model parameters to be modified. Unless complete modal information is available, the system of equations is singular. In the general case of a singular system, a least squared error solution is used to update the model.

Wei and Janter[34] make very compelling arguments for a physical parameter based method using finite element analysis and propose a method to match eigenvalue and eigenvector information by varying physical parameters of a finite element model. The method uses first order Taylor series expansions to construct a Jacobian matrix for each iteration. The algorithm uses frequency matching combined with checks of mass and stiffness matrix

orthogonality. While the method was demonstrated using simulated data, the "T" plate structure used is more realistic that the lumped parameter models often used. Wei and Janter suggest the advantages of an optimization-based procedure operating on parameters of a finite element model:

-Optimization yields readily interpretable results

-Engineering judgement can be brought to bear more readily

-Since the optimization process is defined in terms of design variables, it is convenient to include design criteria

-Updated model is compatible with whatever pre- and post-processors which can be applied to the finite element model

-Procedure is compatible with current analysis practices - insight into finite element modelling is directly applicable

-A correctly formulated approach based on finite element analysis would be general so that new elements could be added without changing the process

They point out two problems which must be considered by anyone implementing such a method. These are that sensitivity calculations can be difficult and numerically intensive and that errors committed in the finite element modelling process are carried through and will affect the answer from the identification algorithm.

These arguments notwithstanding, update methods based on finite element models hold much promise. Work by Ewing and Venkayya[35] and Ewing and Kolonay[36] addresses

many of the limitations of previous methods. The finite element correction problem is formulated in the context of a large, general purpose structural analysis program. Such a approach would be very useful for the wind tunnel model designer.

In this work, a set of design variables is defined using parameters from the finite element model and a new model formulated for each iteration. An error function is defined as the sum of the squares of the differences between desired and calculated frequencies or mode shapes. Stiffness terms are not included in the objective function.

Two types of constraints are defined. The first defines limits on the error function used as an objective. The second is an equality constraint which forces the total mass of the final design to match some desired value. An experimental code was developed by Gibson[37] using the methods developed in References 35 and 36.

Another physically-based parameter update scheme has been documented by Hunt and Blelloch[38]. While based on physical parameters, the method seeks to minimize the amount of data needed for the model update. This is done by using the cross-orthogonality matrix to measure the correlation between the test and analysis generated mode shapes.

A good example of a 'real world' application of structural identification is presented by West[39]. A Modal Assurance Criteria (MAC) method[40] was used to quantify the changes

to an aft bulkhead from the space shuttle due to exposure to extreme levels of acoustic energy. MAC generates a single number for each measured mode shape which describes the correlation between measured and calculated mode shapes, with a coefficient of 1.0 indicating perfect correlation. In this work the MAC coefficients for the first 30 modes of the bulkhead were compared before and after testing to highlight changes in modal response due to damage.

None of the physical parameter updates methods presented are directly useful for the model design problem. However, they offer a strong foundation for a new method. References 35-37 in particular embody many of the features needed for wind tunnel model design.

All of the methods described so far use frequency domain data. A large subset of work in parameter identification methods, however, is devoted to time domain problems. These methods are not needed for a wind tunnel model design method. Readers interested in time domain methods are directed to References 38-45.

## 2.2 Aeroelastic Optimization

The model problem described so far is loosely related to aeroelastic optimization work. The basic goal of most aeroelastic optimization programs is to include aeroelastic constraints in an optimization method to design aircraft structures. Typically, the objective function for the problem is mass and the design variables are parameters of the mathematical representation of the structure. Often, other constraints such as maximum stress are applied along with the aeroelastic constraints.

Optimization of aircraft structures using aeroelastic constraints has been an active research topic for several decades. Early work was strictly analytical[46]. Improvements in computer technology, however, resulted in the development of large optimization codes which used aeroelastic constraints. TSO[47] used a Rayleigh-Ritz approximation of wing structures combined with nonlinear programming techniques to design wings subject to aeroelastic constraints. FASTOP[48] introduced finite element-based structural approximations. The development of ASTROS[49] introduced aeroelastic constraints in the framework of a large, general-purpose finite element based optimization program. ASTROS allows for optimization of a general structure subject to frequency, displacement, stress and aeroelastic constraints. Mass is used as an objective function, although an effort is under way to allow user-defined objective function.

These codes, though loosely related, are not applicable to the wind tunnel model design problem. The reason lies in the basic design of the program. The designer of a full scale vehicle is not likely to be concerned with stiffness distributions or modal behavior of the final design as long as it satisfies performance, strength and stability constraints and meets weight goals. The model designer has a much more specific goal in that the aeroelastically scaled model must have a predetermined weight, stiffness distribution and modal response.

## 2.3 Active Systems

An intersection of fields of parameter identification and aeroelasticity has resulted in the idea of active flutter suppression. The basic idea of flutter suppression is that it may be more efficient to avoid lifting surface flutter by using a control surface driven by a feedback control system to change the dynamic response of a flight vehicle so that flutter is avoided. A flight test was conducted by the Air Force using an F-4 to prove the concept[50,51]. Later a flutter suppression system was included on the F/A-18 currently in service with the U.S. Navy.

The problem with flutter suppression is that, as the flight conditions of the vehicle change (changes in speed, altitude, etc) and the configuration of the vehicle changes (fuel being burned, stores being released, etc) the requirements on the flutter suppression system

change. The F/A-18 system uses a look-up table approach, but a much more flexible approach is to include sensors (typically accelerometers) and some sort of identification capability in the control system to develop appropriate control laws in real time. This concept was demonstrated in a series of wind tunnel tests using aeroelastically scaled YF-17 and F-16 models[52-54]. Other representative work on adaptive flutter suppression are presented in Reference 55.

Wind tunnel models intended to simulate the behavior of lifting surfaces which include active control surfaces must themselves have active control surfaces. This work, however, is limited to passive wind tunnel models.

## 2.4 Wind Tunnel Model Design Methods

In preliminary work, I showed that scaled stiffness properties could be matched using structural optimization.[56-58] In this work, I used structural optimization to determine the element sizes for a finite element model of the scaled model structure so that the desired stiffness characteristics were obtained. Stiffness tests were then performed to show that the actual stiffness characteristics matched predictions.

I cast the model design problem as a constrained optimization problem and showed that stiffness characteristics could be matched by using incomplete information from the flexibility matrix of the full sized structure. Recall that the $i^{th}$ column of the flexibility matrix is the displacement vector due to a unit load applied at the $i^{th}$ degree of freedom. Thus, a set of displacement constraints was written for each column of the flexibility matrix. Constraints were written for elements in the flexibility matrix in the form.

$$g = \delta_{ij} - x_{ij} \leq 0 \qquad (3)$$

Where $\delta_{ij}$ is the $ij^{th}$ element of the desired flexibility matrix and $x_{ij}$ is ij element of the calculated flexibility matrix.

If all the constraints were exactly satisfied, the stiffness properties of the model structure would match the scaled stiffness properties of the full sized structure. However, using the complete set of constraints would result in a very large problem and might result in an overconstrained one. I showed in references 57 and 58 that a relatively small subset of the possible set of constraints is adequate. For instance, of a possible 28 columns of the stiffness matrix, I found that using four columns corresponding to four widely spaced points on the wing resulted in closely matched stiffness characteristics.

I used two different objective functions in previous work: mass and a squared error function. Mass was used for an effort which used existing software. The error function was used in a program written specifically to solve the model design problem. Using the squared error function as the objective, the optimization problem was written as

$$\text{Minimize:} \quad F = \sum_{i=1}^{n} k[g_i(x)]^2$$

$$\text{Subject to:} \quad g_1(x) = \left( \frac{x_1 - \delta_1}{\delta_1} \right) \leq 0 \qquad (4)$$

$$\vdots$$

$$g_n(x) = \left( \frac{x_n - \delta_n}{\delta_n} \right) \leq 0$$

where $x_i$ is the calculated displacement at the $i^{th}$ degree of freedom due to a unit load, $\delta_i$ is the desired displacement at the $i^{th}$ degree of freedom, n is the number of constraints to be applied and k is a constant.

My previous model design efforts were limited to matching stiffness characteristics. Obtaining the desired stiffness characteristics is necessary, but not sufficient for problems in which structural dynamics are important. For such problems, modal characteristics of the model are critical and mass properties must be matched as well.

## 2.5 Requirements For A New Method

This summary describes a cross section of published work which would be of use in designing the structure for an aeroelastically scaled wind tunnel model along with the

limitations of the different methods. From this background survey, I have concluded that any method proposed for model design must have the following characteristics:

-Distributed parameter systems should be accurately modelled

-No unrealistic structural approximations should be required

-No preprocessing of full scale data should be required

-The number of degrees of freedom desired for the scaled model should be completely independent of the number available for the full scale structure

-The model design method should work with very incomplete sets of modal and displacement data. Missing modes and displacement data from a limited number of degrees of freedom must be allowable

-The finished scaled model should accurately predict the results of untested loading conditions

-The model design method should not require an accurate initial design

-The model stiffness and mass matrices must be accurate by themselves, not just as elements in an equation of motion

-Updated mass and stiffness matrices must be symmetric

-Mode shapes calculated from the updated model must be orthogonal

-The results of the model design method must contain enough information to allow fabrication of the model structure. No interpretation of results should be required

-The method should be general enough to be applicable to any type of model structure

-The method must be modular so that new numerical algorithms can be substituted easily

-The method should modify physically meaningful parameters so that engineering judgement can be applied during the design process

-Manufacturing concerns must be included in the method so that the resulting design can be readily fabricated

Chapter III

## Theoretical Development

The new model design method presented here addresses the requirements identified in the Background section. It uses incomplete stiffness and modal information from a full scale structure as a staring point. It then updates a finite element idealization of the model structure with a numerical optimization procedure based on sensitivity calculations. The initial design of the model structure is merely a starting point for the optimization method. While starting at a point in design space close to the optimum speeds convergence, the initial design does not have to be close to the final design.

Design variables for the optimization process are the sizes of the elements in the finite element representation of the model structure. Thus, the result of the optimization procedure is the description of a model structure which can be directly fabricated. Post-processing of the data is not required. Also, consistency of the numerical representation is assured; the mass and stiffness matrices are, by definition symmetric and the eigenvectors calculated from the updated model are, by definition, orthogonal.

The finite element based procedure allows modelling of general structures. There is no need to assume a model structure any more simplified than that desired by the model builder. Particularly, there is no need for unrealistic structural assumptions such as assuming the wing structure can be accurately represented by a single beam. Furthermore, the mathematical representation of the model structure can have any number of degrees of freedom, so very complex model can be designed.

The method uses stiffness information the form of elements of the flexibility matrix and modal information in the form of natural frequencies and mode shapes. Both are readily available from any finite element model of the full scale structure. If the data is experimental, there is no requirement that the mode shapes be exactly orthogonal (although non-orthogonality of measured modes may be indicative of some problem in the test results).

A modest number of basic assumptions is made during the derivation. These are:

-The geometry chosen for the scaled model structure can, with correct element sizes and masses, reproduce the desired static and dynamic response

-Both the full scale structure and the model structure are linear,

-Information from the full scale structure is accurate (this must, by definition be true of all scaled model design methods).

-The scaled stiffness and mass properties of the full scale structure can be represented with sufficient accuracy using the assumed structural geometry of the scaled model.

-The model structure without tuning masses is lighter than the target weight

-The natural frequencies of the model structure without tuning masses are higher than the target frequencies

-Scaled response which is due to active elements in the full scale structure can be adequately modelled by a model control system which feeds back displacement, velocity and acceleration

Although it is currently fashionable to formulate optimization problems to operate on all design variables at once, the process here is broken down into two discrete steps. This is done so that the individual matrices will be physically meaningful alone, not just as components of an equation of motion. The steps in the design process are summarized in Figure 2.

The first step in any model design method is to obtain information about the full scale structure. This can come from several sources, but the most common is probably a finite element model. The model may have been tuned using test data. Finite element models are often very complex, so it is assumed that the number of degrees of freedom available for the full scale structure is much greater than is desired for the scaled model.

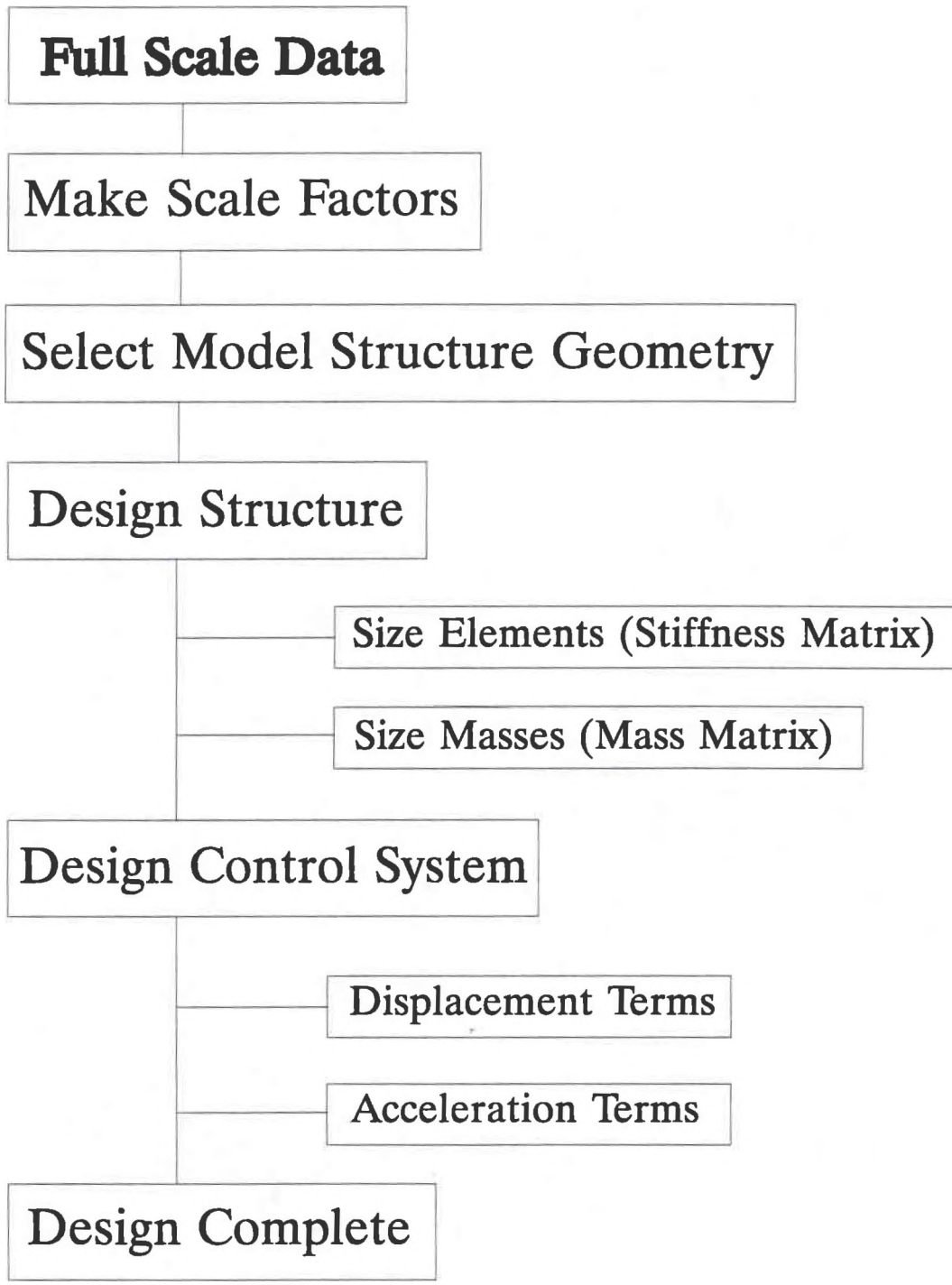


**Figure 2** - Summary of Steps in the Model Design Process

The second step in the process is to form scaling factors for the model. The scale factors depend largely on the tunnel in which the test is being performed. The model must be sized so that wing tips do not get too close to the sides of the tunnel. The dynamic pressure and Mach number available in the tunnel are also of great interest; it is assumed that the designer would like the aeroelastic phenomena to be investigated to be present in the performance envelope of the tunnel. Once the size of the model and the velocity ratio have been selected, the rest of the needed scale factors can be easily calculated.

The third step and final one for which no automatic method exists is choosing the geometry of the model structure, that is grid points and connectivities for the finite element representation of the model structure. It is assumed for this work that the grid points on the model coincide with scaled grid point locations of the full scale structure. There is no assurance that the structural geometry chosen by the model designer can reproduce the scaled response. Since the method is general, the initial model structure can include as many elements as the designer may wish to include. Since every element adds another dimension to the design space, increasing the number elements in the model structure increases the range of possible responses. Elements whose sizes go to zero can be eliminated from the structural model.

Once the model structure geometry is assigned, optimization methods developed below are used to size the elements and concentrated masses so that the stiffness and modal properties of the model match scaled values from the full scale structure. At this point,

the design of a classical passive model is complete. There is, however, the option of including the effect of active structural elements in the design. This is done by using optimization-based methods to determine coefficients in the feedback control system so that the active structure exhibits the desired responses.

## 3.1 Foundations

Before a description of the design methods can take place, scaling laws for the model have to be defined and some basic model structure defined. The aeroelastic model scaling laws are easily derived, but are included here for completeness. The structure of a wind tunnel model is essentially arbitrary. The methods developed here are more clearly presented if done in the context of some assumed model structure. A beam-based structure was used here for manufacturing simplicity and for consistency with a widely used method of designing aeroelastic mode structures.

### 3.1.1 Scaling Parameters

Although the procedure for aeroelastic scaling is not complex[1], a brief description here is useful. The reason for building aeroelastically scaled models is almost always to verify aerodynamic predictions; prediction of unsteady aerodynamic forces has often been the weak point in flutter analysis. It is not surprising then that scaling is driven by the need to match aerodynamic parameters. When scaling a wing, three non-dimensional parameters should be the same for both the full scale wing and the model: Mach number, Reynolds number and reduced frequency. In practice, it is not usually possible to match all three of these quantities so simplifications are often made. If the flow is not dominated by viscous effects, Reynolds number is not matched. If the flow is assumed to be incompressible, Mach number is not matched. Matching Reynolds numbers is usually considered a minimum requirement.

The first step in the scaling process is to define necessary physical properties in non-dimensional terms. In the following notation, the overbar denotes a non-dimensional quantity. Subscript m denotes a model property and subscript w denotes a full scale wing property. Also, l is length, U is velocity and $\rho$ is air density. Time is

$$\bar{t} = \frac{tU}{l} \qquad t = \frac{\bar{t}l}{U} \tag{5}$$

Mass is

$$\bar{m} = \frac{m}{\rho l^3} \qquad m = \bar{m}\rho l^3 \tag{6}$$

Force is

$$\bar{f} = \frac{f}{\rho l^2 U^2} \qquad f = \bar{f}\rho l^2 U^2 \tag{7}$$

Geometry, mass, stiffness and frequency scale factors are needed to scale the model. Typically, wind tunnel size is a driving factor in model design. Thus the geometric scale factor, $l_m/l_w$, is often specified first. The model should flutter inside the performance envelope of the tunnel, so the velocity ratio, $U_m/U_w$ is also specified. The frequency scale factor may be derived two ways, the first is to non-dimensionalize the frequencies and write the ratio of them. Since the units of frequency is 1/time, the frequency ratio is

$$\frac{\omega_m}{\omega_w} = \frac{U_m}{\bar{t} l_m}\frac{\bar{t} l_w}{U_w} = \frac{U_m}{U_w}\frac{l_w}{l_m} \tag{8}$$

The second way to determine the frequency ratio is start with the ratio of reduced frequencies. Reduced frequency is a non-dimensionalized frequency.

$$\frac{k_m}{k_w} = \frac{l_m \omega_m}{U_m}\frac{U_w}{l_w \omega_w} = 1$$

$$\frac{\omega_m}{\omega_w} = \frac{l_w}{l_m}\frac{U_m}{U_w} \tag{9}$$

Since mass is non-dimensionalized using $\rho l^3$, the mass scale factor is written as

$$\frac{M_m}{M_w} = \left(\frac{l_m}{l_w}\right)^3 \frac{\rho_m}{\rho_w} \tag{10}$$

Where $\rho_m$ is the air density in the wind tunnel and $\rho_w$ is the air density at the full scale flight condition. There are two ways to determine the stiffness scale factor. The first is to use the frequency and mass scale factors along with the relationship between frequency, mass and stiffness.

$$\frac{k_m}{k_w} = \frac{\omega_m^2 m_m}{\omega_w^2 m_w} = \left(\frac{l_w^2}{l_m^2}\frac{U_m^2}{U_w^2}\right)\left(\frac{\rho_m l_m^3}{\rho_w l_w^3}\right) = \frac{\rho_m}{\rho_w}\frac{U_m^2}{U_w^2}\frac{l_m}{l_w} \tag{11}$$

The second method stems from the fact that the units for stiffness are force per unit length. The stiffness ratio can be expressed using non-dimensional force and non-dimensional length.

$$\frac{k_m}{k_w} = \frac{\bar{f}\rho_m l_m^2 U_m^2}{\bar{x} l_m}\frac{\bar{x} l_w}{\bar{f}\rho_w l_w^2 U_w^2} = \frac{\rho_m U_m^2 l_m}{\rho_w U_w^2 l_w} \tag{12}$$

One of the most difficult aspects of calculating scaling laws for wind tunnel models is matching the Reynolds number. The Reynolds number is defined as

$$Re = \frac{\rho U l}{\mu} \tag{13}$$

where $\mu$ is viscosity. Matching the Reynolds number requires that the following relation be satisfied

$$\frac{Re_m}{Re_w} = \frac{\rho_m U_m l}{\mu_m} \frac{\mu_w}{\rho_w U_w l_w} = 1 \qquad \textbf{(14)}$$

Velocity, length and density ratios are defined in previous relations. The preceding relationship can be used to specify a viscosity ratio

$$\frac{\mu_m}{\mu_m} = \frac{\rho_m U_m l_m}{\rho_w U_w l_w} \qquad \textbf{(15)}$$

The obvious problem is that viscosity of the test medium cannot be changed at will. Solutions such as cryogenic tunnels and tunnels using pressurized freon have been successful in the effort to match Reynolds numbers. In many case, though, such facilities are not available and the requirement of matching Reynolds number is not satisfied.

An expression for scaling forces is necessary if any kind of control system is included in the structure. the force scaling ratio is simply expressed as a ratio of the non-dimensional force expressions above.

$$\frac{f_m}{f_w} = \frac{\bar{f} \rho_m l_m^2 u_m^2}{\bar{f} \rho_w l_w^2 u_w^2} = \frac{\rho_m}{\rho_w} \left( \frac{l_m u_m}{l_w u_w} \right)^2 \qquad \textbf{(16)}$$

Several general trends become apparent when looking at model scale factors. The first is that the mass of the model is a very strong function of geometry scale factor. Thus, a small scale model must be a very light model. Another is that stiffness is a strong function of velocity ratio. Thus low speed models are very flexible while high speed

models must be very stiff. The stiffness scale factor plays a large part in determining the construction of the model. Typical construction for an aeroelasticity model uses an aluminum or steel beam structure with a light aerodynamic covering made of foam or balsa. In cases where a light, stiff model is required, construction often involves using composite skins over a foam or nomex core.

### 3.1.2 Model Structure

The method developed here is applicable to any structure which can be modelled using finite elements. For simplicity, the structure of the model designed using the methods presented here is assumed to be a planar array of rectangular cross-section beams. This construction is typical of aeroelasticity models. It is further assumed that some subset of the grid points of the model structure line up with grid points for which structural data is available. It is important to note that the model structure will not necessarily bear any physical resemblance to the structure of the full scale wing. A representative model structure is presented in Figure 3.

Stiffness properties are determined by element connectivity and the cross-sectional shape of the elements. It would be highly unusual for a structure which gave the desired stiffness properties to also have the desired vibrational characteristics. Thus, it is

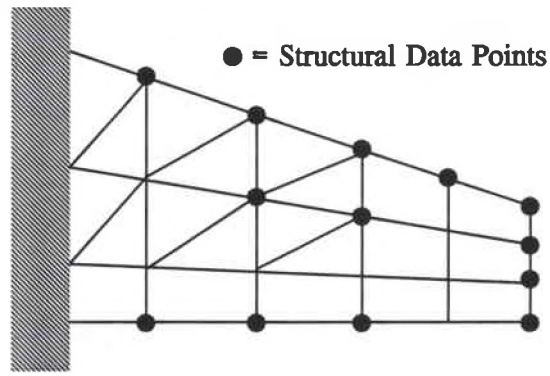


**Figure 3** - Representative Model Structure

common for aeroelasticity models to have masses attached to the structure to tune the frequencies and mode shapes to the desired values. It is assumed that the model structure being designed here will have a concentrated mass at each grid point for use in tuning the vibrational characteristics of the model.

## 3.2 Determining System Parameters

The generic label of system parameters is applied here to any quantity which is used to define the mathematical representation of the model structure. In many of the parametric update schemes developed to date, the term system parameters refers strictly to elements of the global mass, damping and stiffness matrices. Since physical applicability is a

primary goal of this work, system parameters determined here will consist of measurable characteristics of the model such as element dimensions and masses of tuning weights.

The mass and stiffness design methods presented here all have a common philosophy behind them: they all use numerical optimization techniques to minimize some measure of the difference between desired and calculated system response. When formulated properly, this approach meets some of the requirements set forth at the end of Section II. Flexibility is built in by not requiring complete displacement or modal information and by allowing any number of the available elements to be used as design variables.

### 3.2.1 Solution Strategies for Stiffness Design

The strategy for designing the model structure is broken down into two discrete steps. In the first step, the element connectivities are assigned manually and the resulting elements are sized using optimization techniques such that the model has the desired stiffness characteristics. The second step starts with the stiffness designed model. In this step, concentrated masses are sized using optimization techniques so that the resulting structure has the desired modal characteristics. Several approaches are possible for the stiffness and mass design. Computer programs were written to implement each of the

design methods presented below and the results compared in an effort to find the most usable method.

Five different approaches were evaluated for the stiffness design task. In each case, beam heights were assumed to be fixed and the widths were treated as design variables. This resulted in one design variable for each beam element in the finite element model. Input data consisted of grid point geometry, element connectivities, element widths and heights and displacement information.

The first approach treated the design task as an unconstrained minimization problem. An objective function was formed by summing the differences between the desired and actual values of a predetermined set of flexibility coefficients. The objective function to be minimized is

$$F = \sum_{i=1}^{m} \sum_{j=1}^{n} k\,(\delta_{ij} - x_{ij})^2 \qquad (17)$$

where k is a constant used to modify convergence behavior, $\delta_{ij}$ is the value of the ij term of the desired flexibility matrix supplied by the user and $x_{ij}$ is the calculated value of the ij term of the flexibility matrix. m is the number of retained rows of the flexibility matrix and n is the number of retained columns. m and n will, in general, be less than the order of the mathematical representation. It is important to note that the retained rows and columns need not be contiguous. A more complete discussion of the reasons is reserved for a later section.

It is convenient to think of the ij term of the flexibility matrix as the displacement in the $i^{th}$ degree of freedom due to a unit load in the $j^{th}$ degree of freedom. Minimizing the objective function presented in equation 17 is equivalent to finding a least squares fit of the specified terms of the flexibility matrix.

Optimization for all the different design methods was handled using ADS[62] and by a compound scaling method implemented in program FUNOPT[63,64]. Several different unconstrained minimization techniques are available in ADS, but all require objective function gradients to be supplied. The derivative of the function from Equation 17 with respect to some design variable , a, is

$$\frac{\partial f}{\partial a} = \sum_{i=1}^{m} \sum_{j=1}^{n} -2k(\delta_{ij} - x_{ij}) \frac{\partial x_{ij}}{\partial a} \tag{18}$$

The derivative of the displacement $x_{ij}$ with respect to the design variable a is found by implicitly differentiating the matrix equation of equilibrium and solving for the derivative of the displacement vector

$$\begin{aligned} \{F\} &= [K]\{x\} \\ \left\{\frac{\partial F}{\partial a}\right\} &= \left[\frac{\partial K}{\partial a}\right]\{x\} + [K]\left\{\frac{\partial x}{\partial a}\right\} \\ \left\{\frac{\partial x}{\partial a}\right\} &= -[K]^{-1}\left[\frac{\partial K}{\partial a}\right]\{x\} \end{aligned} \tag{19}$$

The second and third approaches examined for the stiffness design used a constrained optimization strategy with mass used as an objective function. The objective function is

$$F = \rho \sum_{i=1}^{n} b_i h_i l_i \tag{20}$$

where $b_i$, $h_i$ and $l_i$ are respectively the width, height and length of the $i^{th}$ element and $\rho$ is the material density. The derivative of the objective function with respect to some beam width, $b_i$, is simply

$$\frac{\partial F}{\partial b_i} = \rho h_i l_i \tag{21}$$

There is one constraint written for each influence coefficient used. Constraints of two different forms were used in the various approached presented here. Strategy two used the method of modified feasible directions[65,66] (MFD) for optimization. A characteristic of MFD is that if the initial design is not feasible or nearly so, there is a good chance that the optimizer will not be able to find the feasible region. For this case, the constraints were of the form

$$g = x_{ij} - \delta_{ij} \leq 0 \tag{22}$$

Thus, a structure for which the deflections are too small is feasible, and a feasible design can be assured by making the element sizes large so that the structure is too stiff. The assumption behind using mass as an objective function is that the lightest feasible structure is the most flexible structure. If this is true, structural mass will reach a

minimum when the maximum number of constraints are exactly satisfied. A secondary reason is to provide a basis to evaluate the use of commercially available optimization packages which often use mass as the default objective function. A recent update to MSC/NASTRAN[67], however, does allow a user-specified objective function.

Strategy three used was an extended interior penalty function[68,69] (IPF) method for optimization. In this method, the values of violated constraints multiplied by some constant are appended to the objective function. If there are no violated constraints, the method becomes an unconstrained minimization method. IPF does a good job of finding a feasible design when the starting point is an infeasible design. Thus, the form of the constraint was modified so that it is violated everywhere except where it is exactly satisfied.

$$g = (\delta_{ij} - x_{ij})^2 \leq 0 \qquad \textbf{(23)}$$

This type of constraint acts like an equality constraint. The feasible region for a group of constraints written in this form is a single point.

The fourth approach used is essentially a mixture of the previous two. A constrained optimization approach is used with the squared error function presented in Equation 17 used as the objective function. The constraints used are of the form presented in Equation 23. The extended interior penalty function was used as an optimization method. The fifth approach used a generalized compound scaling method for optimization. The

displacement error function was used for an objective function and displacements were used to form constraints.

#### 3.2.1.1 Selecting Flexibility Coefficients

One of the requirements stated at the end of Section II is that complete data from the full scale must not be required. A key part of the stiffness design problem, then, is selecting the flexibility coefficients which are to be matched. Full scale flexibility data will likely come from a finite element model (possibly one that has been corrected using ground test data). Production finite element models can be very large, so some means of picking a subset of flexibility coefficients for the stiffness design process must be developed.

Picking the number of flexibility coefficients to be used can be divided into two separate problems. The first is choosing how many columns of the flexibility matrix to retain. The second is to pick which points in those columns to use. In references 59-61, the assumption was made that a model with acceptably correct stiffness properties could be designed using a small subset of the available columns of the flexibility matrix. This proved to be correct. For these efforts, four columns of the flexibility matrix were chosen for the model stiffness design task. These corresponded to grid points at the mid span leading and trailing edge and the tip leading and trailing edge. The intuitive argument

was made that matching displacements due to unit loads at a small number of widely spaced points on the wing would result in a model structure which would have the correct stiffness properties everywhere.

Consider the deformations on the wing structure due to a unit load applied at the tip. Every structural element inboard of the loading point is stressed and so deforms in a way that contains information about the stiffness properties of the structure. Points outboard of the loading point are not stressed, so, even though they deform, they contain no information about the stiffness properties of the wing.

It is apparent that deformations due to a small number of loading conditions (perhaps even a single one) which collectively stress the entire structure might contain enough information to perform a stiffness design. It may even be undesirable to have a single element stressed by more than one loading condition. If the resulting deformation were to be included more than once in figuring out the objective function, that deformation would be given more weight in the optimization process than would a point which was stressed by a single loading condition.

### 3.2.2 Solution Strategies for Mass Design

The first stage of the design process should result in a structure with the correct stiffness characteristics. The second stage of the process is to size concentrated masses to be added to the stiffness design structure so that the resulting system has the desired modal characteristics. Two different methods were used to size the concentrated masses. Both use numerical optimization methods to minimize some measure of the difference between the desired scaled modal response and that calculated from the finite element representation of the model structure.

The first method used an unconstrained minimization approach to match frequencies only. The assumption was that if the stiffness distribution was correct and the frequencies were correct, the resulting mass distribution and, thus, mode shapes would also be correct. The objective function for this method is

$$F = \sum_{i=1}^{n} \left( \frac{\lambda_i - \bar{\lambda}_i}{\bar{\lambda}_i} \right)^2 \qquad (24)$$

Where $\lambda_i$ is the $i^{th}$ eigenvalue of the structure. Overbars indicate desired values input by the user. Minimizing the objective function amounts to finding a least squares fit of the n specified eigenvalues. It is important to note that the difference between the calculated and specified eigenvalues is normalized. If this were not done, the function would be

biased toward the higher eigenvalues where a given percentage error would result in a larger absolute error.

The second method uses a constrained optimization approach to size the concentrated masses. The objective function is a squared error function using mode shapes. The objective function is

$$F = \sum_{i=1}^{m} \sum_{j=1}^{n} \left[ \frac{\overline{x_{ij}} - x_{ij}}{\overline{x_{ij}}} \right]^2 \qquad \textbf{(25)}$$

where m is the number of out of plane degrees of freedom specified by the user, n is the number of modes specified and $x_{ij}$ is the ij element of a matrix whose elements are the out of plane terms of the eigenvector matrix. It is important to note that the terms in Equation 25 are normalized. This has the effect of allowing the same percentage violation for each of the terms and ensures that very small displacements are matched more closely on an absolute scale than are larger displacements. The intent is to make sure that the positions of node lines are determined correctly.

There are two different types of constraints. The first is a set of eigenvalue constraints. Then, appended onto the end of the eigenvalue constraints is a total mass constraint. The constraints are written out as

$$g_1 = \left( \frac{\lambda_1 - \bar{\lambda}_1}{\bar{\lambda}_1} \right)^2 \leq 0$$

$$\vdots \qquad (26)$$

$$g_n = \left( \frac{\lambda_n - \bar{\lambda}_n}{\bar{\lambda}_n} \right)^2 \leq 0$$

$$g_{n+1} = \frac{\bar{m} - m}{\bar{m}} = 0$$

Note that the mass constraint is an equality constraint.

3.2.2.1 Eigenvalue Derivatives

For computational efficiency, having analytical expressions for the objective function gradients is highly desirable. The derivative of the objective function in equation 24 with respect to some design variable a is

$$\frac{\partial F}{\partial a} = \sum_{i=1}^{n} \frac{2}{\bar{\lambda}_i} \left( \frac{\lambda_i - \bar{\lambda}_i}{\bar{\lambda}_i} \right) \frac{\partial \lambda_i}{\partial a} \qquad (27)$$

The derivative of some eigenvalue $\lambda$ can be found by implicitly differentiating the eigenvalue equation

$$[K]\{x\} = \lambda [M]\{x\}$$

$$\left[\frac{\partial K}{\partial a}\right]\{x\} + [K]\left\{\frac{\partial x}{\partial a}\right\} = \frac{\partial \lambda}{\partial a}[M]\{x\} + \lambda\left[\frac{\partial M}{\partial a}\right] + \lambda [M]\left\{\frac{\partial x}{\partial a}\right\} \tag{28}$$

The stiffness matrix [K] is not a function of the concentrated mass values, so the derivative of [K] with respect to a is zero. Now, equation 28 is premultiplied by the transpose of the eigenvector

$$\{x\}^T[K]\left\{\frac{\partial x}{\partial a}\right\} = \frac{\partial \lambda}{\partial a}\{x\}^T[M]\{x\} + \lambda\{x\}^T\left[\frac{\partial M}{\partial a}\right]\{x\} + \lambda\{x\}^T[M]\left\{\frac{\partial x}{\partial a}\right\} \tag{29}$$

and can be slightly re-arranged to yield

$$\{x\}^T[K]\left\{\frac{\partial x}{\partial z}\right\} - \lambda\{x\}^T[M]\left\{\frac{\partial x}{\partial a}\right\} = \frac{\partial \lambda}{\partial a}\{x\}^T[M]\{x\} + \lambda\{x\}^T\left[\frac{\partial M}{\partial a}\right]\{x\} \tag{30}$$

For a symmetric problem

$$\{x\}^T[K] = \lambda\{x\}^T[M] \tag{31}$$

so the left side of Equation 30 is zero and a closed form expression for the eigenvalue derivative results

$$\{x\}^T([K] - \lambda[M])\left\{\frac{\partial x}{\partial a}\right\} = 0 = \frac{\partial \lambda}{\partial a}\{x\}^T[M]\{x\} + \lambda\{x\}^T\left[\frac{\partial M}{\partial a}\right]\{x\}$$

$$\frac{\partial \lambda}{\partial a} = -\frac{\lambda\{x\}^T\left[\frac{\partial M}{\partial a}\right]\{x\}}{\{x\}^T[M]\{x\}} \tag{32}$$

3.2.2.2 Eigenvector Derivatives

A result of using an objective function as defined in Equation 25 is that eigenvector derivative must be determined. The method of Nelson[71,72] was used to calculate eigenvector derivatives. The eigenvalue equation is

$$[K]\{x\} = \lambda[M]\{x\} \tag{33}$$

and a normalization equation can be written

$$\{x\}^T[M]\{x\} = c \tag{34}$$

where c is some constant. Taking the derivative of the eigenvalue equation with respect to some design variable a and rearranging terms yields

$$\left[[K] - \lambda[M]\right]\left\{\frac{\partial x}{\partial a}\right\} = \frac{\partial \lambda}{\partial a}[M]\{x\} - \left[\frac{\partial K}{\partial a}\right]\{x\} + \lambda\left[\frac{\partial M}{\partial a}\right]\{x\} \tag{35}$$

The right hand side of Equation 35 is made up of known quantities, so an $n^{th}$ order linear system is formed. However, the coefficient matrix on the left hand side is singular, so a direct solution is not possible. Instead, assume the solution of Equation 35 is

$$\left\{\frac{\partial x}{\partial a}\right\} = \{V\} + \alpha\{x\} \tag{36}$$

where {V} is the homogeneous solution of Equation 35. The coefficient matrix of Equation 35 is singular, so {V} cannot be solved for directly. Instead, one of the elements of {V} is set equal to zero and Equation 35 is solved for the remaining components.

The coefficient, $\alpha$, can be determined using the normalization equation. Taking the derivative of the normalization equation with respect to a gives

$$\left\{\frac{\partial x}{\partial a}\right\}^T [M]\{x\} + \{x\}^T \left[\frac{\partial M}{\partial a}\right]\{x\} + \{x\}^T [M]\left\{\frac{\partial x}{\partial a}\right\} = 0 \tag{37}$$

Terms can be combined to give

$$\{x\}^T [M]\left\{\frac{\partial x}{\partial a}\right\} = -\frac{1}{2}\{x\}^T \left[\frac{\partial M}{\partial a}\right]\{x\} \tag{38}$$

To find $\alpha$, substitute Equation 38 into Equation 35. The result is

$$\alpha = \frac{1}{c}\left[-\frac{1}{2}\{x\}^T \left[\frac{\partial M}{\partial a}\right]\{x\} - \{x\}^T [M]\{V\}\right] \tag{39}$$

It should be noted that there are many methods available for calculating eigenvector derivatives and that Nelson's method is not always adequate when there are double eigenvalues. An alternative method proposed by Ojalvo[72] is effective in the cases involving double eigenvalues.

Chapter IV

# Numerical Evaluation

## 4.1 Sample Problem

The sample case used for evaluating the methods described in the previous section is a low aspect ratio fighter wing. The planform of the wing is shown in Figure 4. The structure of the wing is built up of shear, membrane and rod elements and is cantilevered at the root. The structure is made completely from aluminum with 12 spars and four ribs. The airfoil section of the wing is NACA 0004. A picture of the finite element model of the wing is shown in Figure 5.

The wing was modeled in ASTROS using 235 finite elements. Thicknesses of these elements are all potential design variables. Using all 235 elements would result in undesirably long run times and would be inconsistent with the detail if the structural and aerodynamic representations. Thus the number of design variables was reduced to 5 using heavy design variable linking. The reduction in the number of design variables greatly reduced the run time for the full scale model and did not qualitatively change the aeroelastic behavior.

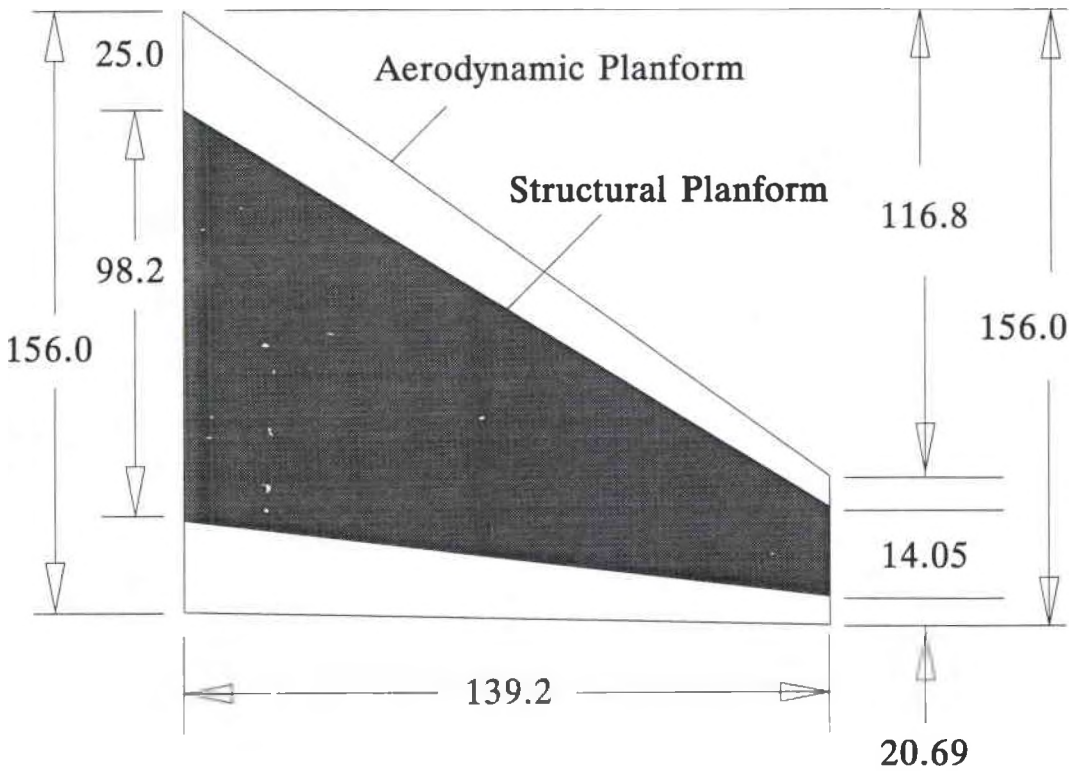


All Dimensions in Inches

**Figure 4** - Wing Planform

The aerodynamic panel model of the wing was kept simple to reduce run times; the aerodynamic representation of the wing used a 6 x 6 panel grid. The wing section is symmetric, so no camber effects were included in the analysis. Thickness effects were assumed to be insignificant and are not modelled either. The aerodynamic box pattern is presented in Figure 6.

Element sizes for the wing were determined by designing the wing for minimum mass using a flutter constraint. ASTROS[51] was used for the design. A flutter velocity of not less than 10000 in/sec was specified at a Mach number of .85. Heavy design variable linking was used to assign five design variables for the wing. After an optimized design was obtained, the Mach number was varied to find a matched point flight condition. The matched point was determined to be Mach .75 at sea level. The first four normal modes were used for the flutter analysis. The modal participation factors for the flutter point are given in Table 1.

Table 1
Modal Participation Factors at Flutter Point

| Mode | Real | Imaginary | Magnitude | Phase (deg) |
|---|---|---|---|---|
| 1 | .9764 | 0.00 | .9764 | 0.0 |
| 2 | .20745 | -.0494 | .2132 | -13.4 |
| 3 | -.01728 | .0309 | .0354 | 119.2 |
| 4 | .00403 | 00002 | .00403 | .28 |

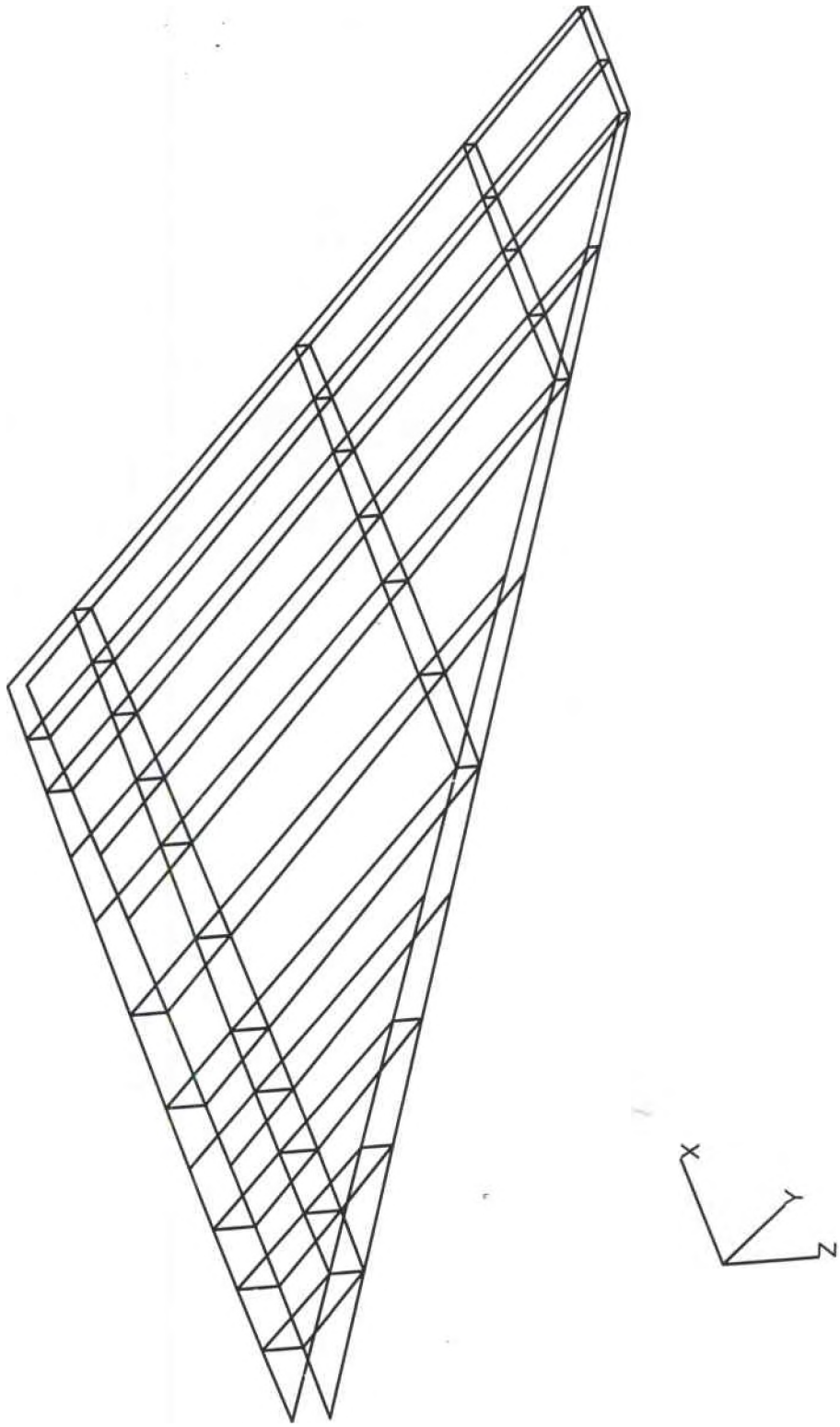


**Figure 5** - Wing Finite Element Model

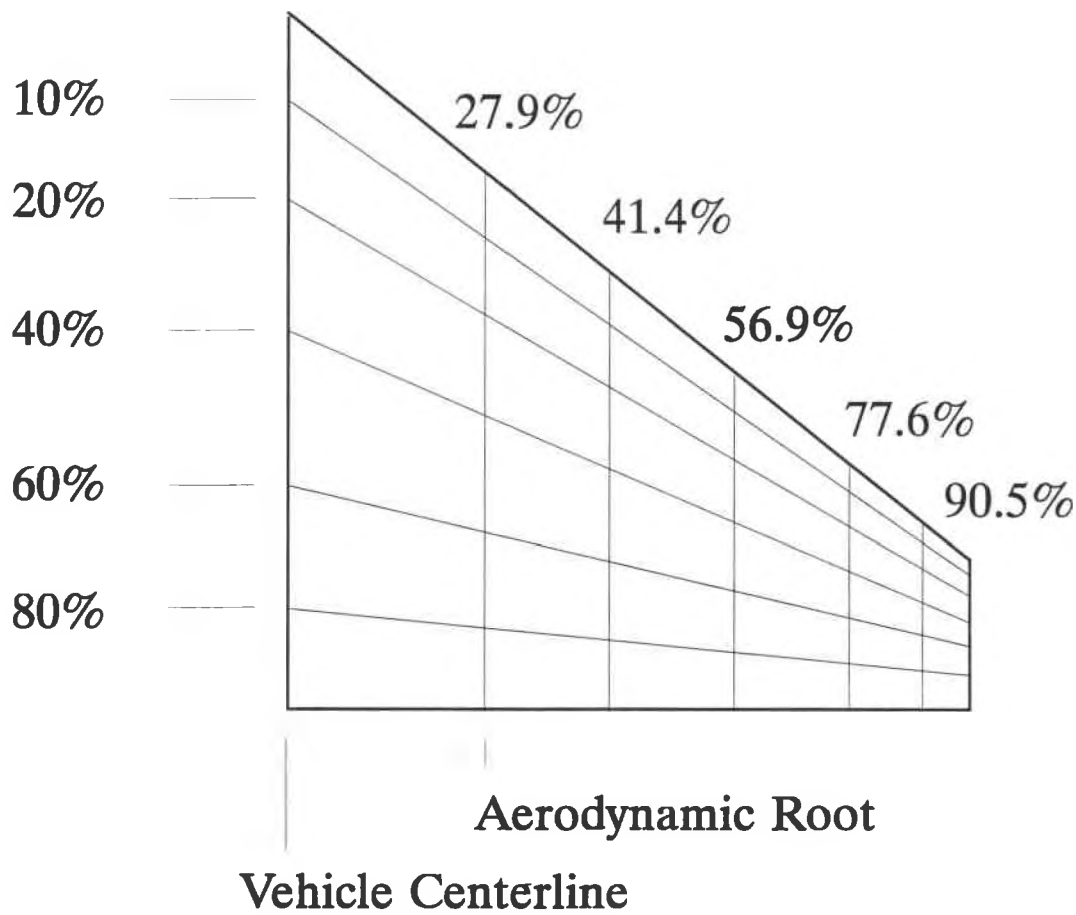


**Figure 6** - Wing Aerodynamic Box Pattern

The flutter mode is assumed to be a summation of in vacuo normal modes multiplied by complex scale factors. These complex scale factors are the modal participation coefficients. The magnitude of the modal participation coefficient of a particular mode is a measure of the extent to which that mode contributes to the flutter mode. It is typical for the magnitude of the modal participation coefficient to decrease as the mode number increases. When the participation coefficient for a mode is small, that mode may be eliminated from the analysis with little effect on the results. It is apparent from the very low magnitude of the modal participation coefficient that the fourth mode does not contribute significantly to the flutter mechanism. The magnitudes of the participation coefficients for higher modes are also small. Thus, only the first three normal modes are included in the remaining analyses. The first three natural frequencies are presented in Table 2. The first three mode shapes are presented in Figures 7, 8 and 9 respectively.

Table 2
Natural Frequencies of Full Scale Wing

| Mode | Frequency (hz) |
|---|---|
| 1 | 3.58 |
| 2 | 11.35 |
| 3 | 14.96 |

At Mach .75 the flutter velocity was 820.5 ft/sec and the flutter frequency was 5.81 hz. The V-G plot resulting from this analysis is presented in Figure 10. The V-ω plot resulting from the flutter analysis is presented in Figure 11.

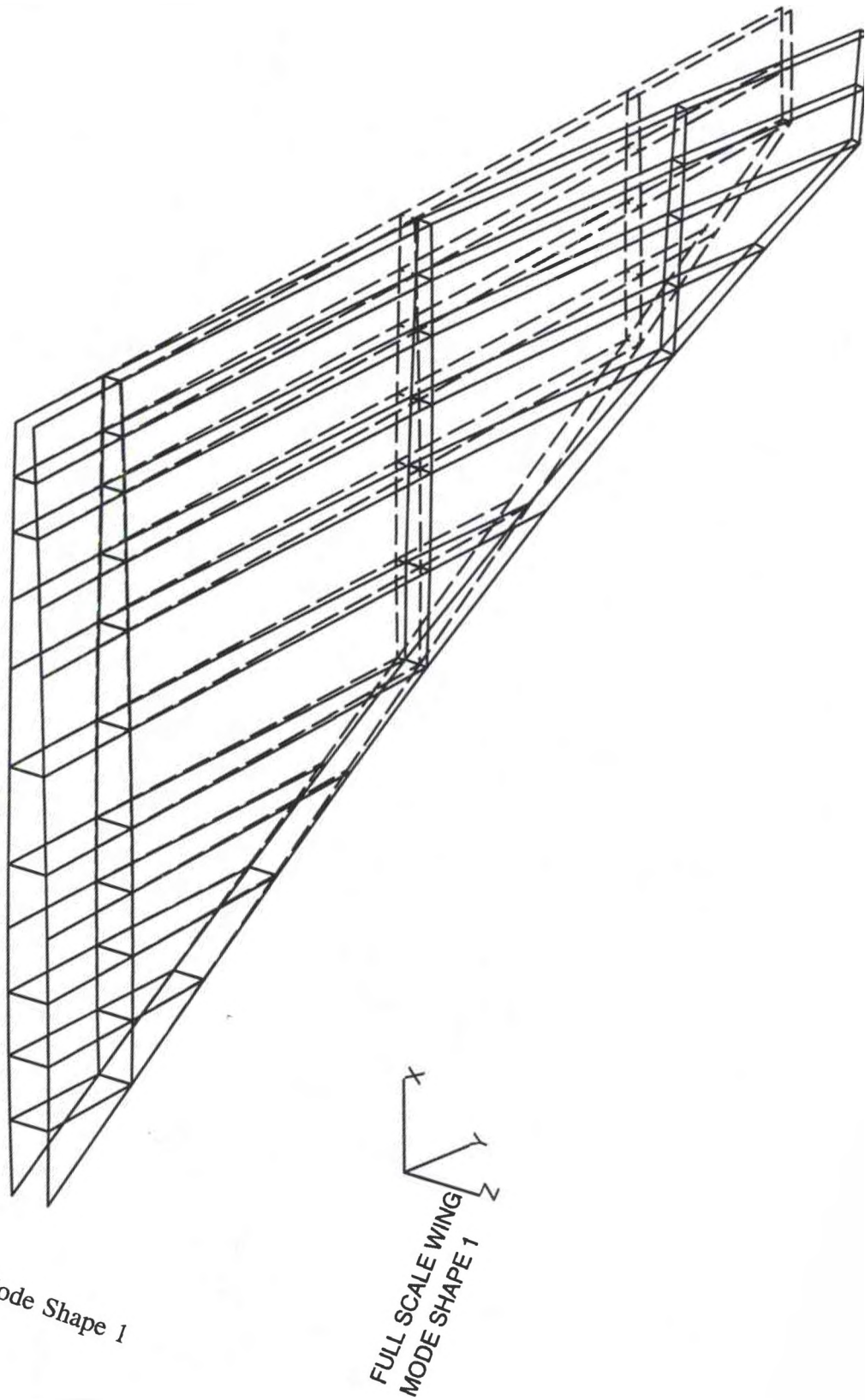


**Figure 7** - Full Scale Wing Mode Shape 1

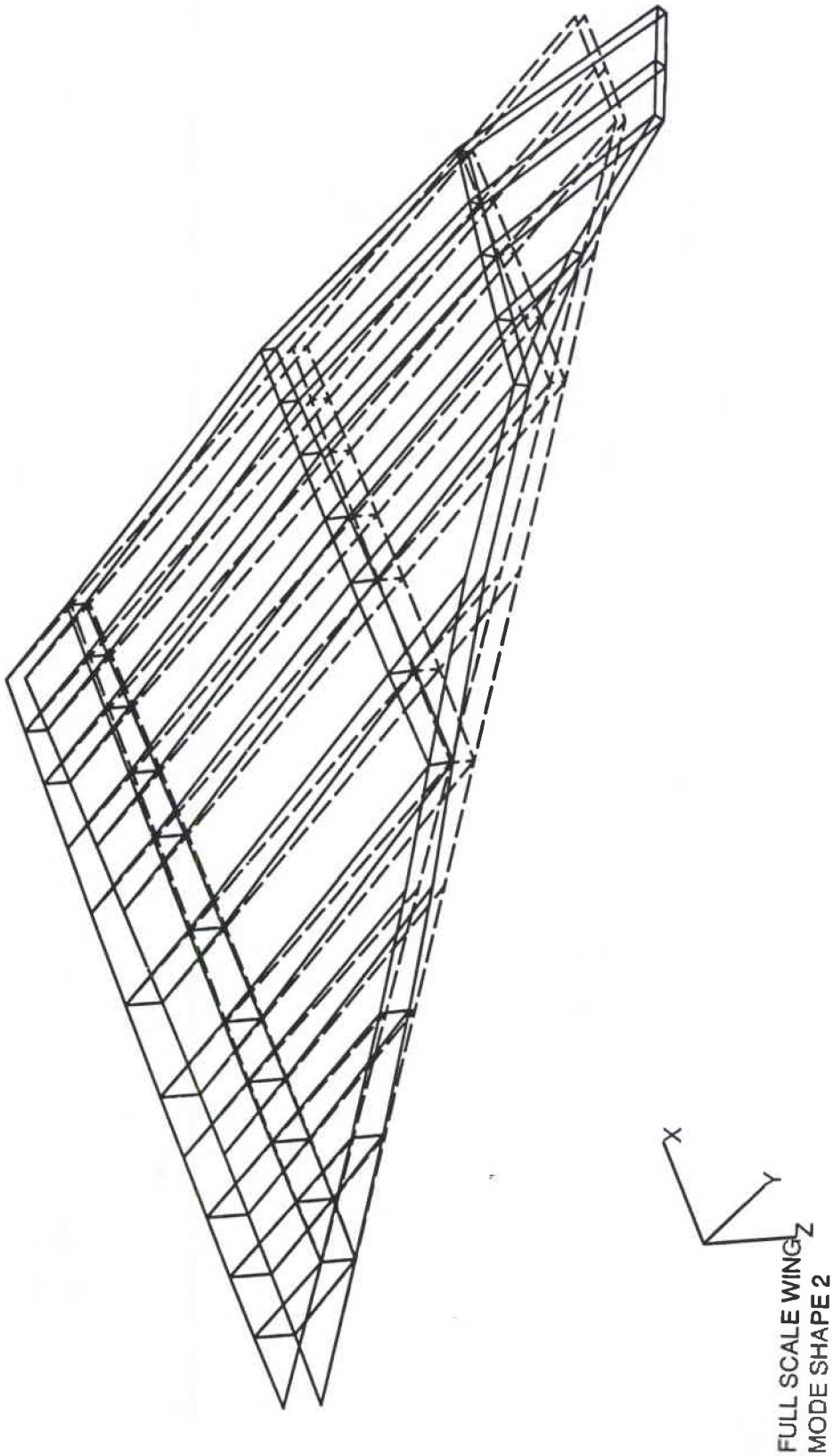


**Figure 8** - Full Scale Wing Mode Shape 2

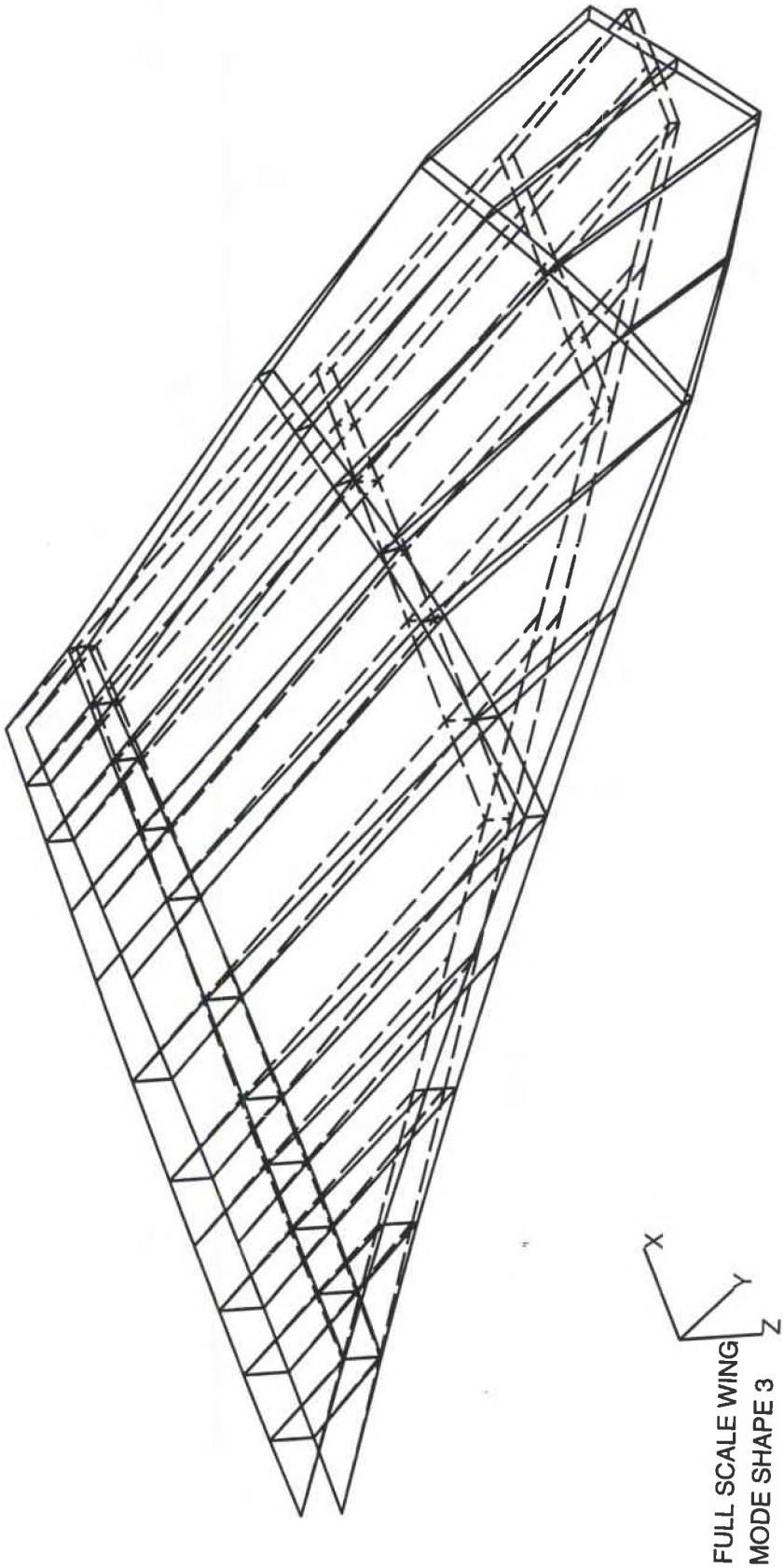


**Figure 9** - Full Scale Wing Mode Shape 3

**Figure 10** - V-G Plot for Wing

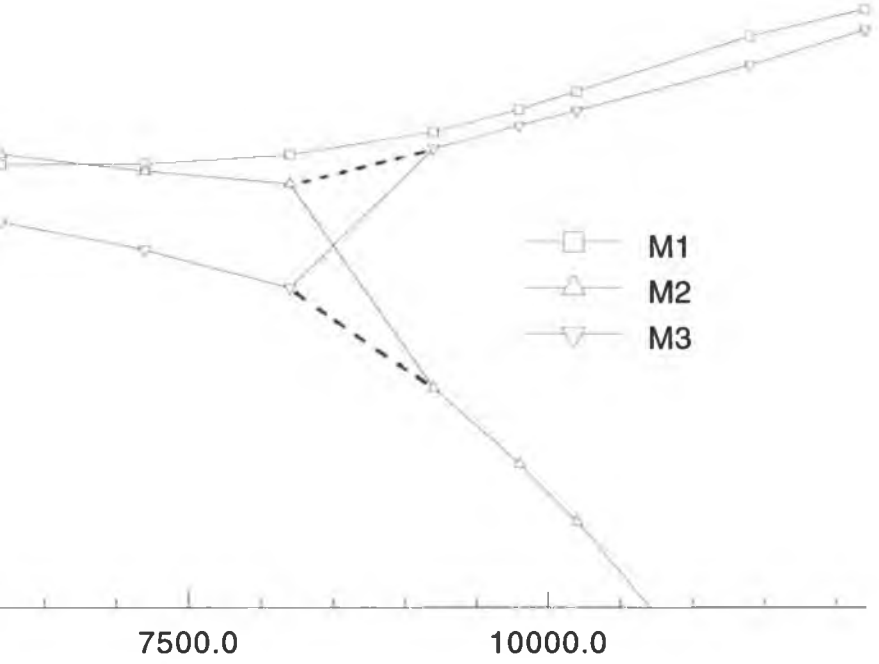


Velocity (in/sec)

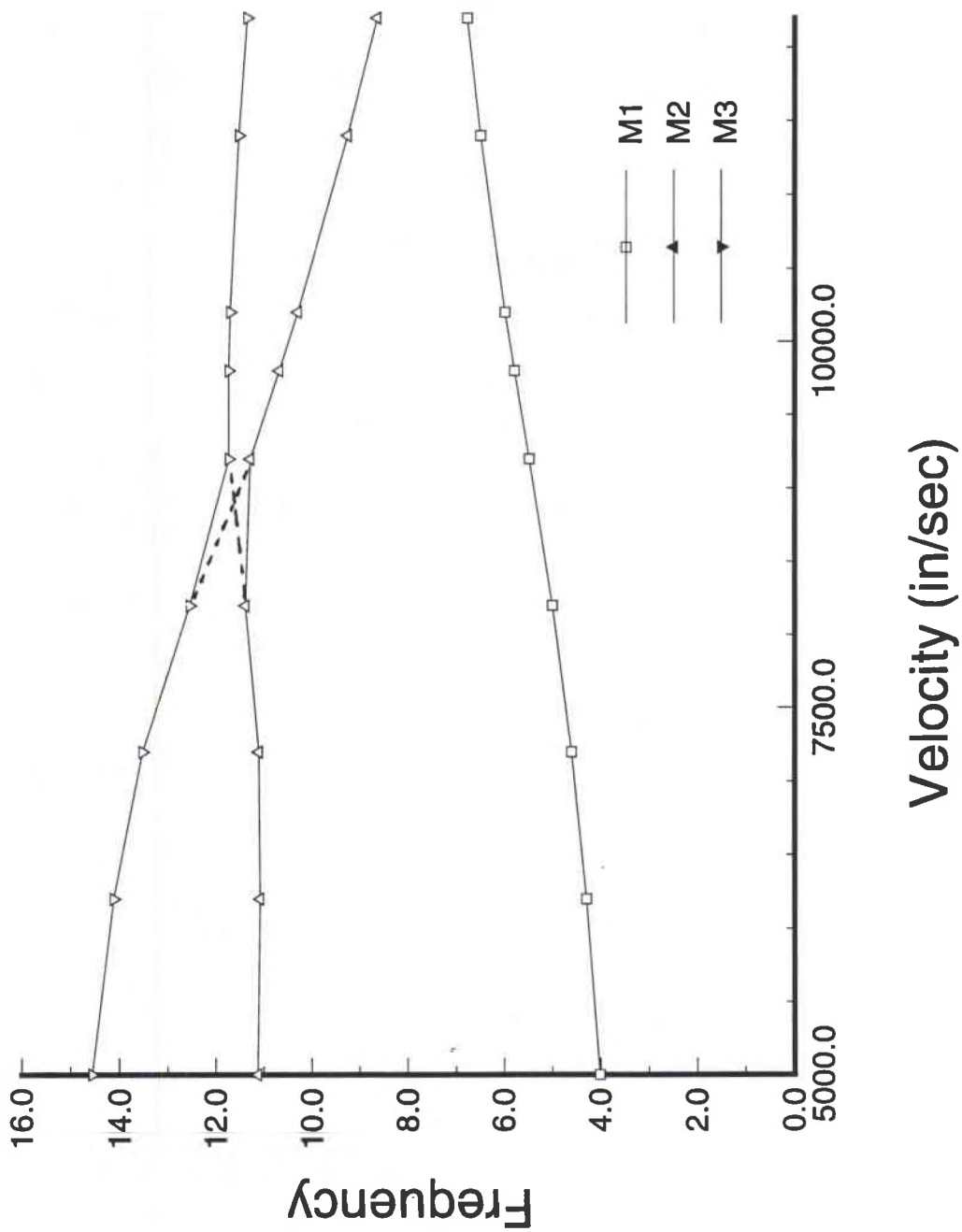


**Figure 11** - V-ω Plot for Wing

## 4.2 Determining Structural Parameters

An aeroelastically scaled model was designed to model the flutter characteristics of the low aspect ratio fighter wing described above. The scale factors were determined without a specific wind tunnel in mind. It was assumed that the geometric scale factor was 1/10. The velocity and density ratios were both assumed to be unity. Thus, we have a 1/10 scale model which will be run in a wind tunnel at Mach .75 with sea level air density. The scale factors are presented in Table 3.

Table 3
Wing Model Scale Factors

| | |
|---|---|
| Length | 1/10 |
| Stiffness | 1/10 |
| Frequency | 10 |
| Mass | 1/1000 |

A subset of grid points from the full scale finite element model was used to develop a finite element representation for the scale model. The assumptions was made earlier that the model structure would be a collection of constant cross section beams which run between the geometrically scaled grid point locations from the full scale wing. There is no guarantee that any chosen model geometry can reproduce the desired stiffness and mass properties. The more elements which are present in the model, the more design variables are created. Each additional design variable adds a dimension to the design space which may be searched and increases the likelihood that the desired stiffness and

modal properties can be duplicated. Initial model representations used very few elements. Initial design studies showed, however, that the desired stiffness properties could not be duplicated. Adding additional elements to the subscale model structure greatly increased the accuracy with which the desired stiffness properties could be matched. The resulting finite element representation of the beam lattice model structure is presented in Figure 12. It is this model which was used for the studies presented here.

It should be noted that the beam lattice structure for the subscale model was chosen for ease of manufacture. The methods presented here are general and may be applied to any type of structure which can be accurately described with a finite element model.

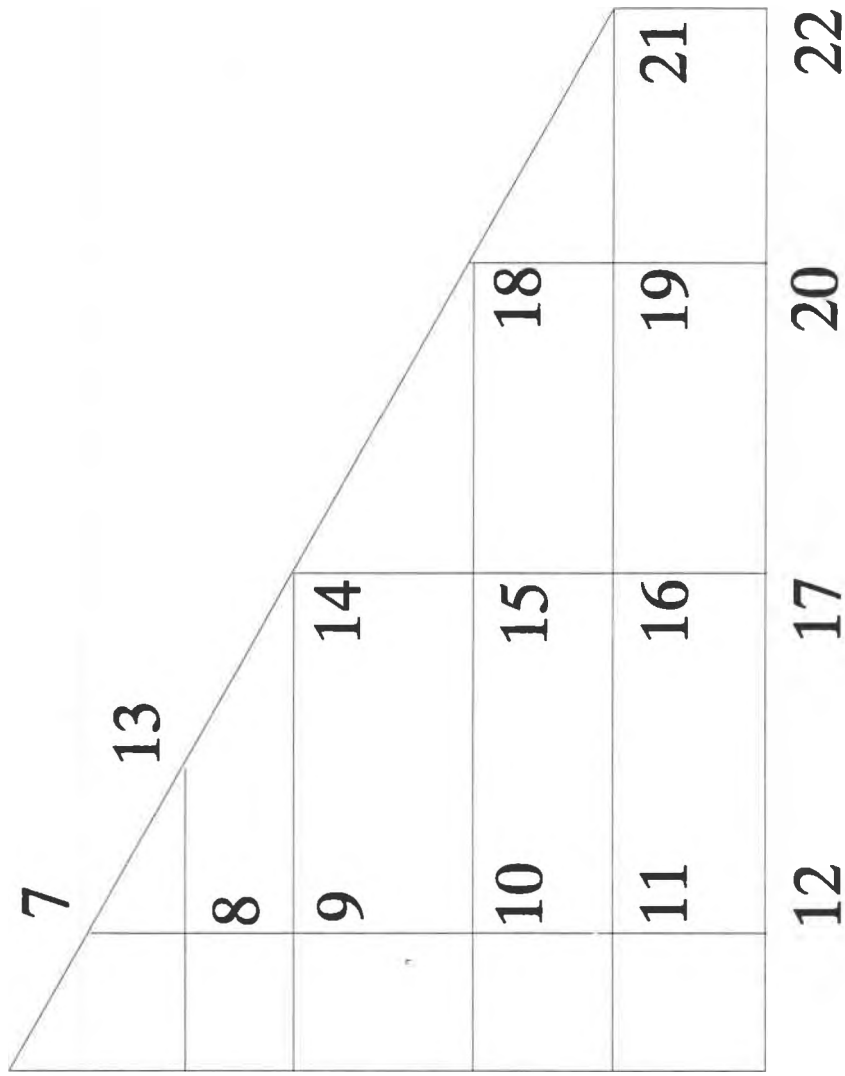


**Figure 12** - Finite Element Representation of Scaled Model

### 4.2.1 Stiffness Design

The first step in the design process for the structure is to determine the element cross-sections such that the stiffness distribution of the model matches the scaled stiffness distribution of the full scale wing. As described above, elements of the flexibility matrix are used to form an objective function, constraints or both. To match the stiffness characteristics exactly, every element of the flexibility matrix would be needed. To do this, though, would result in an extremely large and possibly overconstrained problem. It has been shown that using the columns of the flexibility matrix corresponding to a small number of points can result in a design which has the correct stiffness characteristics[59-61].

Four columns of the flexibility matrix have been chosen to be used in designing the stiffness scaled model. They correspond to vertical displacements at points 14, 17, 21 and 22. These points are respectively mid span leading edge, mid span trailing edge, tip leading edge and tip trailing edge points. The model flexibility coefficients are greater by a factor of 10 than the full scale wing coefficients. This is due to the stiffness scaling relationship presented in equations 11 and 12.

The desired displacements of the stiffness scaled model due to a unit vertical load at point 14 are presented in Figure 13. The desired displacements of the stiffness scaled model due to a unit vertical load at point 17 are presented in Figure 14. The desired

displacements of the stiffness scaled model due to a unit vertical load at point 21 are presented in Figure 15. Finally, The desired displacements of the stiffness scaled model due to a unit vertical load at point 22 are given in Figure 16.

Initially, all four load conditions were used for the stiffness design of wing model 1. An initial design was chosen without using any calculations, since one goal was to allow an essentially arbitrary initial design. The error function for the initial design was approximately 25.6. The scaling factor, k, was chosen to be $10^4$ and was unchanged for all remaining calculations. Aluminum was originally chosen for the material, but preliminary runs showed that some of the element sizes were too large to be practical. Thus, steel was used for the remainder of the design effort. The initial design is given in Table 4.

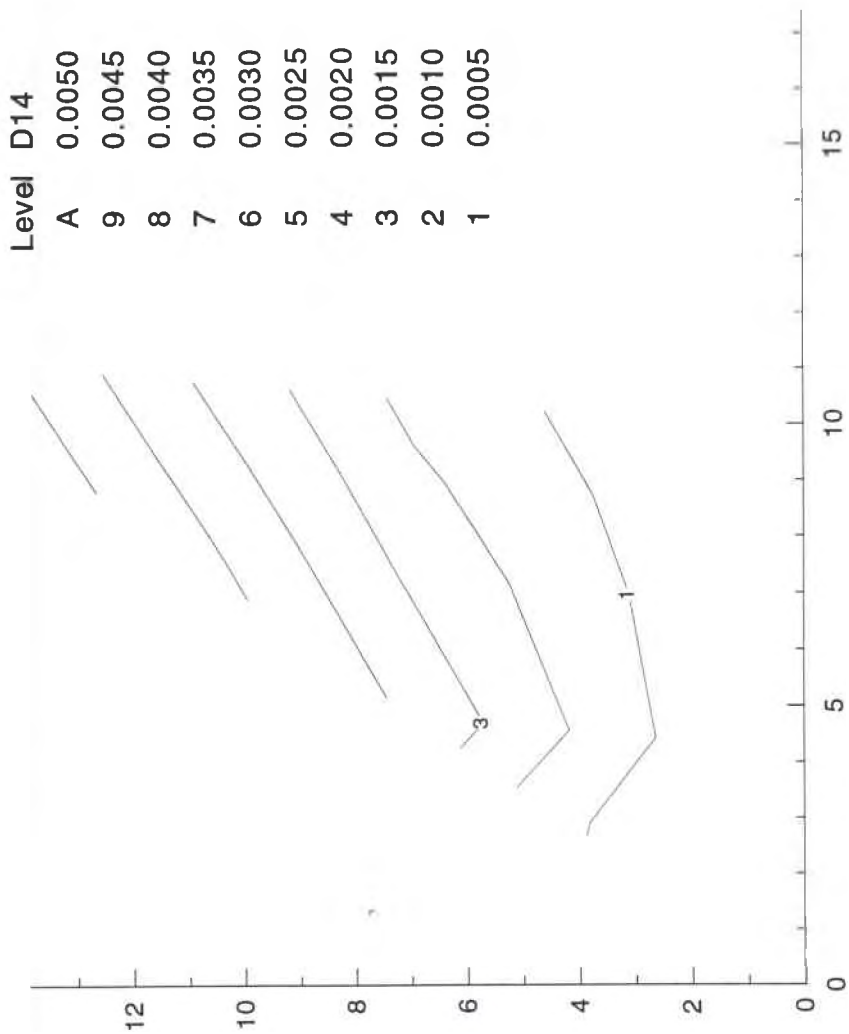


**Figure 13** - Desired Model Displacements Due to A Unit Load at Point 14

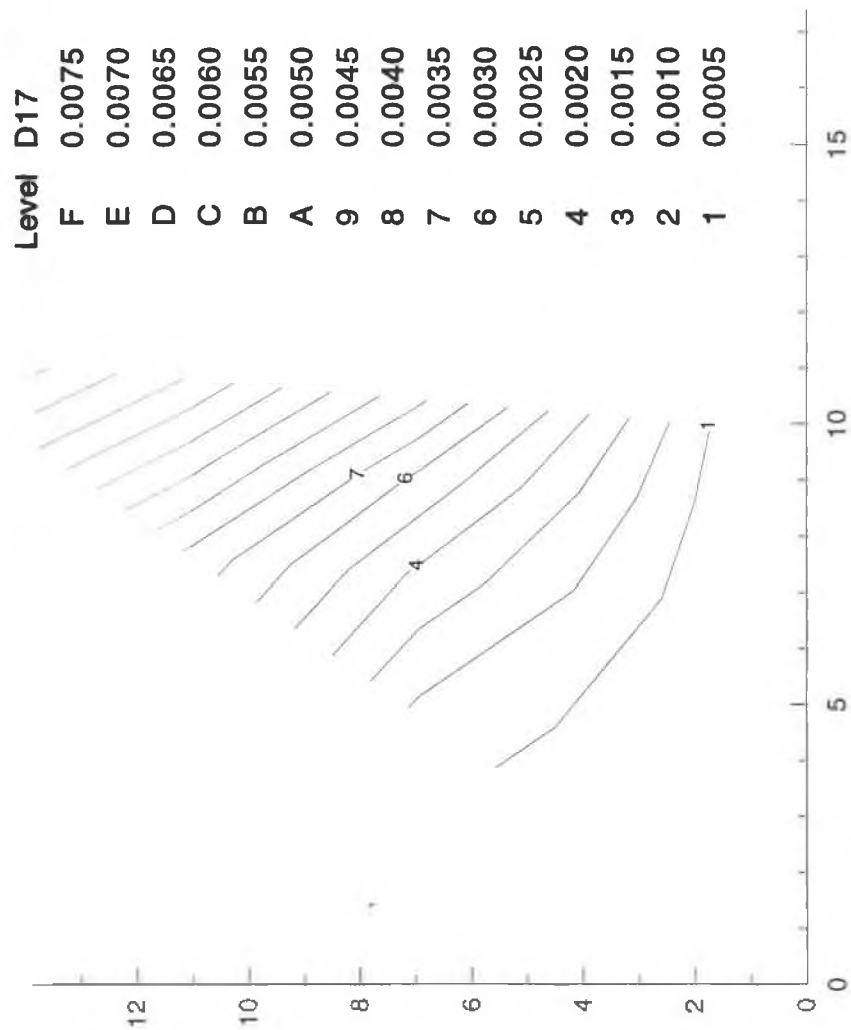


**Figure 14** - Desired Model Displacements Due To A Unit Load At Point 17

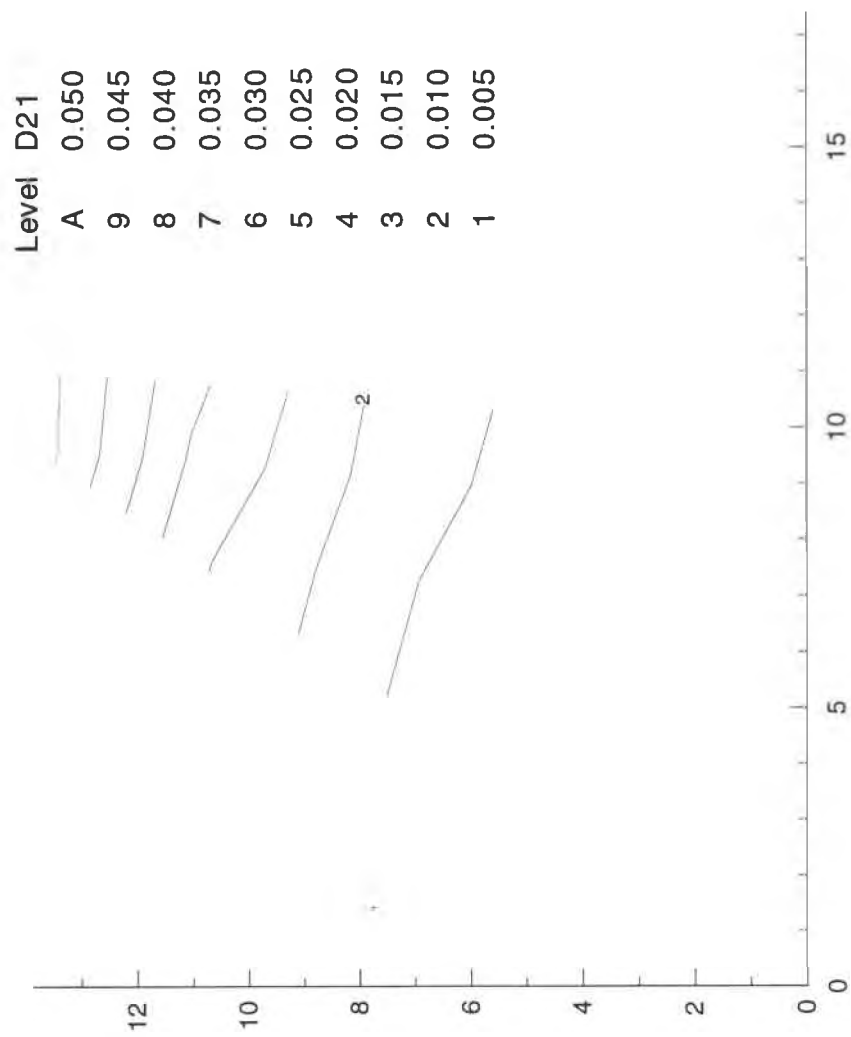


**Figure 15** - Desired Model Displacements Due To A Unit Load at Point 21

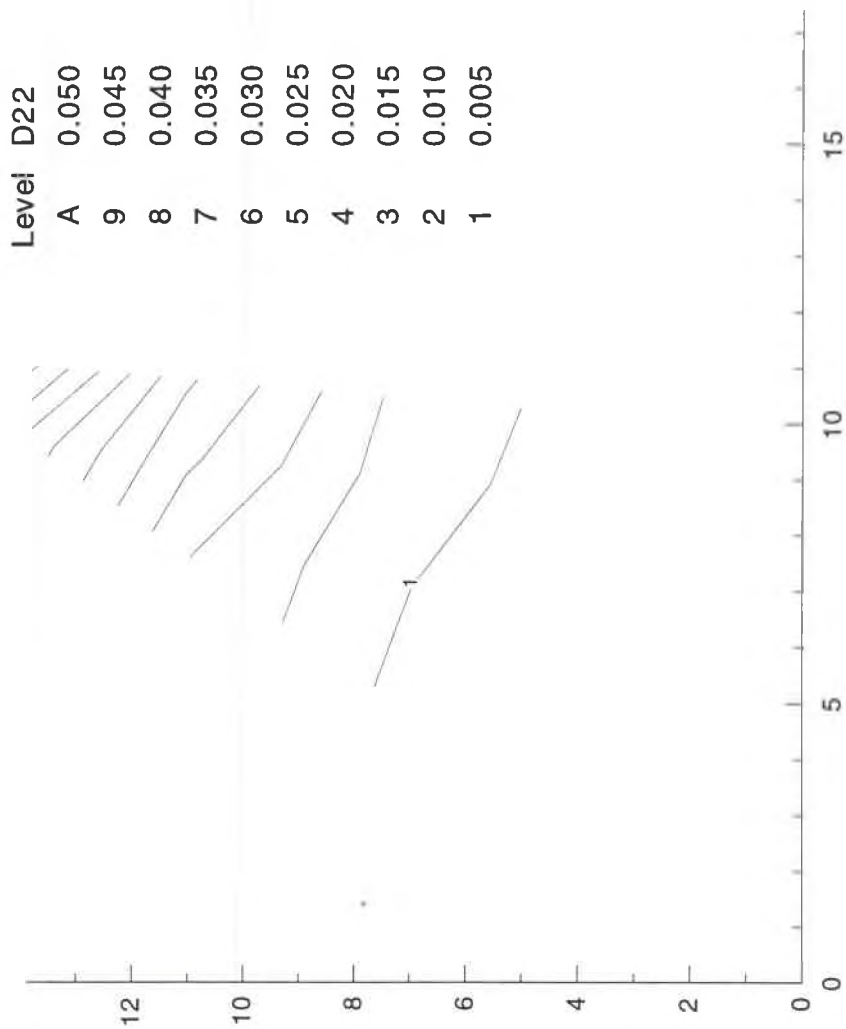


**Figure 16** - Desired Model Displacements Due To A Unit Load At Point 22

Table 4
Initial Design For Wing Model

| Beam | Width (b) | Height (h) |
|---|---|---|
| 1 | .200 | .52 |
| 2 | .200 | .57 |
| 3 | .200 | .56 |
| 4 | .200 | .46 |
| 5 | .200 | .37 |
| 6 | .200 | .27 |
| 7 | .200 | .52 |
| 8 | .200 | .56 |
| 9 | .200 | .46 |
| 10 | .200 | .37 |
| 11 | .200 | .27 |
| 12 | .200 | .43 |
| 13 | .200 | .43 |
| 14 | .200 | .35 |
| 15 | .200 | .35 |
| 16 | .200 | .38 |
| 17 | .200 | .31 |
| 18 | .200 | .22 |
| 19 | .200 | .35 |
| 20 | .200 | .31 |
| 21 | .200 | .22 |
| 22 | .200 | .22 |
| 23 | .200 | .22 |
| 24 | .200 | .24 |
| 25 | .200 | .18 |
| 26 | .150 | .22 |
| 27 | .150 | .18 |
| 28 | .150 | .14 |
| 29 | .150 | .14 |
| 30 | .150 | .14 |
| 31 | .150 | .14 |

#### 4.2.1.1 Comparison Of Methods

For the first four strategies, initial convergence was fast. It slowed considerably, however, as an optimal design was approached. From the initial design, it was typical for the error function to be lowered by an order of magnitude in a few iterations. Lowering the error function from 2 or 3 to an acceptable final value (something on the order of .05) often took dozens more iterations. This combined with the fact that ADS does not stop until it satisfies its own termination criteria meant that the optimization process was not a fast one. This limitation was thought to be acceptable since the task at hand is not a production task, but one which crops up fairly infrequently. In such a case, getting the best possible answer is more important than getting an acceptable answer quickly. The five different design strategies were described earlier. For clarity, they are presented in Table 5.

Table 5
Stiffness Design Methods

| Strategy | Method | Objective Function | Constraints |
|---|---|---|---|
| 1 | unconstrained minimization | displacement error function | none |
| 2 | modified feasible directions | mass | displacements |
| 3 | exterior penalty function | mass | displacements squared |
| 4 | exterior penalty function | displacement error function | displacements squared |
| 5 | compound scaling | displacement error function | displacements |

At this point in the discussion, it is customary to plot the objective function vs the number of iterations. These plots are omitted here because of problem in defining an iteration. The optimization methods used in approaches 1-4 require an analysis for each design cycle and a gradient calculation only periodically. The compound scaling routine requires an analysis and a gradient calculation for each design cycle.

Method 1 produced good results as measured by the final value of the objective function, but had extreme problems satisfying the ADS exit criteria. The final objective function was .0883. The initial convergence was quick; the objective function was reduced from 25.9 to .094 after 1 gradient calculation and 5 analyses. The convergence after this point, however, was negligible. The final design was reached after 570 analyses and 37 gradient calculations.

A notable feature of the final design was that many of the design variables were unchanged from the initial design. This was due to the fact that the only design variables which were modified were the one which corresponded to the largest terms in the objective function gradient. There were no constraint surfaces to bump into, so if a design variable had little effect on the objective function, it was changed very little.

Methods 2 and 3 were developed to evaluate optimization strategies used in MSC NASTRAN and ASTROS. Both programs use mass as the objective function and both allow displacement constraints. Mass is not the desired objective function, so the assumption must be made that the lightest structure is the most flexible one. If this were true, the lightest structure would exactly satisfy a complete set of maximum displacement constraints. In the course of testing methods 2 and 3, it became clear that the fewer the number of load paths, the more reliable this assumption became. As the number of possible load paths increased, instances in which this assumption was not completely adequate became more common.

A basic problem with methods 2 and 3 is that the quantity being minimized is not the one which has been defined as determining the optimal design. In many cases during the testing of methods 2 and 3, the final (lowest mass) design had a larger value for the error function than did some of the intermediate designs. In spite of the problems discussed above, the final design produced using method 2 had a very low total error measurement of .0016. Reaching this result took 371 function evaluations and 29 gradient evaluations.

Method 3 yielded a final error function .of .0307 and reached this result in 473 function evaluations and 88 gradient evaluations.

One benefit of using mass as an objective function is that it drives the element widths to the lowest possible values, lowering the structural mass. Small widths help ensure that the length to width ratios of the elements are high enough that they can still be considered beams. Reducing structural mass is very important to model designers who often have problems meeting the weight requirement which result from the scaling laws.

The results of method 4 are discussed in the next section. The behavior of method 5 differed qualitatively from the that of the other four methods. The compound scaling algorithm was evaluated here for two reasons. The first is that, for sample problems, it has been shown to be able to find the feasible region in one or two iterations. The second is that in an earlier work[60] on wind tunnel model design, a developmental version of the compound scaling algorithm was able to find the intersection of over sixty constraints very consistently while Modified Feasible Directions wasn't able to find the intersection of more than 25.

The version of compound scaling available at the time of this work was less successful, though. It was typical for the other four methods to converge very rapidly for the first 10-15 design cycles and then converge very slowly after that. Method five converged slowly throughout the run and did not produce a usable design. It should be noted that

the algorithm used here was still under development and that previous versions of compound scaling[63,64] worked very well.

The compound scaling method used here searches for the boundary of the feasible region and moves the design there in such a way that the objective function is reduced. When one or more of the constraints becomes active, the optimizer 'pushes off' from the boundary back into the feasible region and searches for the boundary again. This action produced two effects which made convergence poor. The first was that it was unusual for more than a few constraints to be active at once; a good design has many, hopefully all, of the constraints exactly satisfied. The second problem was that when the optimizer pushed off from the boundary, the objective function increased dramatically. It was typical for the error function to go from a value of 3 or 4 when one of the constraints was satisfied to 50 or 60 after it pushed off. The result was that the lowest error function obtainable with the compound scaling method was approximately 2.5, several orders of magnitude higher than that obtainable with the other methods.

#### 4.2.1.2 Final Stiffness Design

Overall, method 4 appeared to consistently yield the lowest final error function, so it was used to design the test structure. Method 4 was used in an iterative fashion to ensure a

producible design resulted. A preliminary design was produced using the initial design presented in Table 4. All beam heights were set at the maximum allowed by the aerodynamic envelope formed by the upper and lower surfaces of the wing. The final error function was .0038. This was acceptable, however many of the element widths were too small to be easily machined. The preliminary design was modified so that no element widths were smaller than .050 inches.

Wherever element widths were increased, the element height was decreased so that the area moment of inertia remained unchanged. This was done so that the bending stiffness of the element normal to the plane of the wing was not altered and a complete redesign would not be required. After the necessary modifications were made, the result was used as the starting point for another design cycle using method 4. This was done to ensure that the modifications to the element sizes did not adversely effect the error function.

This second design cycle also resulted in some elements which were too small to be machined, so the element widths were increased where necessary. Again element heights were decreased so that area moments of inertia remained unchanged. This time, modifications were minor enough that another design cycle was not necessary. The final design is given in Table 6.

While not used for the design of the test structure in this work. Method 1 was used in subsequent model design efforts to quickly move an arbitrary starting design to a point

close to the optimum. This design was then used as the starting design for method 4, which converged more slowly, but consistently produced better designs.

It is necessary at this point to make some kind of comparison between the stiffness characteristics of the final design and the desired stiffness characteristics. This was done by preparing contour plots of the differences between calculated and desired displacements due to unit loads at various grid points on the structure.

Initially, the four points previously identified (14, 17, 21 and 22) were used to make the stiffness design. Figure 17 presents differences in displacements over the structure due to a unit load at grid point 14. Figure 18 presents differences over the structure due to a unit load at grid point 17.

It should be noted that, since there are no external loads outboard of the grid points at which the loads were applied, there should be no spanwise curvature of the structure there either. Thus, the extent to which displacements outboard of an applied load are matched is a measure of how well the displacement slopes on the inboard section of the wing are matched. Figures 19 and 20 present differences in displacements due to loads at points 21 and 22.

One conclusion from the end of Section II was that the new method should be able to accurately predict the response to loading conditions not used to design the structure.

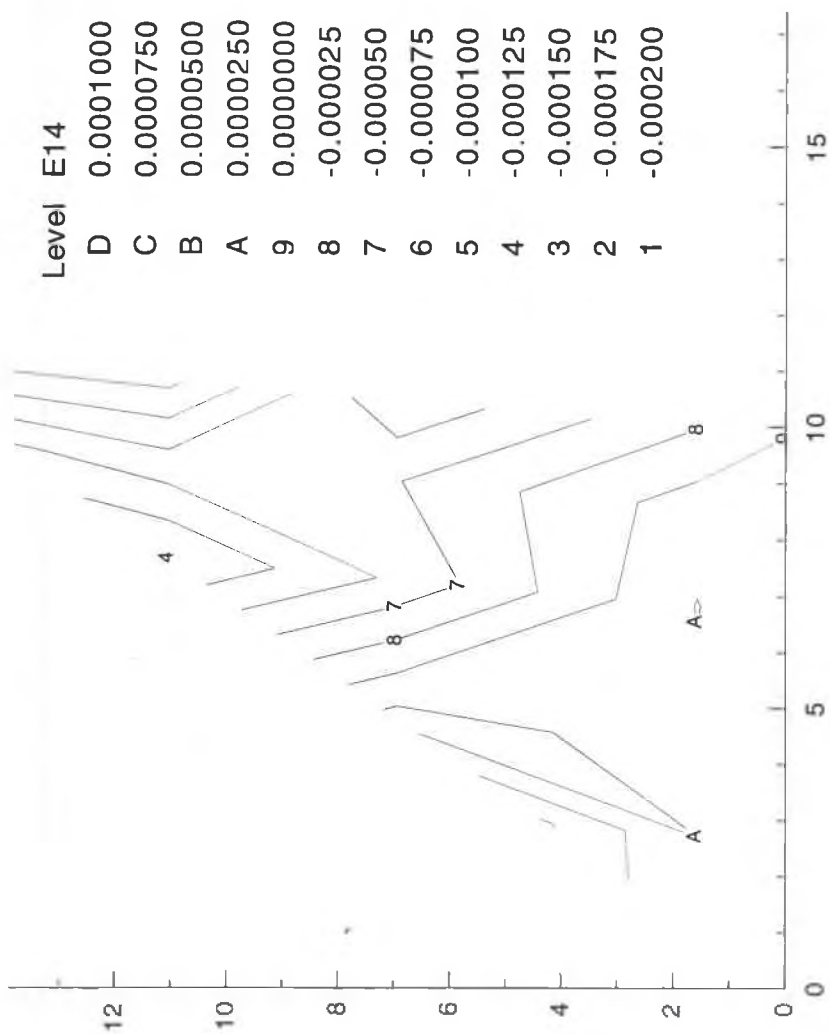


**Figure 17** - Difference Between Desired and Predicted Displacements Due to A Unit Load At Point 14

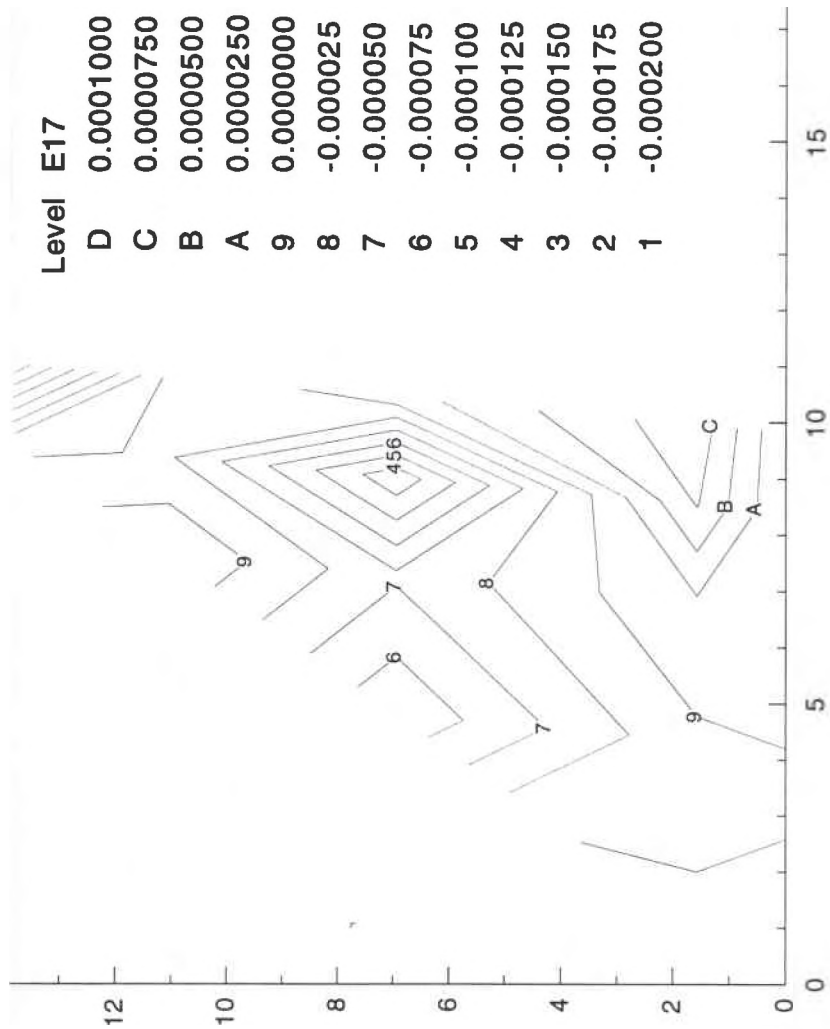


**Figure 18** - Difference Between Desired And Predicted Displacements Due to A Unit Load At Point 17

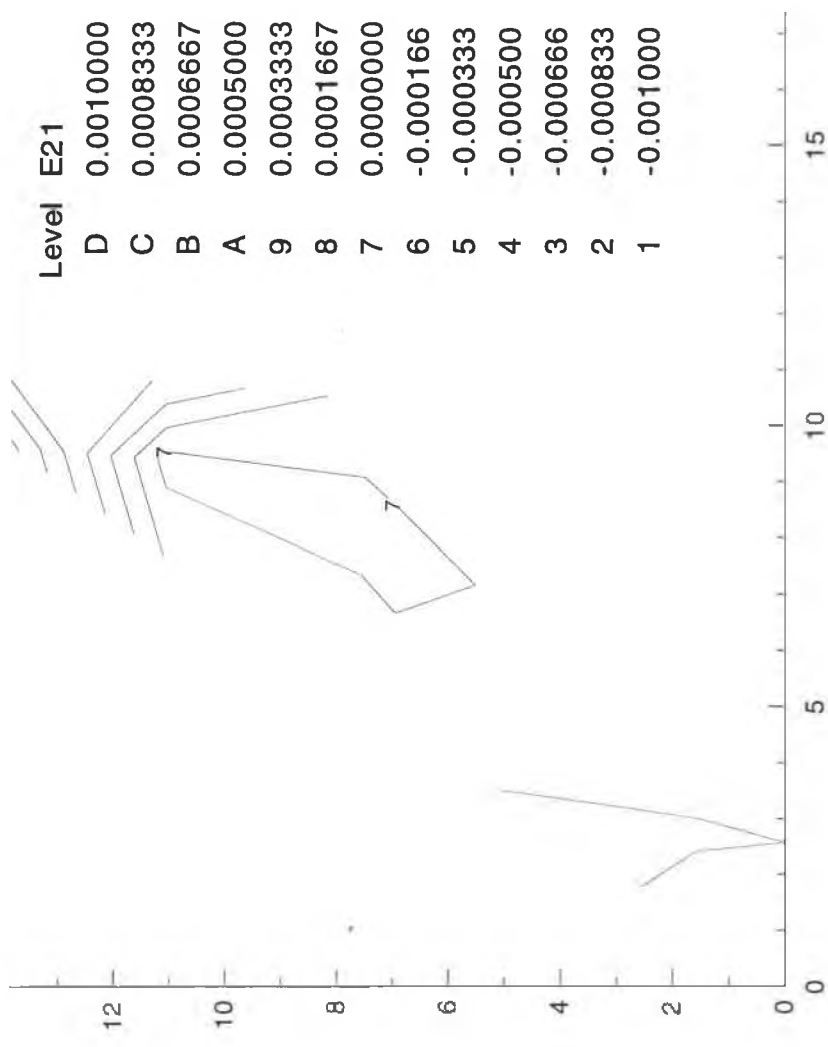


**Figure 19**- Difference Between Desired and Predicted Displacements Due To A Unit Load At Point 21

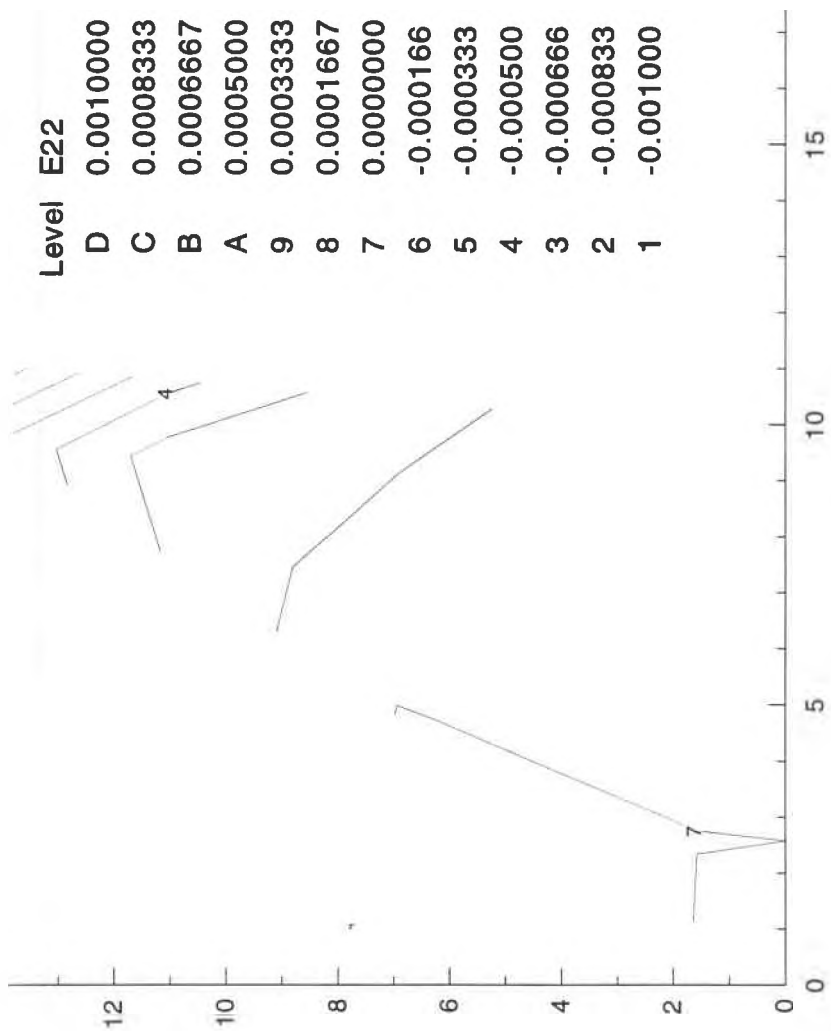


**Figure 20** - Difference Between Predicted And Desired Displacements Due To A Unit Load At Point 22

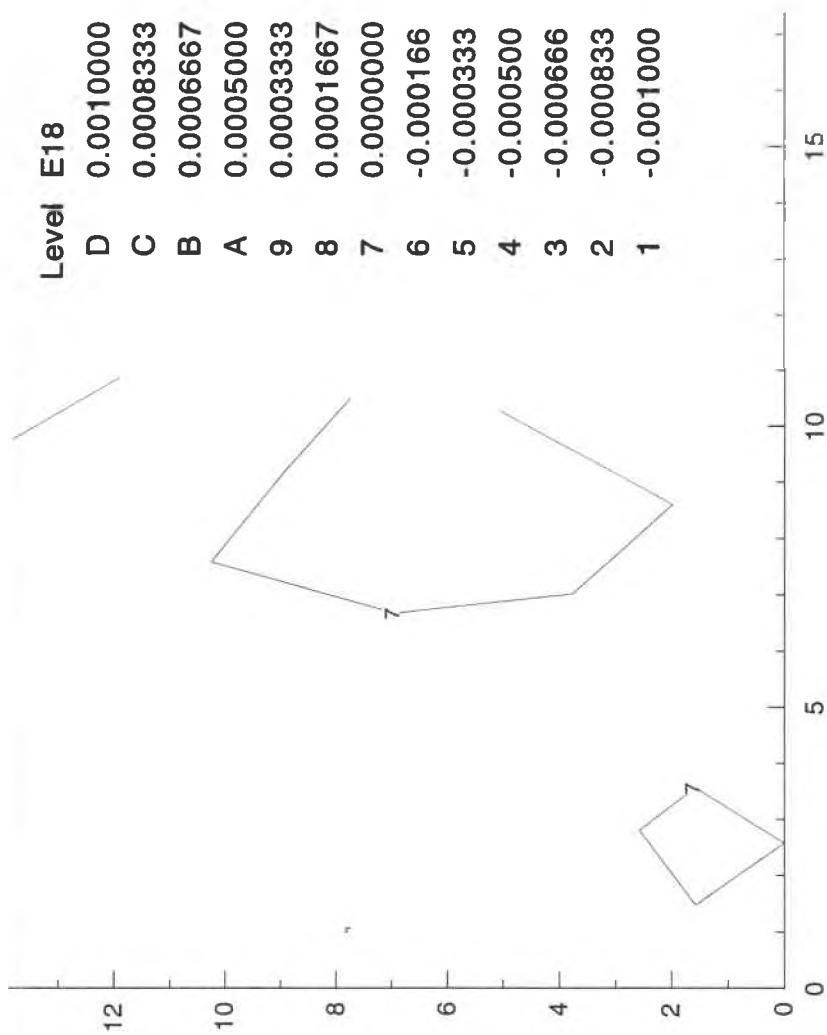


**Figure 21** - Difference Between Desired and Predicted Displacements Due To A Unit Load at Point 18

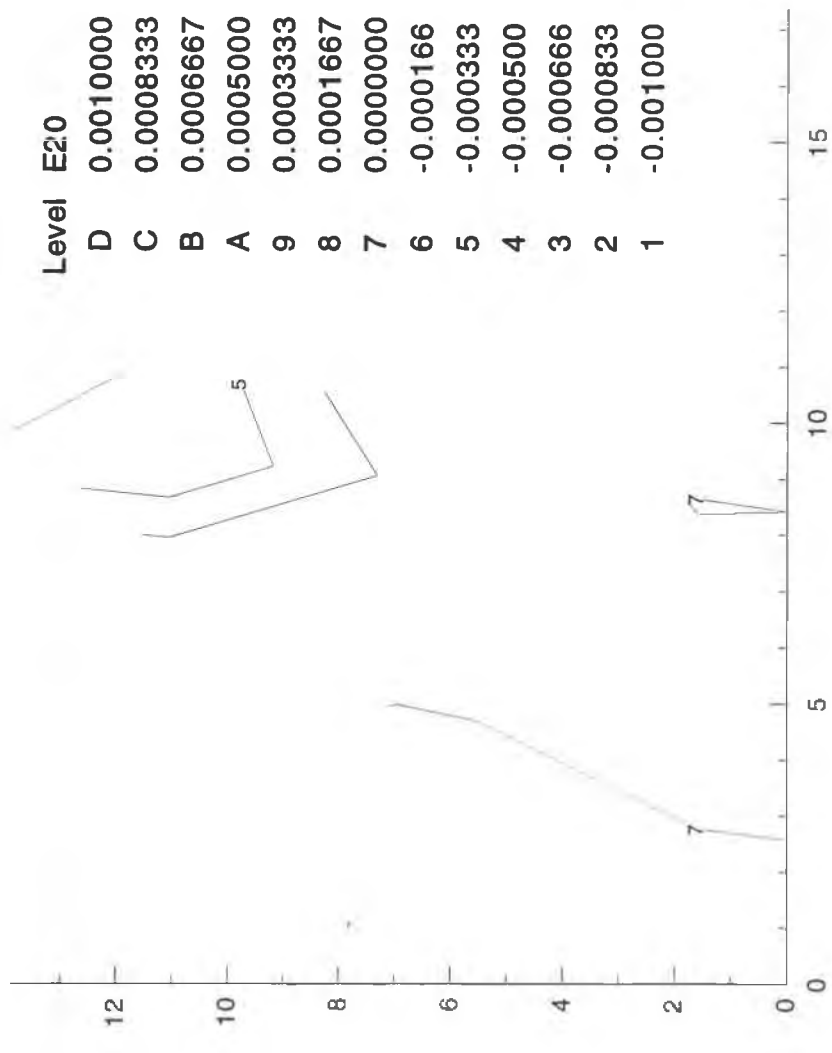


**Figure 22** - Difference Between Desired And Predicted Displacements Due To A Unit Load At Point 20

Loads at points 18 and 20 were not used in designing the model. It can be seen from the surface plots presented in Figures 21 and 22 that the agreement between desired and calculated displacements is very good. This is taken as an indication that a sufficient number of unit loads were applied to result in a correct overall stiffness of the structure.

Table 6

Final Element Sizes For Stiffness Design of Wing Model

| Element | Width | Height |
|---|---|---|
| 1 | .500 | .520 |
| 2 | .077 | .520 |
| 3 | .050 | .258 |
| 4 | .062 | .460 |
| 5 | .119 | .370 |
| 6 | .118 | .270 |
| 7 | .452 | .311 |
| 8 | .050 | .530 |
| 9 | .125 | .269 |
| 10 | .050 | .251 |
| 11 | .493 | .270 |
| 12 | .050 | .325 |
| 13 | .135 | .430 |
| 14 | .086 | .350 |
| 15 | .123 | .350 |
| 16 | .141 | .380 |
| 17 | .182 | .310 |
| 18 | .211 | .220 |
| 19 | .213 | .350 |
| 20 | .050 | .215 |
| 21 | .486 | .220 |
| 22 | .103 | .220 |
| 23 | .068 | .220 |
| 24 | .089 | .240 |
| 25 | .076 | .150 |
| 26 | .178 | .220 |
| 27 | .162 | .175 |
| 28 | .050 | .080 |
| 29 | .124 | .140 |
| 30 | .084 | .140 |
| 31 | .050 | .069 |

4.2.2 Mass Design

During the experimental effort to validate the analytical results, frequencies and mode shapes of the bare structure will be compared to the predicted values. They will be used as a measure of how well the test article duplicates the mathematical model of the structure. The first three predicted natural frequencies of the bare structure are presented in Table 7 along with the scaled natural frequencies from the full scale wing.

Table 7
Predicted Natural Frequencies of Model Before Mass Balancing

| Mode | Frequency (hz) | Desired Frequency (Hz) |
|---|---|---|
| 1 | 76.42 | 35.8 |
| 2 | 216.7 | 113.5 |
| 3 | 246.7 | 149.6 |

It can be seen that the frequencies of the model structure before mass balancing are significantly higher than the desired values. This, along with lower than desired final weight indicate that there is room to mass balance the wing model. The first three normal mode shapes for the structure before mass balancing are presented in Figures 23, 24 and 25.

The element sizes have been determined such that the structure has the desired stiffness characteristics. Now the values of the concentrated masses must be determined so that

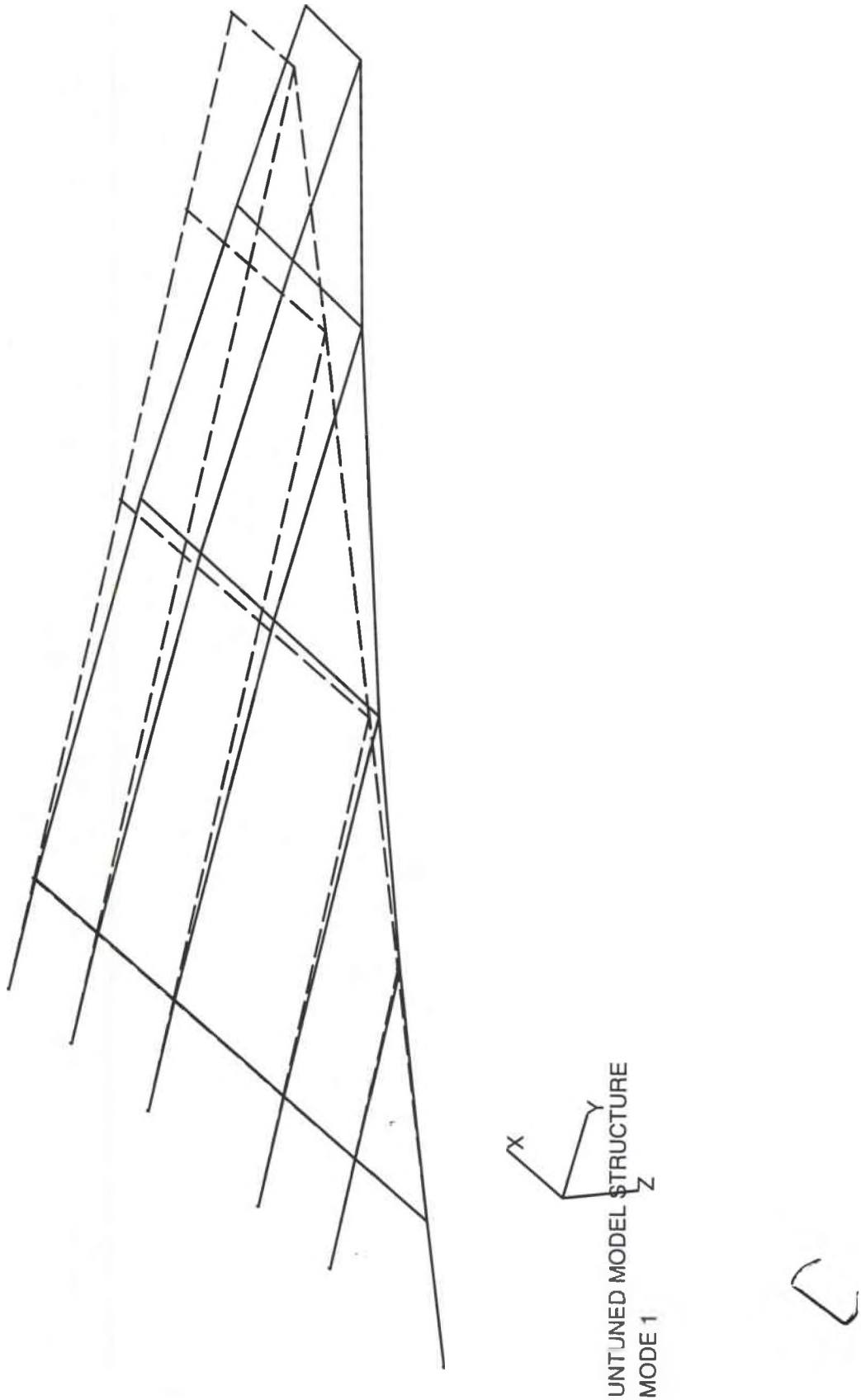


**Figure 23** - First Mode Shape of Model Before Mass Balancing

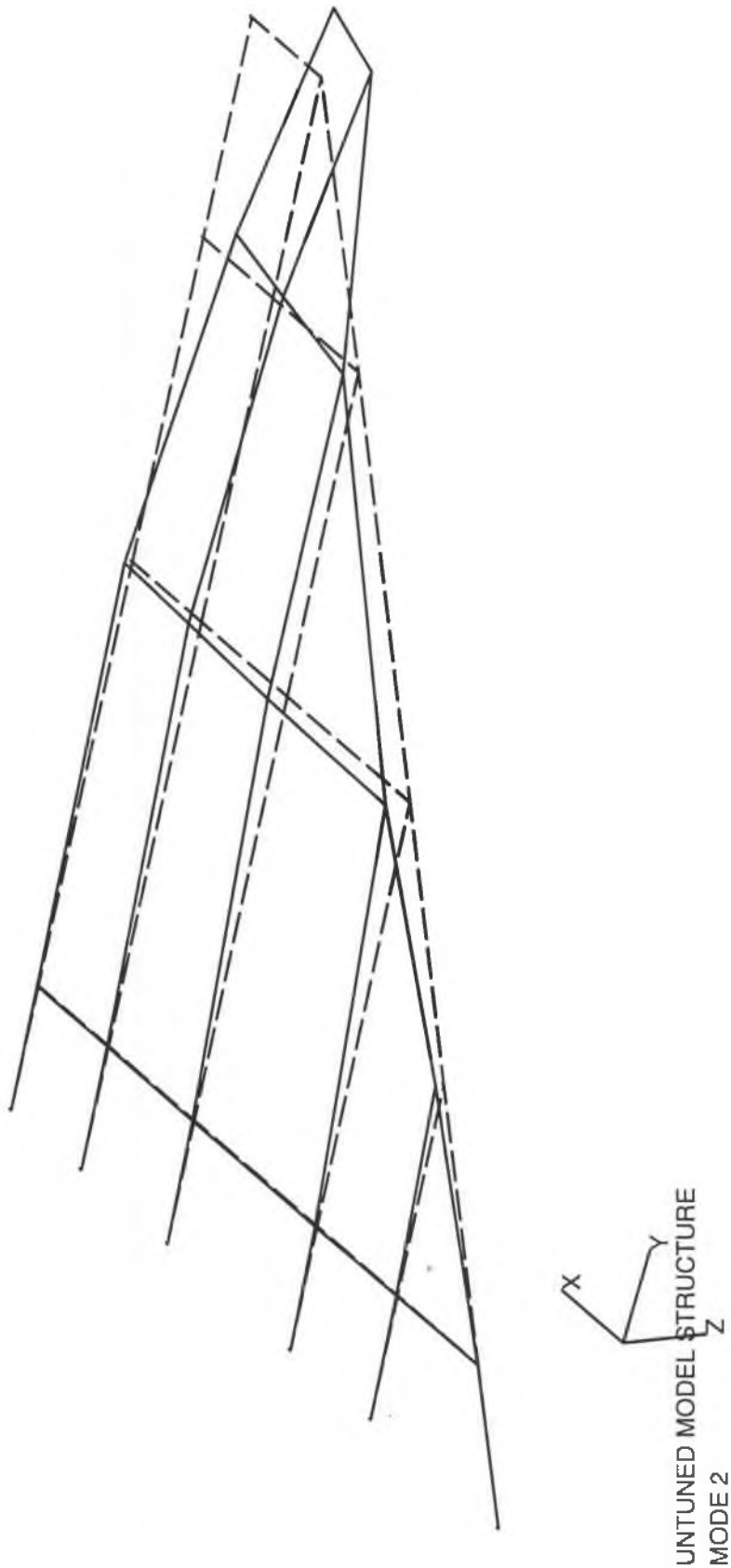


**Figure 24** - Second Mode Shape of Model Before Mass Balancing

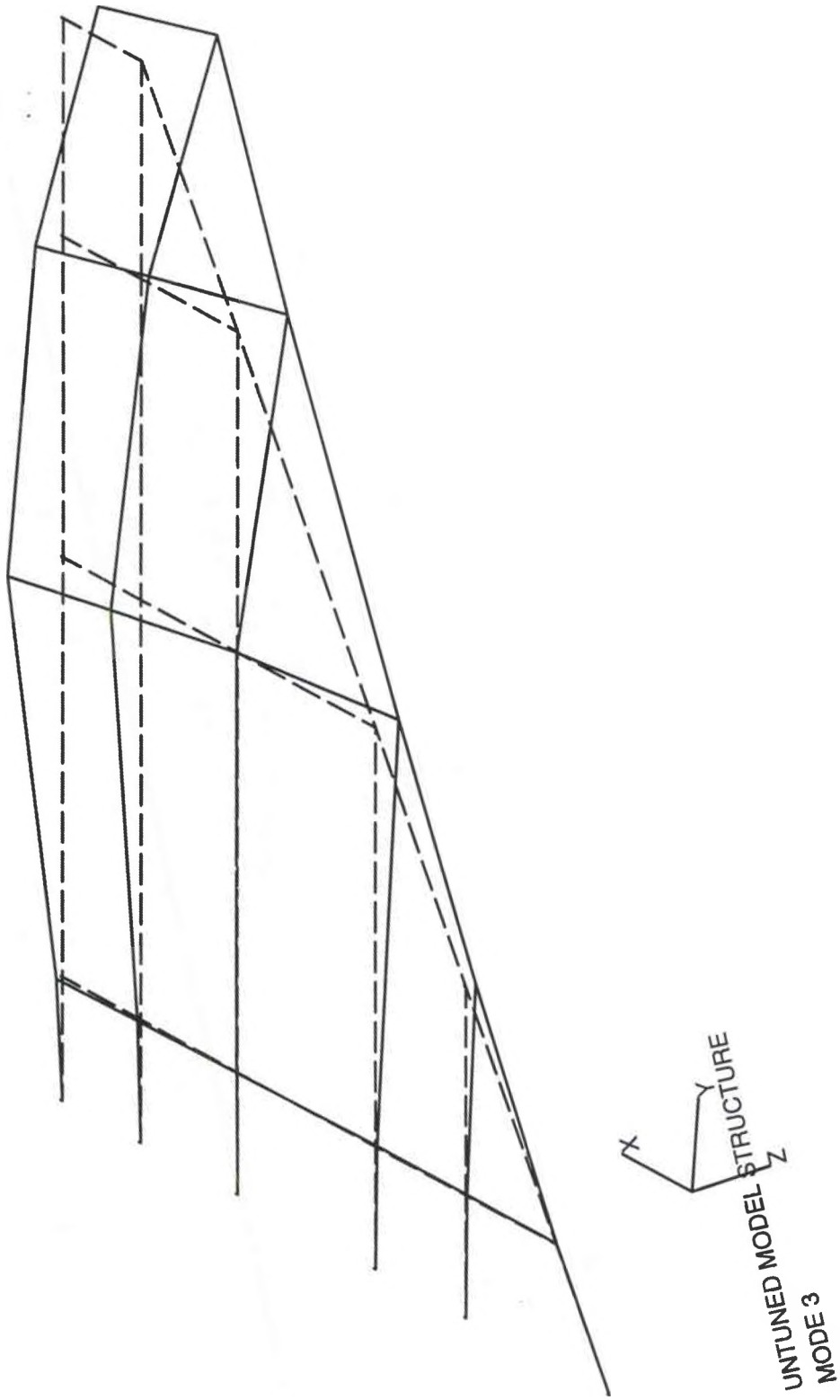


**Figure 25** - Third Mode Shape of Model Before Mass Balancing

the resulting system has the desired frequencies and mode shapes. Two methods were evaluated for sizing the concentrated masses. The methods are outlined in Table 8.

Table 8
Mass Design Methods

| Method | Objective | Constraints | Optimizer |
|---|---|---|---|
| 1 | Frequency Error Function | None | Unconstrained Minimization |
| 2 | Mode Shape Error Function | Frequency Squared, Total Mass | Interior Penalty Function |

Design method 1 was found to be unacceptable; it consistently gave designs with the incorrect total mass and with unrealistic mass distributions. The assumption behind method 1 was that, if the stiffness was correct and masses were sized such that frequencies were correct, it should follow that overall mass and mode shapes should be correct. This is true if complete scaled stiffness and modal information is available. Consider the familiar eigenvalue equation

$$[K]\{x\} = \omega^2 [M]\{x\} \tag{40}$$

The mass matrix, [M], can be written as the sum of the initial guess and the correction terms

$$[K]\{x\} = \omega^2 \left( [M] + [\Delta M] \right) \{x\} \tag{41}$$

In the case of complete information, the only unknown term in the previous equation is [ΔM]. The preceding equation can be written as

$$[\Delta M]\{x\} = \frac{1}{\omega^2}[K]\{x\} - [M]\{x\} \quad \textbf{(42)}$$

which forms a system of equations of n equations and $n^2$ unknowns. If all eigenvalues are known and all eigenvectors are known completely and are orthogonal, the unique value of [ΔM] can be determined. These restrictions are unrealistic. Furthermore, even if complete modal information is available, the computed [ΔM] may not be useful. Adding concentrated masses to the structure changes only the diagonal terms of the mass matrix. It would be extremely difficult to place distributed masses on a structure such that off-diagonal terms of the mass matrix were modified. Such would require masses which connected two or more grid points without changing the stiffness of the structure. An alternate approach would require that the effect of the added mass on the stiffness of the structure were accounted for during the stiffness design process. This may be possible if mass and stiffness design were integrated into a single step.

Since, for this work, only the diagonal elements of the mass matrix can be modified, a unique solution to the model design problem is impossible. the necessity of finding an approximate solution suggests that an optimization-based method is required.

In testing the computer program, it became apparent that the frequency error function used as the objective function had many local minima. It was common for the optimizer to hit a local minima fairly quickly and get stuck on a poor design. Furthermore, the method had a tendency to vary the values of a small number of masses on the structure

and leave the remaining ones largely unchanged. It was common for inboard grid points to remain unchanged since deflections were low there and changing them had little effect on the frequencies. One check used to determine whether the optimization process was producing a consistent final design was to start with varying initial designs and compare the final designs. It was found that relatively small changes in the starting design resulted in very large changes in the final design.

The absolute test of whether this mass design method worked was to perform a flutter analysis using the previously determined stiffness design and a mass design from method 1. An initial mass of .001 lb-sec$^2$/in was specified for all masses in the wing. The first three natural frequencies of the resulting design are presented in Table 9 along with the desired frequencies.

Table 9

Natural Frequencies of Model Using Mass Design Method 1

| Mode | Desired Freq (Hz) | Calculated Freq (Hz) |
|---|---|---|
| 1 | 35.8 | 31.48 |
| 2 | 113.5 | 121.7 |
| 3 | 149.6 | 149.9 |

A flutter analysis of the beam lattice model using the element sizes from Table 6 and the masses from Table nn above predicted no flutter points below 1083 ft/sec (roughly the speed of sound at sea level). The object was to find a more robust method than this, so the second method was evaluated.

Design method 2 was more successful. The addition of a total mass constraint had the effect that, as outboard masses were varied to alter the frequencies, the inboard masses had to change to maintain the correct overall mass. Flutter may be thought of as an energy transfer mechanism in which kinetic energy in the flow in converted to kinetic energy in the wing. If the mass of the scaled model is incorrect, correct flutter response would require a change in the kinetic energy of the wing. As an example of this effect, a flutter analysis of the full scale wing was run with the elastic modulus and mass of the material doubled. The ratio of mass to stiffness and, thus, natural frequencies of the wing are unchanged. The resulting flutter velocity, however, is 1074 ft/sec with a corresponding flutter frequency of 5.94 Hz. The flutter speed of the unmodified full scale wing is 820 ft/sec and flutter frequency is 5.81 Hz. While the frequency changed very little (about 2%) the computed flutter velocity increased by 31%.

The convergence was much faster for the mass design problem than for the stiffness design problem. The exit criteria was satisfied after 43 analyses and 8 gradient evaluations. Furthermore, the total mass of the final design matched almost exactly the desired value. The total mass of the final design was .00461 lb-sec$^2$/in and the desired value was .00460 lb-sec$^2$/in (2.97 lb). Desired mass was determined by adding the structural and non-structural masses and multiplying the total by the mass scale factor of 1/1000. Table 10 presents a comparison of the desired vs the calculated frequencies for the passive model with tuning masses added.

Table 10
Summary of Calculated Vs Desired Natural Frequencies

| Mode | Calculated Frequency (hz) | Specified Frequency (hz) | Difference (%) |
|---|---|---|---|
| 1 | 36.883 | 35.810 | 3.0 |
| 2 | 115.35 | 113.525 | 1.6 |
| 3 | 147.41 | 149.62 | -1.5 |

An initial value of .000125 lb-sec$^2$/in was specified for all of the masses on the structure. The final values of the concentrated masses are presented in Table 11. Masses are in slinches (lb - sec$^2$ / in).

Table 11
Concentrated Mass Values of Final Design

| Mass Number | Grid Point | Mass Value |
|---|---|---|
| 1 | 7 | .00009885 |
| 2 | 8 | .00009841 |
| 3 | 9 | .00009768 |
| 4 | 10 | .000100 |
| 5 | 11 | .0001039 |
| 6 | 12 | .0001107 |
| 7 | 13 | .00008297 |
| 8 | 14 | .0001037 |
| 9 | 15 | .0001247 |
| 10 | 16 | .0001515 |
| 11 | 17 | .0001510 |
| 12 | 18 | .0001149 |
| 13 | 19 | .0001274 |
| 14 | 20 | .0001285 |
| 15 | 21 | .0001237 |
| 16 | 22 | .0001215 |

The first three calculated mode shapes are presented in figures 26, 27 and 28. The tuning masses changed the frequencies noticeably, the mode shapes changed very little.

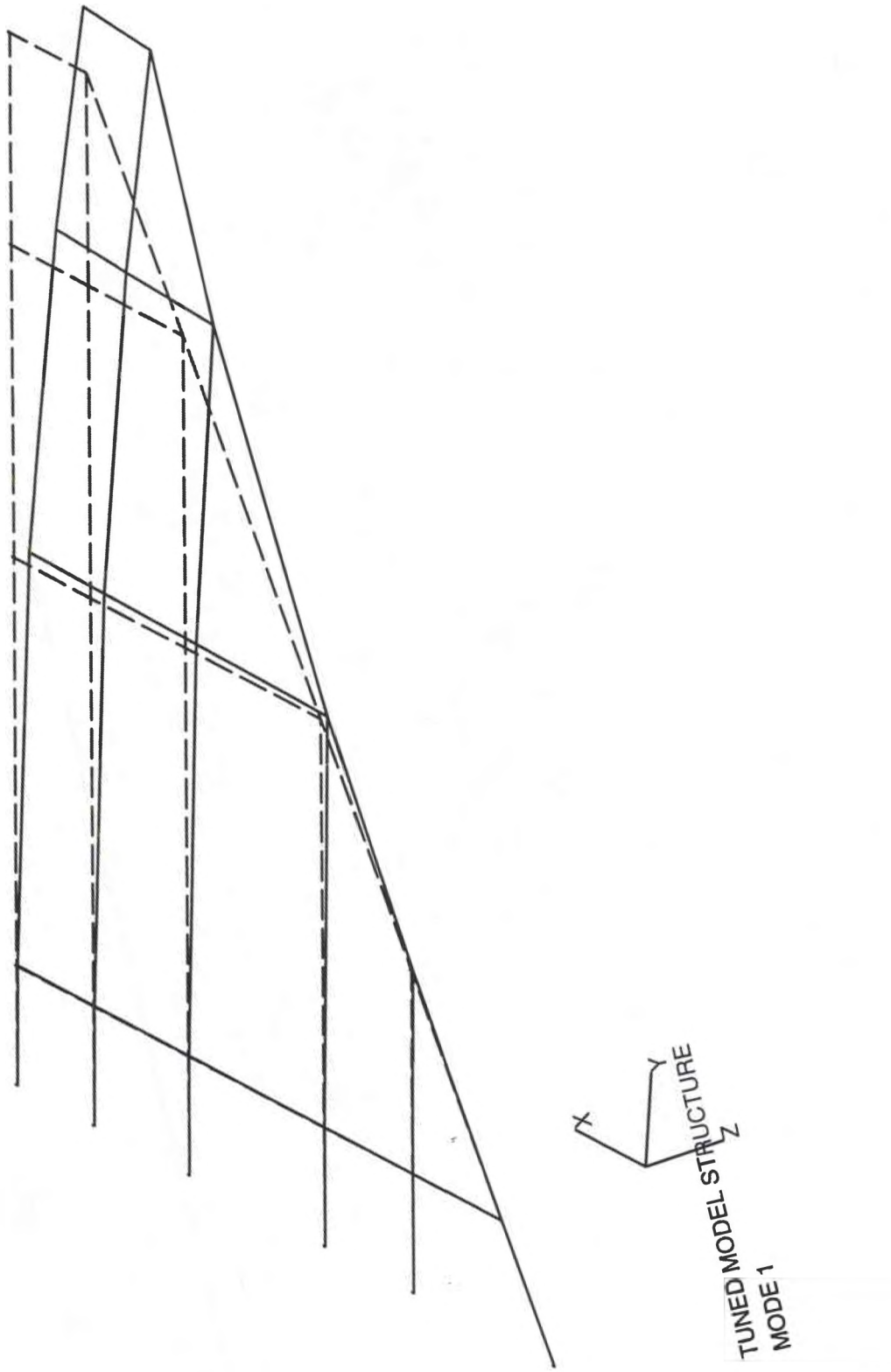


**Figure 26** - First Mode Shape of Wing Model With Concentrated Masses

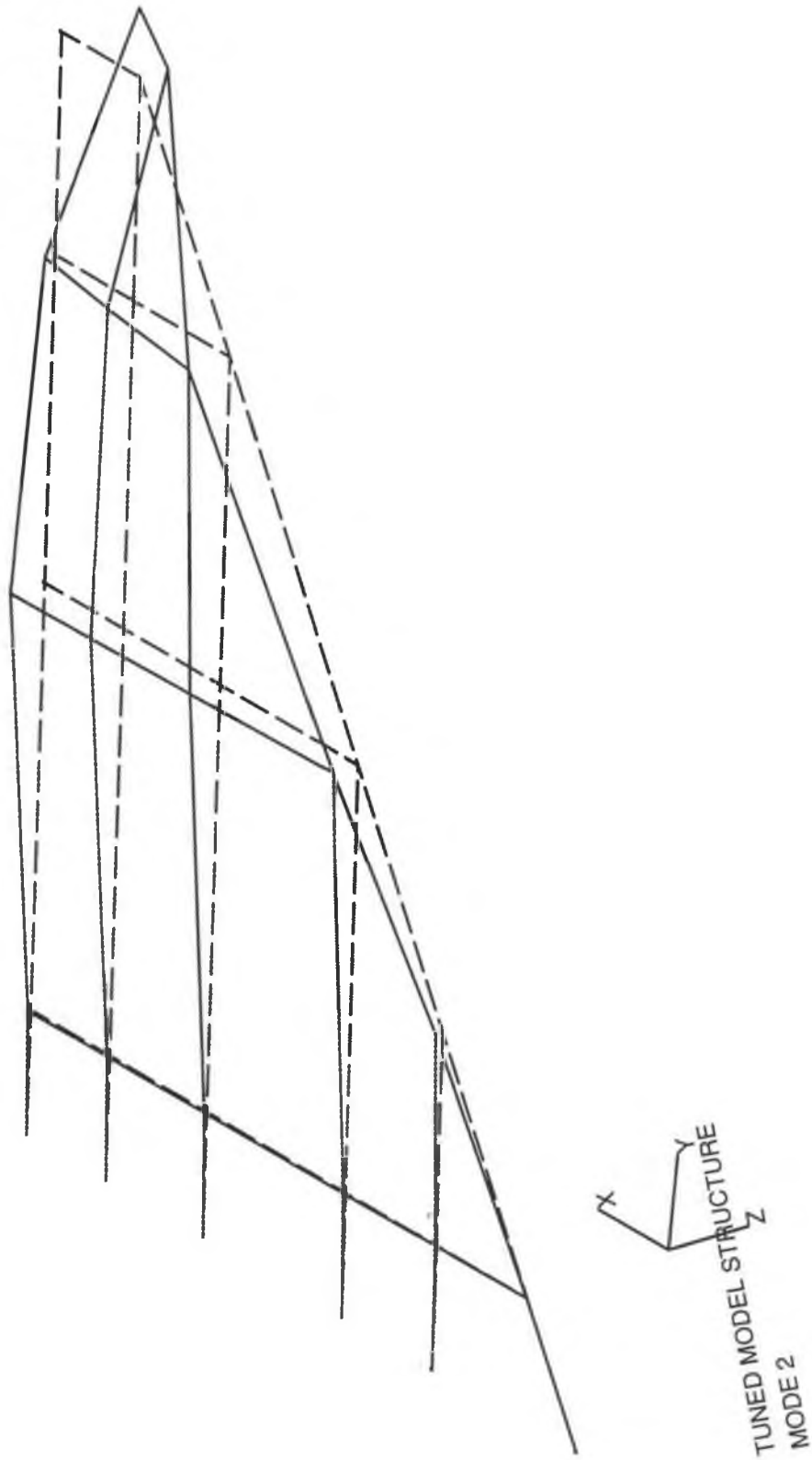


**Figure 27** - Second Mode Shape of Wing Model With Concentrated Masses

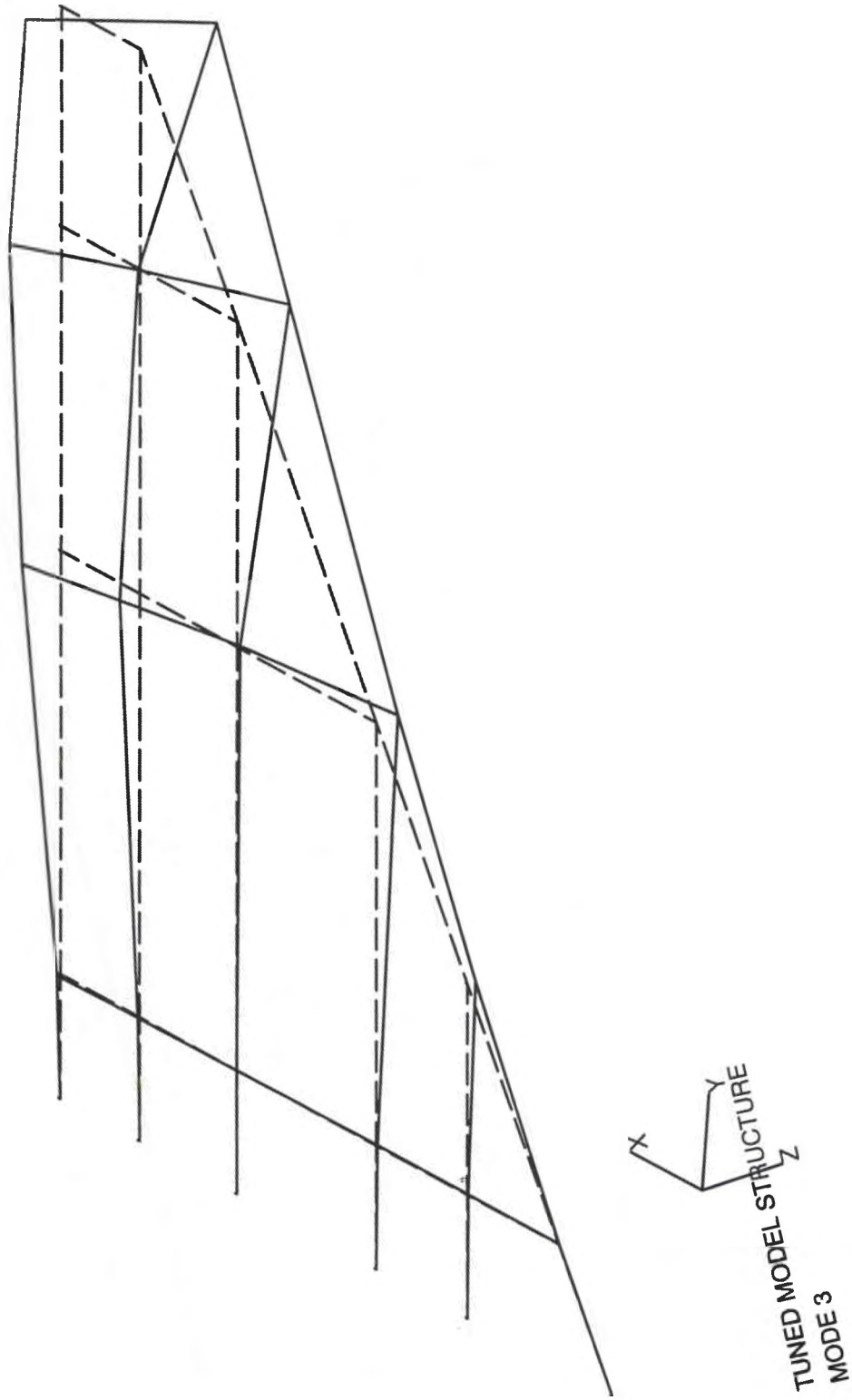


**Figure 28** - Third Mode Shape of Wing Model With Concentrated Masses

### 4.2.3 Flutter Analysis of Wing Model

The true measure of whether a flutter model had been correctly designed is how well its flutter characteristics duplicate those of the full scale wing. Not only must the model have the correct flutter velocity and frequency, the mechanism must also be correct. A flutter analysis was carried out on the final subscale model design (Masses presented in Table 11 and element sizes presented in Table 6). The subscale model analysis used the same Mach number, reduced frequencies and aerodynamic box pattern as was used in the analysis of the full scale wing. Table 12 presents a comparison between the desired and calculated flutter velocities and frequencies.

Table 12
Desired Vs Predicted Flutter Parameters For Low AR Wing Model

| Parameter | Desired Scaled Value | Predicted Value |
|---|---|---|
| Flutter Vel (in/sec) | 9846 | 9109 |
| Flutter Freq (hz) | 58.1 | 58.1 |

A measure of whether the correct flutter mechanism is being predicted is to compare the modal participation coefficients for the flutter mode. Table 13 presents modal participation coefficients predicted for the model flutter mode. These values can be compared to those presented in Table 1 for the full scale wing.

Table 13
Modal Participation Coefficients For Low AR Wing Model

| | | | Model | | Full Scale | |
|---|---|---|---|---|---|---|
| Mode | Real | Imag | Mag | Phase | Mag | Phase |
| 1 | .9799 | 0.00 | .9779 | 0.0 | .9764 | 0.0 |
| 2 | .1907 | -.0437 | .1956 | -12.91 | .2132 | -13.4 |
| 3 | -.00973 | .0382 | .0394 | 104.3 | .0354 | 119.2 |

Another measure of whether flutter characteristics are being accurately predicted is to compare V-G and V-ω plots. The V-G plot for the wing model is presented in Figure 29. The V-ω plot is presented in Figure 30. Note that mode switching has occurred in the V-G plot and that the correct branches are added with dashed lines.

The flutter results and modal participation coefficients (both phase and magnitude) at flutter are very close for the model and full scale wing. The V-G and V-Ω plots are not exact copies of each other, though. The second and third modes on the V-G plot cross slightly earlier for the model than for the full scale wing. Also, separation between mode 3 and the other two on the V-Ω is slightly greater for the full scale wing than for the model. These differences are very small, probably resulting from the slight differences between the desired model characteristics and those achieved.

**Figure 29** - V-G Plot For Wing Model

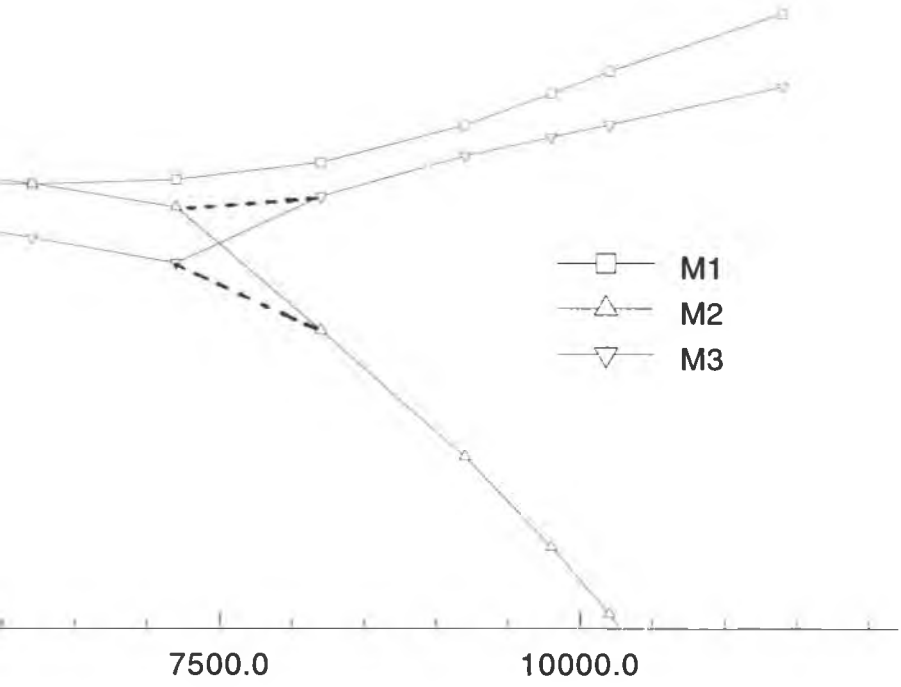


Velocity (in/sec)

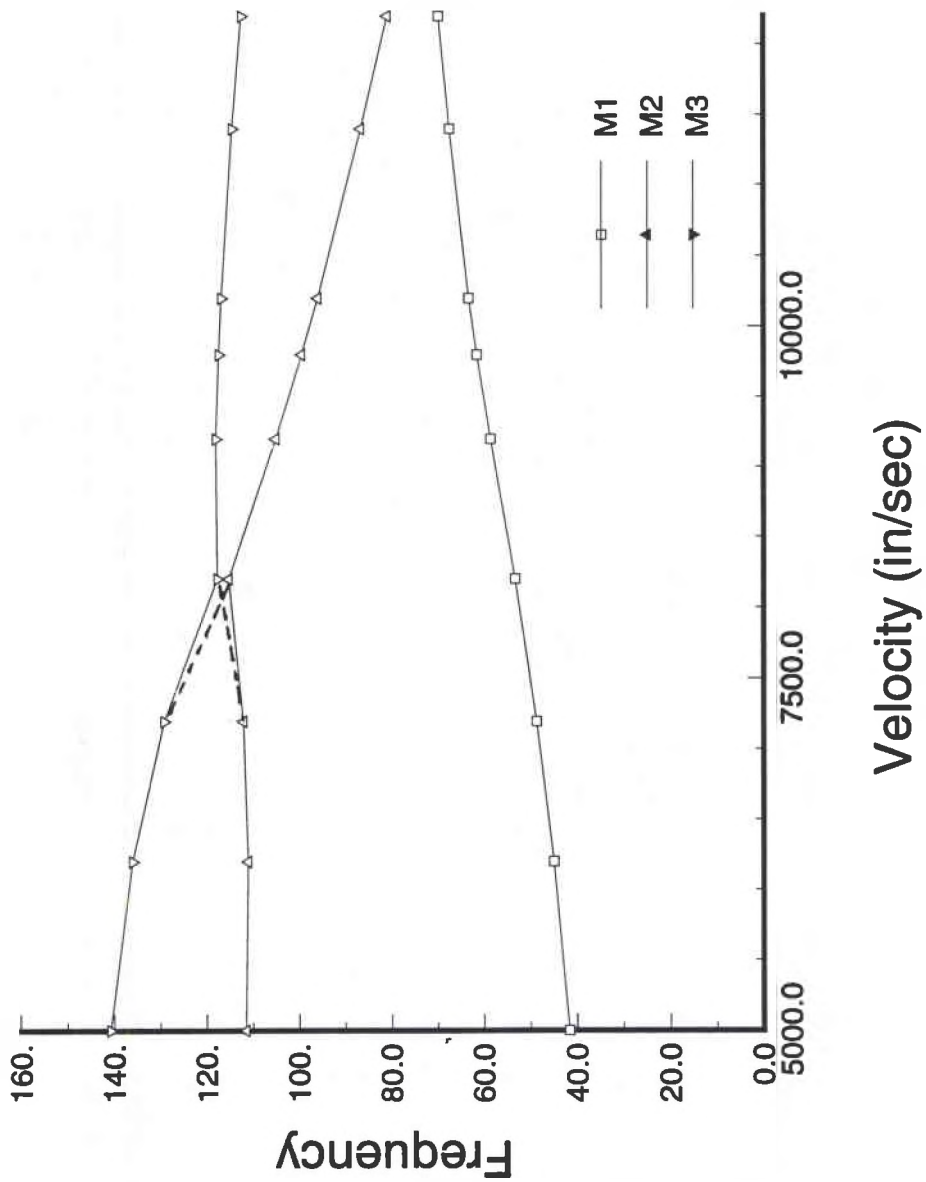


**Figure 30**- V - Ω Plot For Wing Model

Chapter 5

## Experimental Validation of Analysis

The investigation has so far has been all numerical. However, an experimental effort was performed to check the analytical results. The finite element model used for the analyses so far has been very simple and, at first glance, there seems to be little need for experimental verification of the results. However, there are several problems involved in fabricating a real world structure from the beam lattice finite element model.

A sample model structure was fabricated from 4130 steel plate for static and dynamic testing. A clamped boundary condition at the wing root was achieved by bolting the wing into a very heavy steel test fixture. Two different series of tests were performed on the model: a static test to measure the stiffness characteristics of the wing and a dynamic test to measure the natural frequencies and mode shapes of the wing before and after mass balancing. All testing was done with laser interferometric methods.

The beam lattice finite element model of the structure uses mathematically ideal beam elements. Some of the assumptions used in deriving the beam elements are not strictly borne out in the actual structure. The most notable potential discrepancy is at the joints.

In the mathematical model, the beam elements are line segments with no cross-sectional area. Thus, they come together only at the grid points. In a real structure, however, the elements have width and height and intersect at some radius from the grid point location. Furthermore, the structure was machined on an end mill with .250 inch diameter cutter. So, any intersection of beam elements also has a .125 inch radius. See Figure 31 for an illustration of a typical joint.

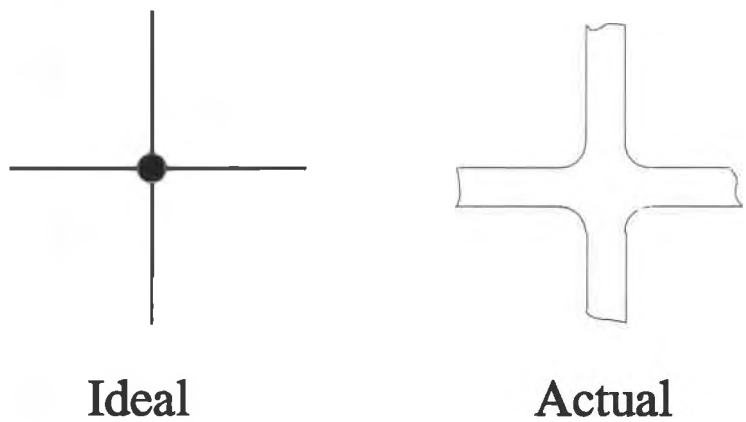


**Figure 31** - Idealized Vs Actual Joint

Another problem with joints is that the height of the different beams coming together is not usually the same. Thus, some standard means had to be developed for determining the height of the material in the joint area. The solution eventually settled on was to mill the joint area off at the height of the highest element at the joint. The other elements

were milled to the correct height, but the cutter was stopped when it got to within .125 inches of the grid point location for the joint.

The result is that there is an excess of material at the joints. This makes the area near the joints stiffer than predicted by the simple finite element model used so far. It also makes the mass of the area near the joints difficult to quantify. The basic objective of the stiffness and modal testing was to determine how much these differences in joint characteristics affected the stiffness and modal characteristics of the structure.

Another potential source of errors is that the finite element model assumes the structure to be symmetric about the midplane of the wing. However, the structure was machined with one side being flat. While this makes the wing slightly asymmetric, it greatly reduces manufacturing problems. A picture of the wing is presented in Figure 32.

The most immediately quantifiable source of error in getting experimental data is error in manufacturing the test structure. Desired element widths and heights were specified to three decimal places, but problems with the lighter elements flexing during the machining process meant that the elements are not all exactly of the design sizes. Table 14 presents the specified and measured dimensions of the beam elements. The manufacturing errors are small and were assumed to be negligible.

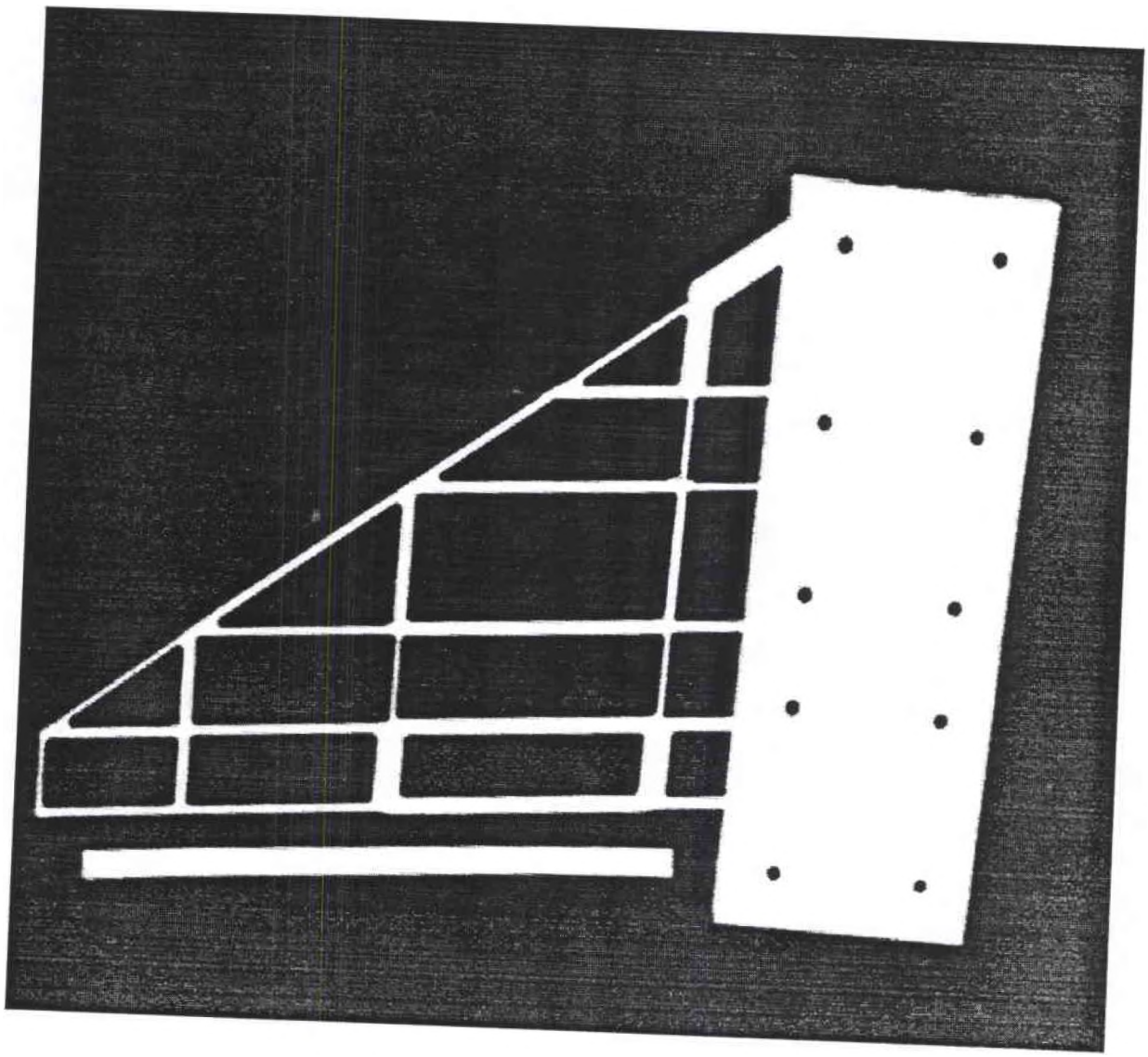

**Figure 32** Test Structure Before Installation in Mounting Fixture.

Table 14
Specified vs Measured Element Sizes

| Element No | G1 | G2 | Design Width | Measured Width | Design Height | Measured Height |
|---|---|---|---|---|---|---|
| 1 | 1 | 7 | .500 | .51 | .520 | .53 |
| 2 | 2 | 8 | .070 | .09 | .520 | .52 |
| 3 | 3 | 9 | .050 | .07 | .258 | .26 |
| 4 | 4 | 10 | .062 | .07 | .460 | .46 |
| 5 | 5 | 11 | .119 | .13 | .370 | .38 |
| 6 | 6 | 12 | .118 | .13 | .270 | .27 |
| 7 | 7 | 8 | .452 | .47 | .311 | .31 |
| 8 | 8 | 9 | .050 | .06 | .530 | .53 |
| 9 | 9 | 10 | .125 | .13 | .269 | .27 |
| 10 | 10 | 11 | .050 | .07 | .251 | .25 |
| 11 | 11 | 12 | .493 | .50 | .270 | .27 |
| 12 | 7 | 13 | .050 | .07 | .325 | .33 |
| 13 | 8 | 13 | .135 | .14 | .430 | .43 |
| 14 | 13 | 14 | .086 | .09 | .350 | .35 |
| 15 | 9 | 14 | .123 | .13 | .350 | .35 |
| 16 | 10 | 15 | .141 | .15 | .380 | .38 |
| 17 | 11 | 16 | .182 | .19 | .310 | .31 |
| 18 | 12 | 17 | .211 | .22 | .220 | .22 |
| 19 | 14 | 15 | .213 | .22 | .350 | .35 |
| 20 | 15 | 16 | .050 | .06 | .215 | .21 |
| 21 | 16 | 17 | .486 | .50 | .220 | .22 |
| 22 | 14 | 18 | .103 | .12 | .220 | .22 |
| 23 | 15 | 18 | .068 | .09 | .220 | .22 |
| 24 | 16 | 19 | .089 | .11 | .240 | .24 |
| 25 | 17 | 20 | .076 | .08 | .150 | .16 |
| 26 | 18 | 19 | .178 | .19 | .220 | .22 |
| 27 | 19 | 20 | .162 | .18 | .175 | .18 |
| 28 | 18 | 21 | .050 | .06 | .080 | .09 |
| 29 | 19 | 21 | .124 | .14 | .140 | .15 |
| 30 | 20 | 22 | .084 | .09 | .140 | .14 |
| 31 | 21 | 22 | .050 | .06 | .069 | .07 |

## 5.1 Mounting Fixture

In most testing situations, the mounting fixture is not an object of much attention. Previous work with laser interferometry experiments has shown that a poorly designed mounting fixture can be a source of many headaches. The basic problem is that it is common for holography tests to assume a clamped boundary condition, but actually achieving a clamped boundary condition is very difficult. Laser measuring techniques are so sensitive that extremely small deformations in the clamping fixture can be detected. Furthermore, this sensitivity allows the effect of imperfect boundary conditions on structural behavior to readily detected. The solution is to make the fixture very stiff and very massive.

The fixture used for this series of tests was designed for the work presented in References 59, 60 and 61, but was thought to be well suited to the present work as well. It is made of 1 inch steel plate joined together with hardened 3/8 inch bolts. The test specimen is sandwiched between two heavy plates joined by 1/4 inch hardened bolts. The general arrangement of the test structure and mounting fixture is shown in Figure 33. A picture of the test structure installed in the mounting fixture is presented in Figure 34.

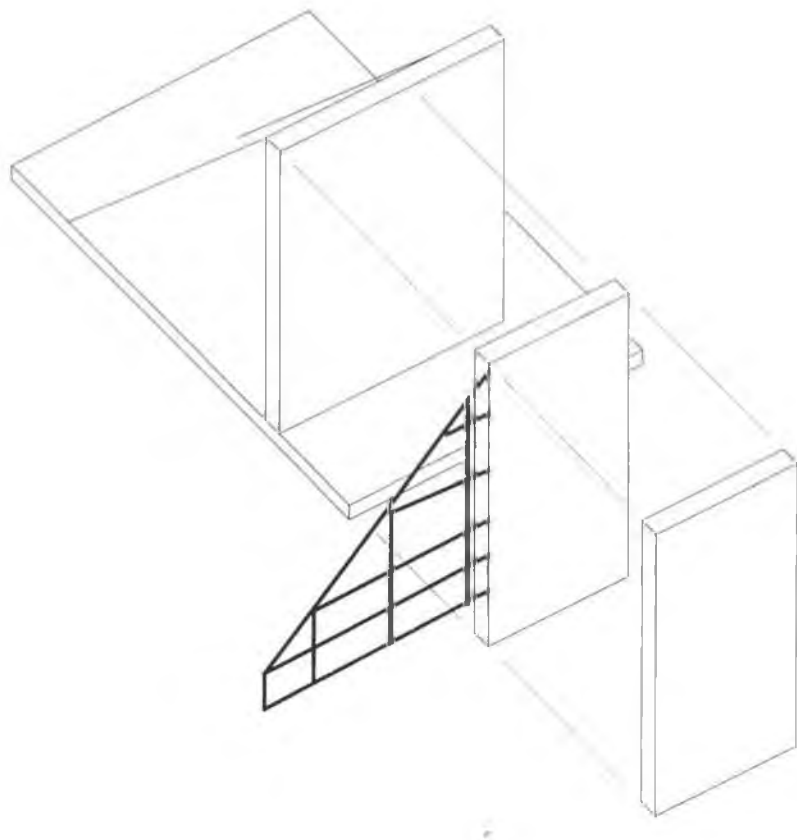

**Figure 33** - Test Structure and Mounting Fixture

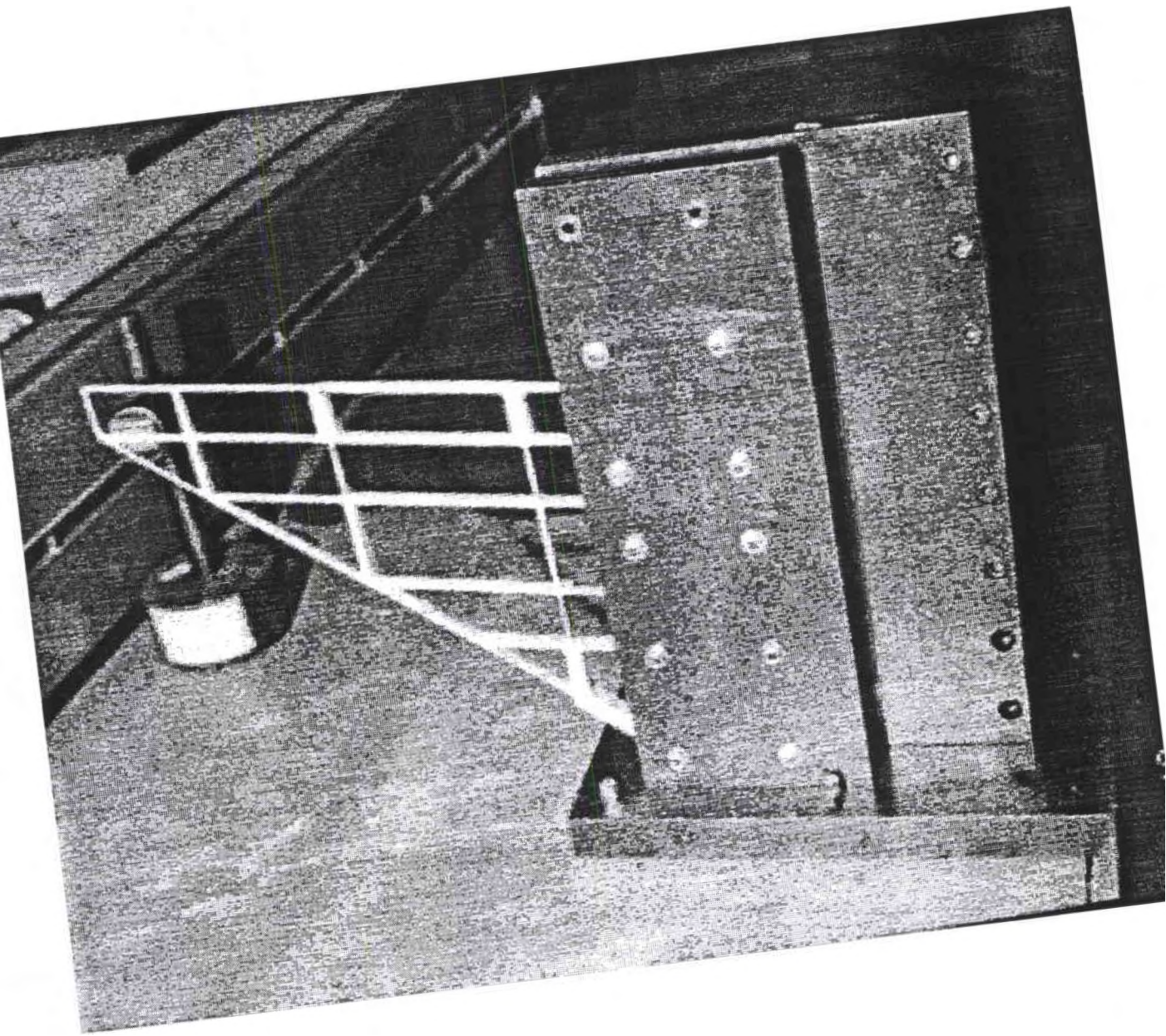

**Figure 34** - Test Structure and Mounting Fixture On Testing Table

## 5.2 Static Testing

### 5.2.1 Static Test Procedure

The first set of experiments measured static deflections of the structure. Two types of static tests were conducted. In the first test, a deflection was applied to the structure with a pointed probe attached to a fine thread micrometer. A picture of the setup is presented in Figure 35. In the second, a known load was applied to induce a displacement. When only a known displacement is applied, the resulting displacement elsewhere on the structure must all be normalized for comparison with other enforced displacement tests. Only when a known load is applied can an absolute comparison be made between different tests.

One of the strengths of the laser measurement techniques used for this work is the extreme sensitivity of measurements. Deflections of a few tens of micro-inches are easily resolved. This sensitivity can also be a problem. Known deflections must be applied to the structure with a fine thread micrometer. If the deflection is too large, the holographic image will literally be black with fringes. A bigger problem is applying a known load of the magnitude required for laser interferometric measurements. Static tests on model structures typically involve suspending weights on the order of a pound or two from the structure and measuring the resulting deflections. With laser methods, however, the

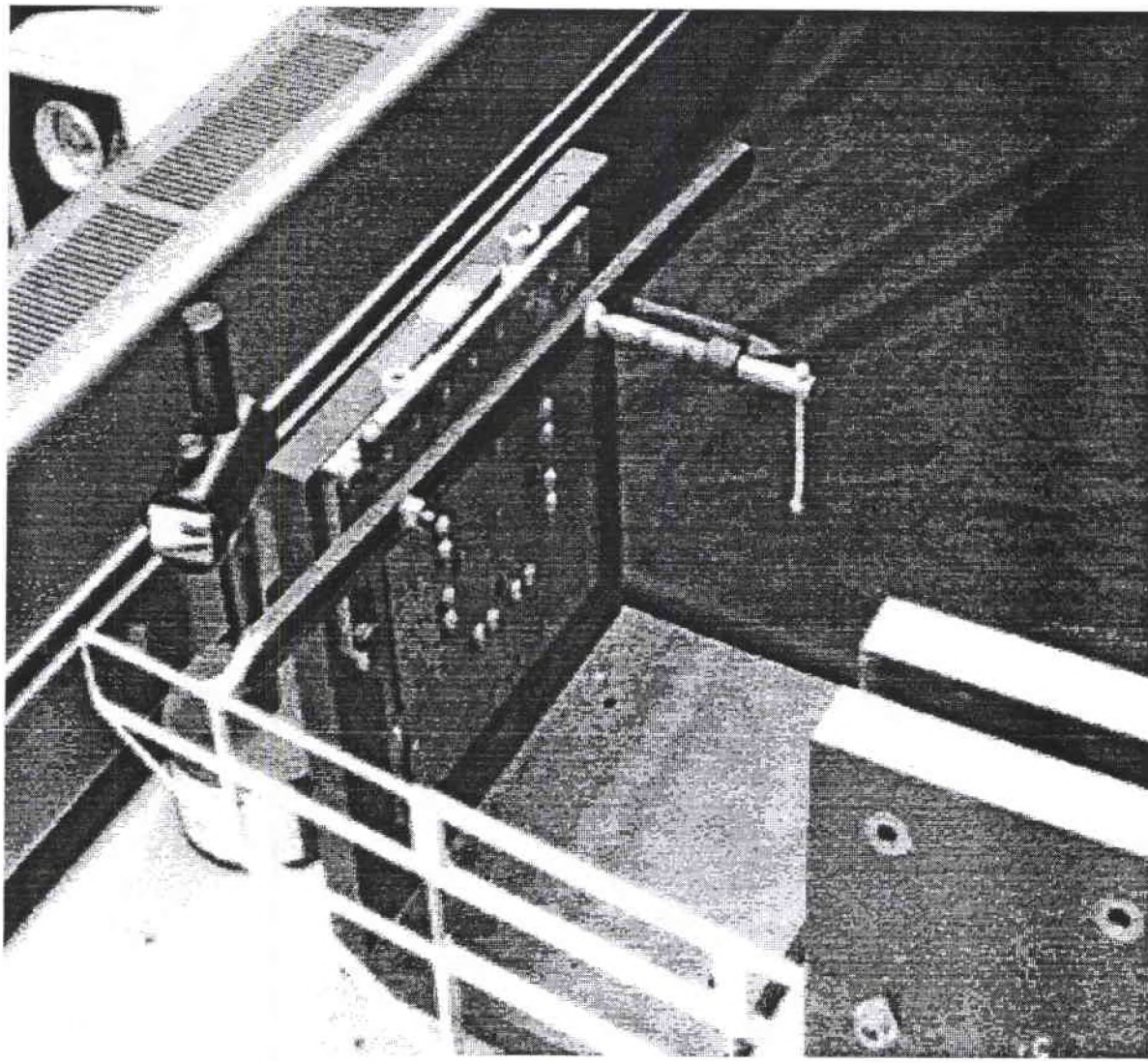

**Figure 35** - Test Structure in Mounting Fixture With Probe Assembly

required deflections are so small that weight on the order of a few grams are often needed. There are definite problems with applying a load this small with accuracy.

The desired method would be to design a fixture in such a way that the weight could be simply hung from the structure. This is not practical for the tests here because the laser and associated equipment are set up on a very heavy table with the beam horizontal and the plane of the wing vertical. The whole setup would have to be rotated 90 degrees so that the wing was horizontal and the beam looked down vertically on it.

Another obvious possibility would be to hang the weight over a pulley by a fine piece of string. The problem is that the friction in the pulley would likely be on the order of the weight being used. The option finally settled on was to hang the weight by a piece of string running over a support suspended on a knife edge. The arrangement is shown schematically in Figure 36.

The knife edge reduces friction to very low levels and allows very small loads to be transmitted accurately. The fixture was fabricated from steel and proved to have very low friction, but also relatively high inertia. The balance assembly was found to be able to swing for 5 to 10 minutes when the string and weight were not in place.

A simpler, and ultimately more successful, approach for applying small loads was suggested by Dr R. Pryputniewicz. It uses light string suspended from a rigid support at

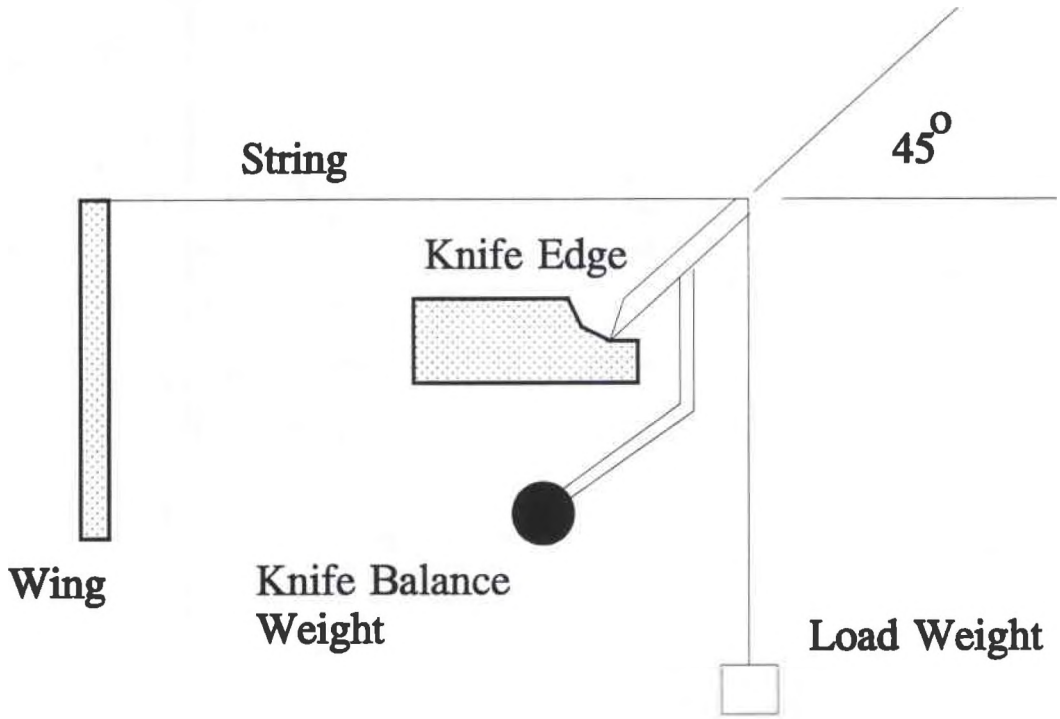


**Figure 36** - Schematic of Knife Edge Balance

a 45 degree angle to take the place of the knife edge balance. It is shown schematically in Figure 37.

Deflections were applied at six different points on the wing: grid points 14, 17, 18, 20, 21 and 22. Due to limited testing time and experimental problems, loads were applied only at points 17, 20, 21 and 22. A hologram was made for each of the test points. The quality of the images varied, but usable data could be extracted from most of the images. In a few cases, however, the resolution of the fringes was too poor get useful data.

The first set of tests used an applied deflection. Typical test procedure was to set the probe up so that it contacted the plate at the correct point and allow 10-15 minutes for slippage and for vibrations to die down. The first exposure was made and then a full turn applied to the micrometer. After a minute or two for vibrations to die down, a second exposure was made.

The second set of static tests applied a known load to the structure. The test procedure was to set up the load fixture with both a tare load and a differential load being applied. 10-15 minutes were allowed for vibrations to damp out before the first exposure was taken. Then the differential load was removed and 5 minutes allowed for vibrations to damp out before the second exposure was taken.

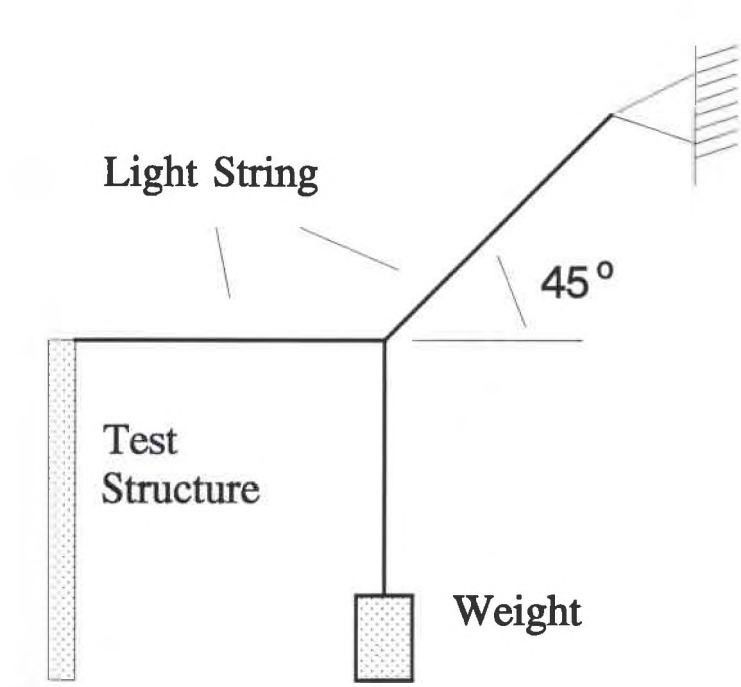


**Figure 37** - Schematic of String Load Fixture

Experience gained over several days of trying showed that the knife edge fixture could not be reliably used to apply loads. It was proved impossible to completely stop the balance assembly from swinging. Increasing amounts of time were allowed for vibrations to damp out, but air currents in the room and vibrations in the building kept the balance from being perfectly stationary. The result was that the deflection was changing while the shutter was open and the fringes came out too blurry to be used.

The string system proved to be much more workable, but only after some means was found for damping out swinging motion of the weight. Initially, the tare weight was partially submerged in a cup of water, but damping was still not adequate. Finally, the tare weight was partially submerged in a cup (actually a hamster dish) filled with glycerin. This combined with 5-10 minute waiting periods before the exposure resulted in clear fringe patterns.

Another problem encountered was that different weights were needed depending on where the load was being applied. The objective was to have 10-20 fringes along the rear spar, so a relatively large load was applied to the inboard point. The load was decreased as the load application point moved outboard. The loads and application points are presented in Table 15

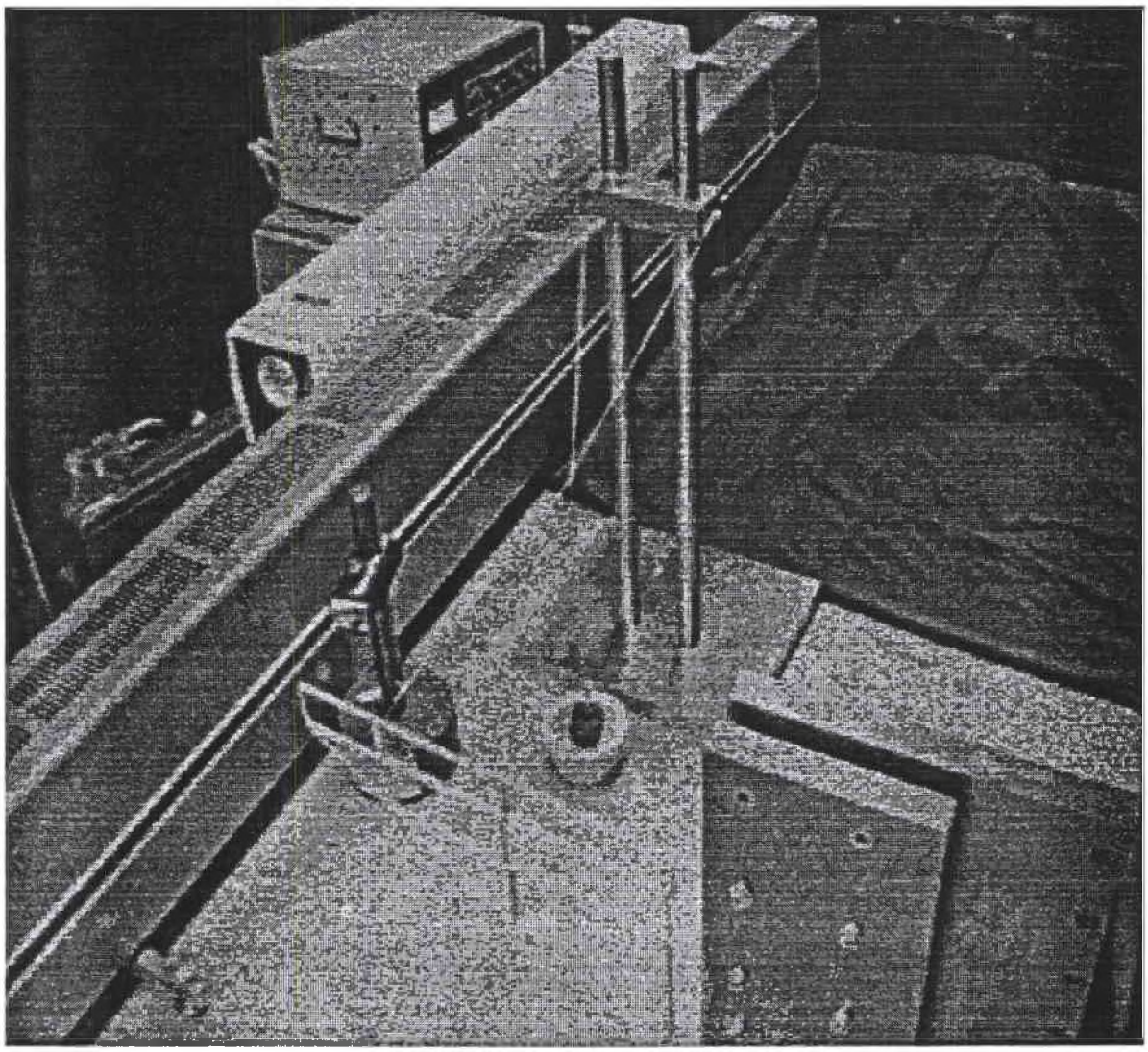

**Figure 38** - Load Application Using String Arrangement

Table 15
Loads And Application Points

| Number | Weight (gm) | Grid Point(s) |
|---|---|---|
| 1 | 22.44 | 17 |
| 2 | 10.09 | 20 |
| 3 | 6.18 | 21, 22 |

### 5.2.2 Static Test Data Reduction and Results

A hologram containing fringe patterns was produced for each test case described above. The hologram were then processed electronically to obtain numerical values for fringe orders and locations along the spars. Previously, deflection data has been presented in the form of contour plots. This was not possible for the experimental data, since the holograms were not always of high enough quality to allow fringes to be counted everywhere on the structure. Instead, plots are presented which show experimental deflection along the wing spar compared to deflections predicted by the finite element model.

The electronic processing was done using a specialized computer system. The hardware consists of an Everex 486/33 PC with a video camera system and second monitor for display of the video images. The software was a package called Optimas which runs under Windows 3.0/DOS 5.0. Optimas is a very sophisticated image processing package

which allows the user to scan in images, process the images to highlight desired features and extract quantitative data from them.

Image processing ranged from simple brightness and contrast changes through pixel averaging schemes to 2-d Fast Fourier Transforms. Very little processing of this type was done on the images produced for this effort. In one case, however, a poor reconstruction was improved by averaging scanning the image four times and averaging the results the form a single image of much higher quality.

For this effort, the true value of Optimas lay in data collection. The data collection process was as follows. Each image was scanned into the computer and stored as a Tagged Information File Format (TIFF) file. The first step was to scale the image on the screen. To do this, a line is drawn joining two known locations on the wing and a length input. The points used for scaling were the root and tip of the trailing edge. Optimas has the ability to count light and dark fringes along some specified line, so the next step is to draw a line on the image. This is done by using the mouse to mark endpoints. When this is done, a plot of luminance versus distance is generated and the fringe locations marked automatically on the image.

There are various parameters which can be modified to make sure all the fringes are marked. In addition, fringe locations can be marked manually using the mouse to click on the desired location. Finally a table containing locations of fringes along the line is

written to the disk. The images were not clear enough for fringes to be counted along all the spars. Typically, data was collected for the three rear spars. For purposes of terminology, the structure can be thought of as consisting of a leading edge and five spars, with the fifth spar forming the trailing edge.

Correlation of test data raises the problem of what value should be assigned to individual fringes. If the displacement of the structure is normal to the bisector of the angle formed by the object beam before and after it is reflected off the object, an individual fringe represents about 12.5 microinches displacement. However, the displacement of the structure is not normal to the bisector, so some correction must be made. A simpler solution is to use a fringe as a dimensionless unit. For the cases in which a displacement was applied to the structure, correlation with the finite element model becomes simple. An arbitrary displacement value is assigned for each fringe and the finite element results are then normalized. If the displacement at the load point was measured to be 10 fringes, a displacement of .10 inches is applied on the finite element model and all displacements are divided by .01 inches to non-dimensionalize the displacements.

It is not clear how much data should be presented before it starts to become redundant. Deflections along the rear three spars due to loads applied at six points along the wing are presented here. There was not enough resolution on most of the images to count fringes along the leading edge and the two forward spars are relatively stiff. Thus, it was assumed that sufficient deflection information could be obtained from the rear three.

Plots 40, 41 and 42 are deflections along spars 3, 4 and 5 due to a deflection applied at grid point 17. Correlation between analytical and experimental results is good in all three figures. An interesting feature apparent in the plots is a change in curvature outboard of the loading point. This initially raised some concern over the experimental results, but was also found to be present in the finite element results. The curvature change appears to be due to the fact that the beam on which the load was applied is connected to several others on which there are no loads placed.

Deflections along spars 4 and 5 due to a deflection applied at grid point 19 are presented in Figures 43 and 44. Image quality on the hologram plate was poor for the area around spar 3, so no data for that area could be obtained. Correlation between analysis and experiment is extremely good for the remaining two spars. It is interesting to note that there is a slight change of curvature along spar 5 similar to that found in Figure 44.

Deflections along spars 3, 4 and 5 due to a deflection applied at grid point 21 are presented in Figures 45, 46 and 47. Again, correlation is good between analysis and experiment was very good with the two curves lying virtually on top of each other in all three cases.

Deflections along spars 4 and 5 due to a deflection at grid point 22 are presented in Figures 48 and 49. Correlation is good, but there is some discrepancy at the tip of spar 4.

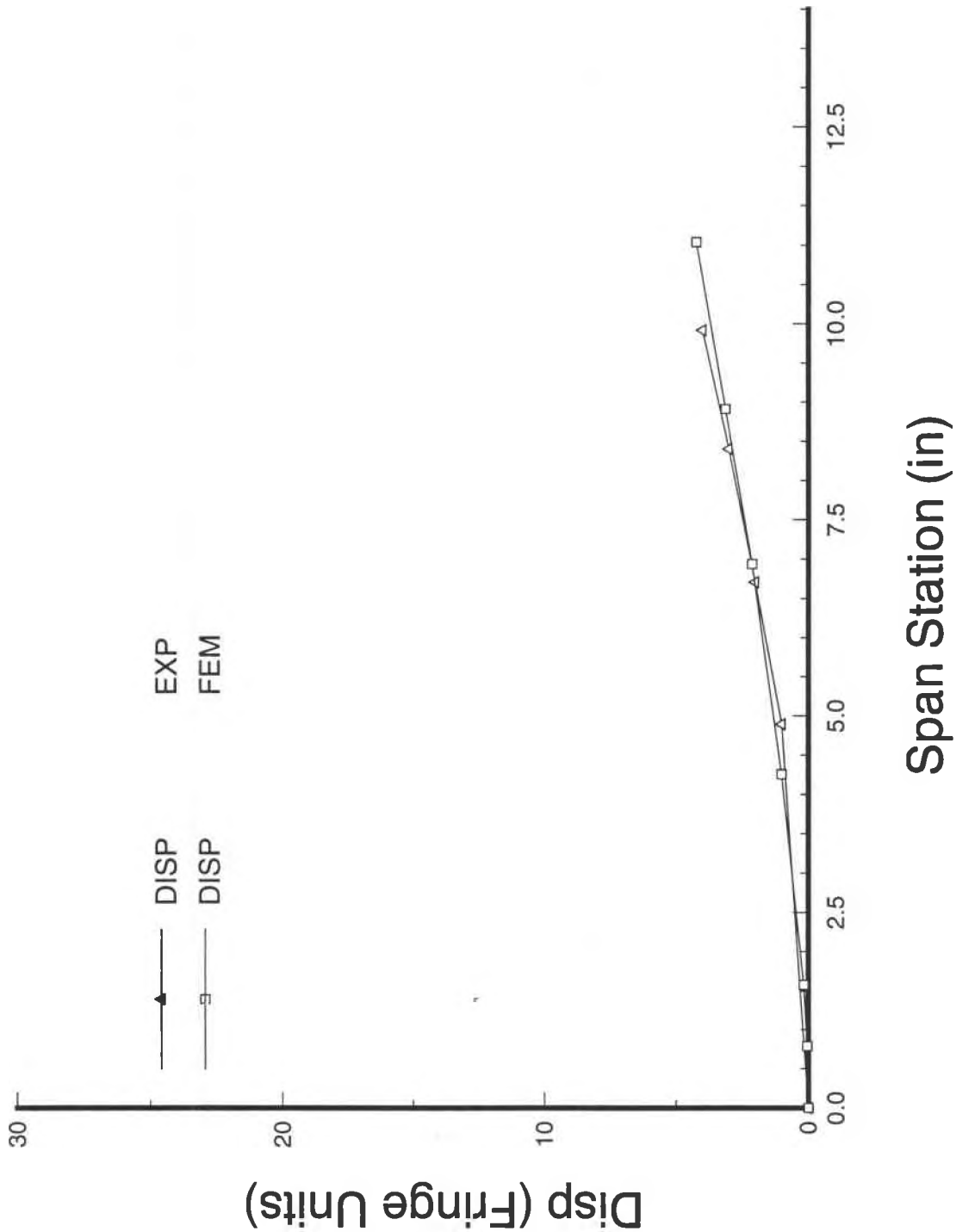


**Figure 39** - Deflections Along Spar 3 Due To Deflection At Grid Pt 17

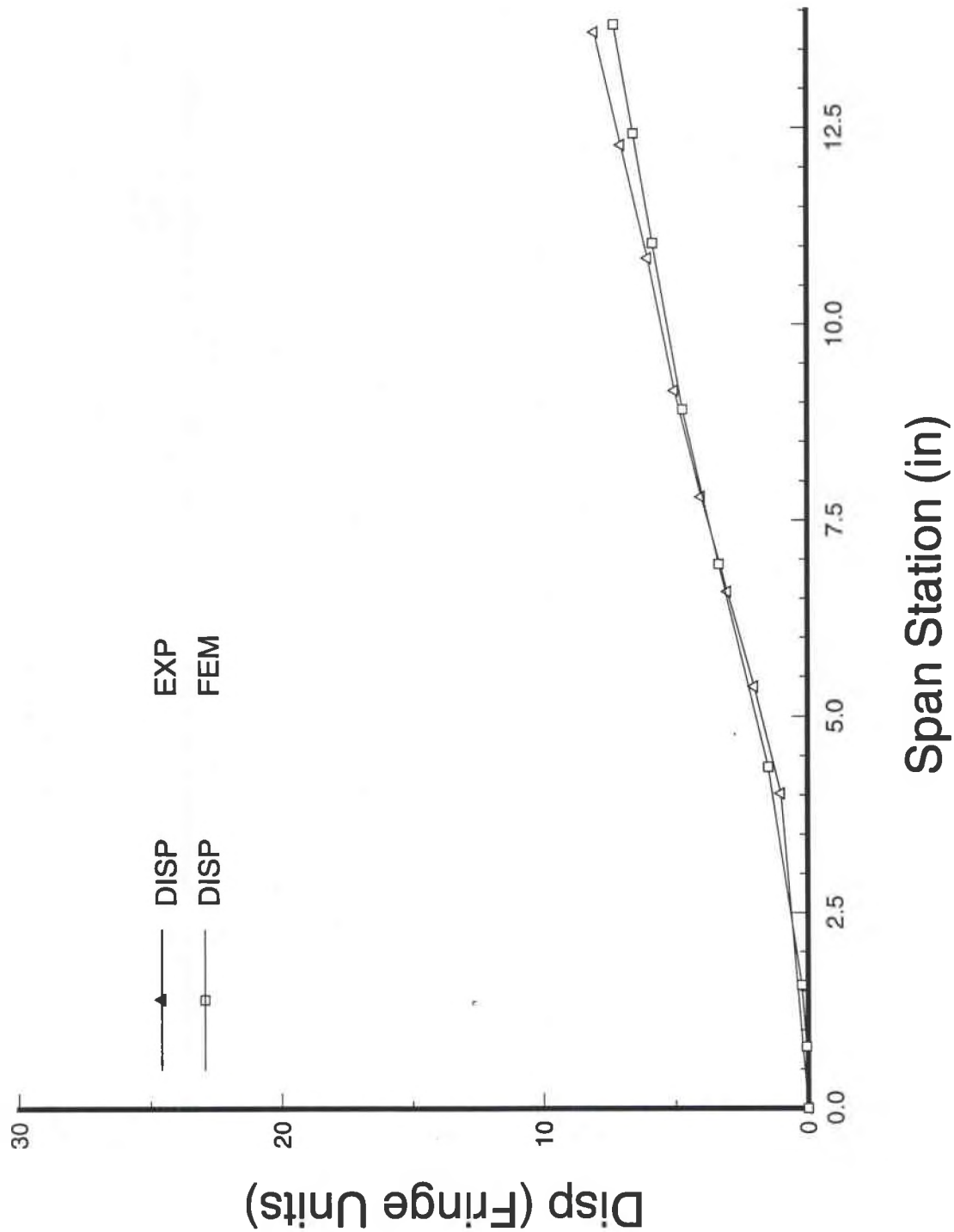


**Figure 40** - Deflections Along Spar 4 Due To Deflection at Grid Pt 17

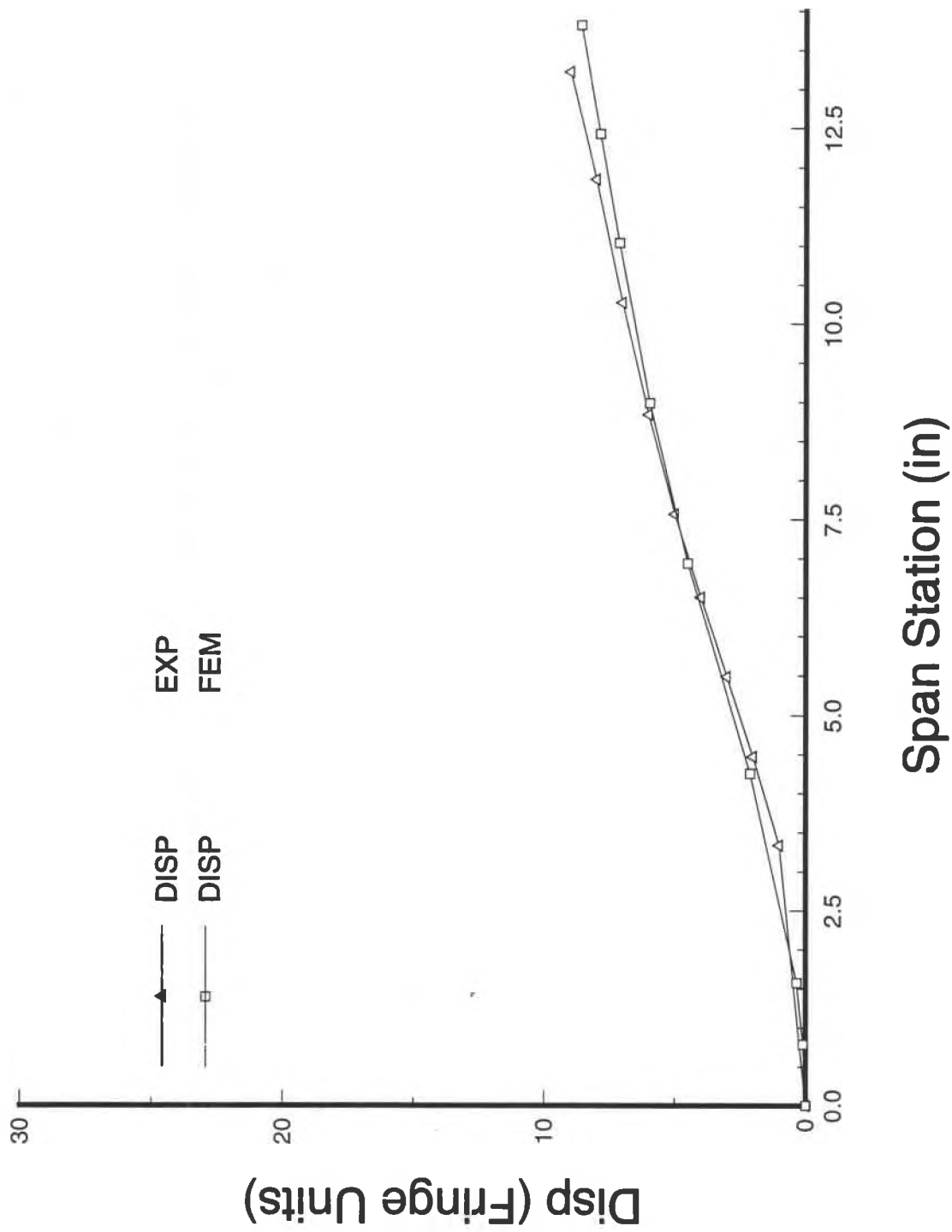


**Figure 41** - Deflections Along Spar 5 Due To Deflection At Grid Pt 17

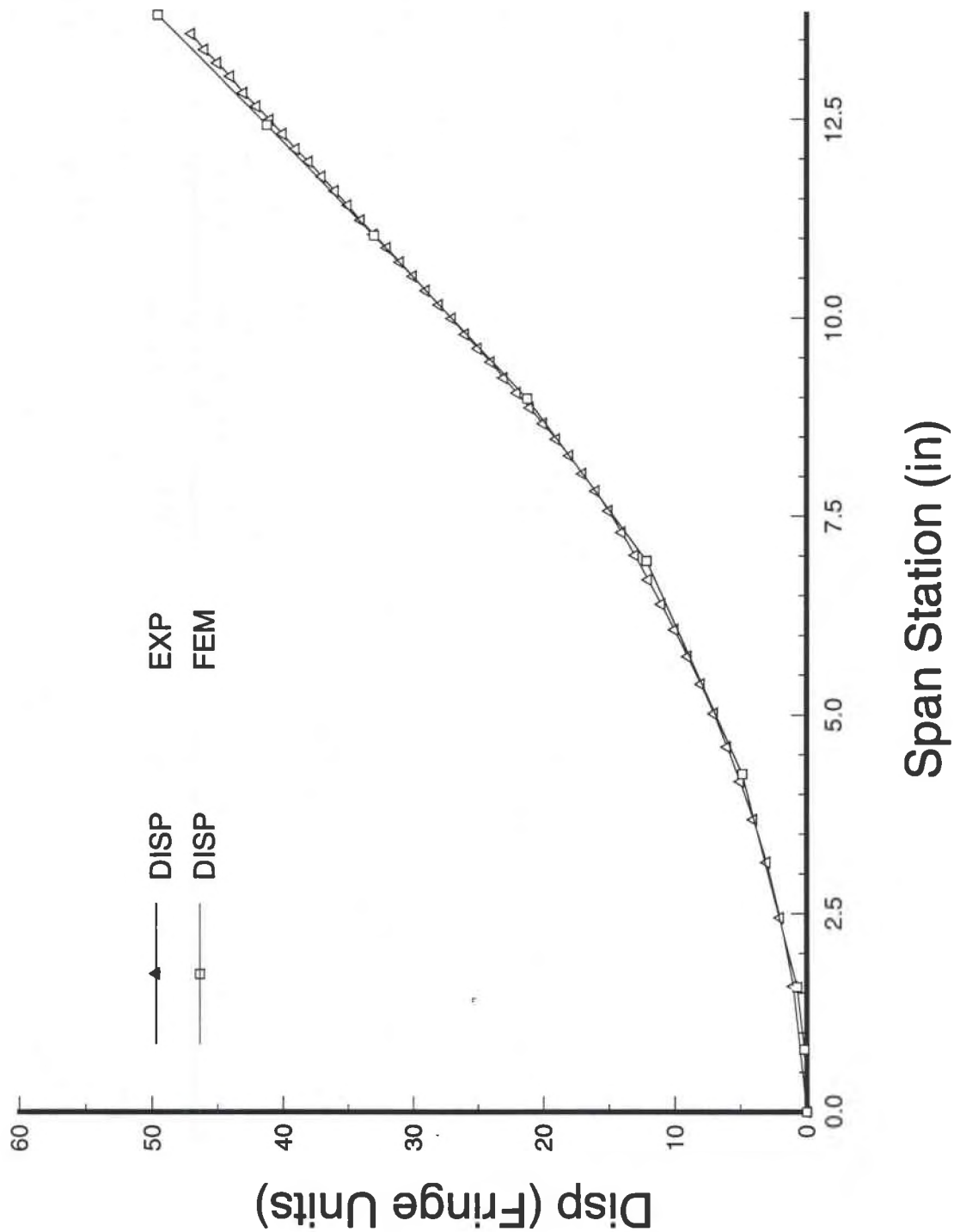


**Figure 42** - Deflections Along Spar 4 Due To A Deflection At Grid Pt 19

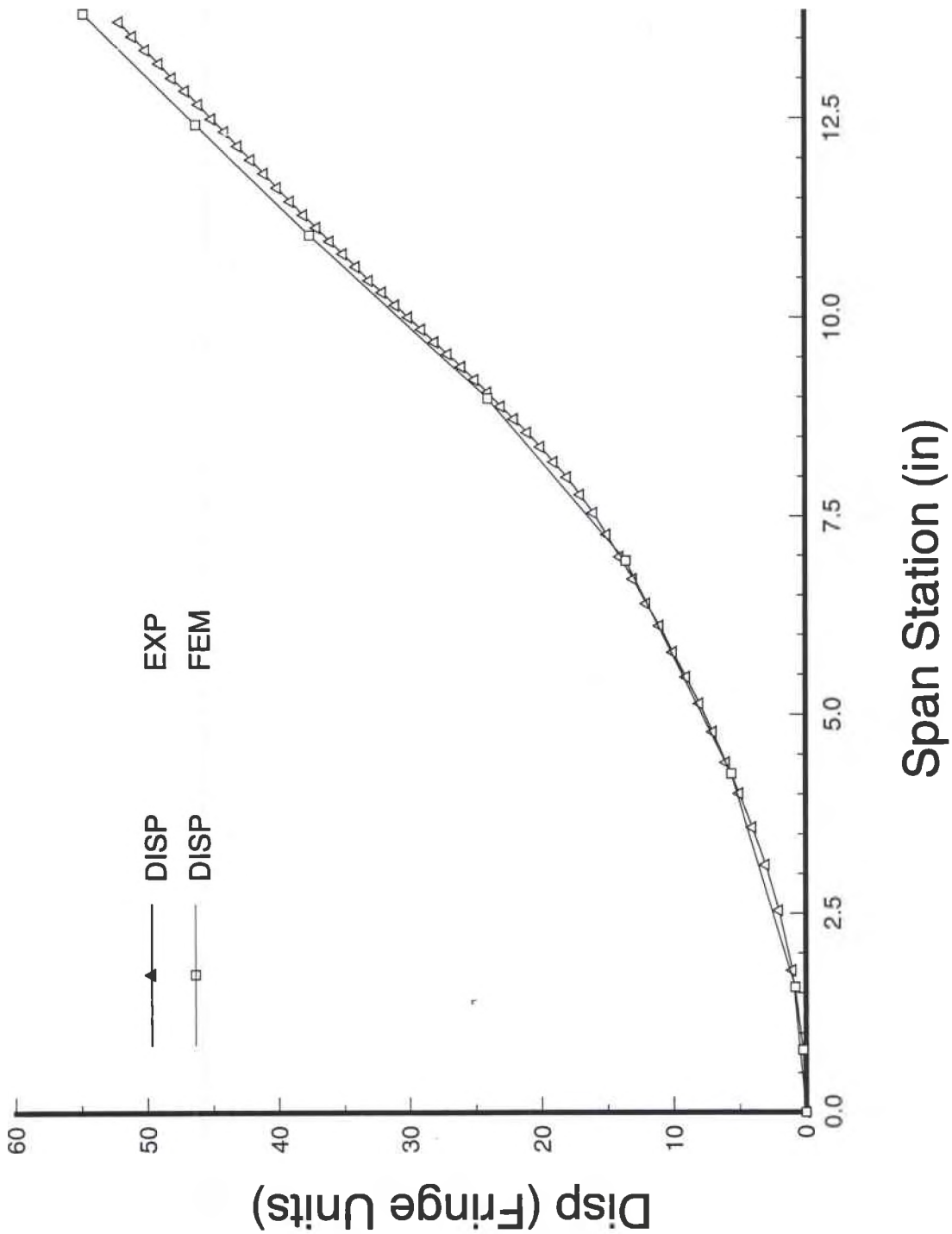


**Figure 43** - Deflections Along Spar 5 Due To A Deflection At Grid Pt 19

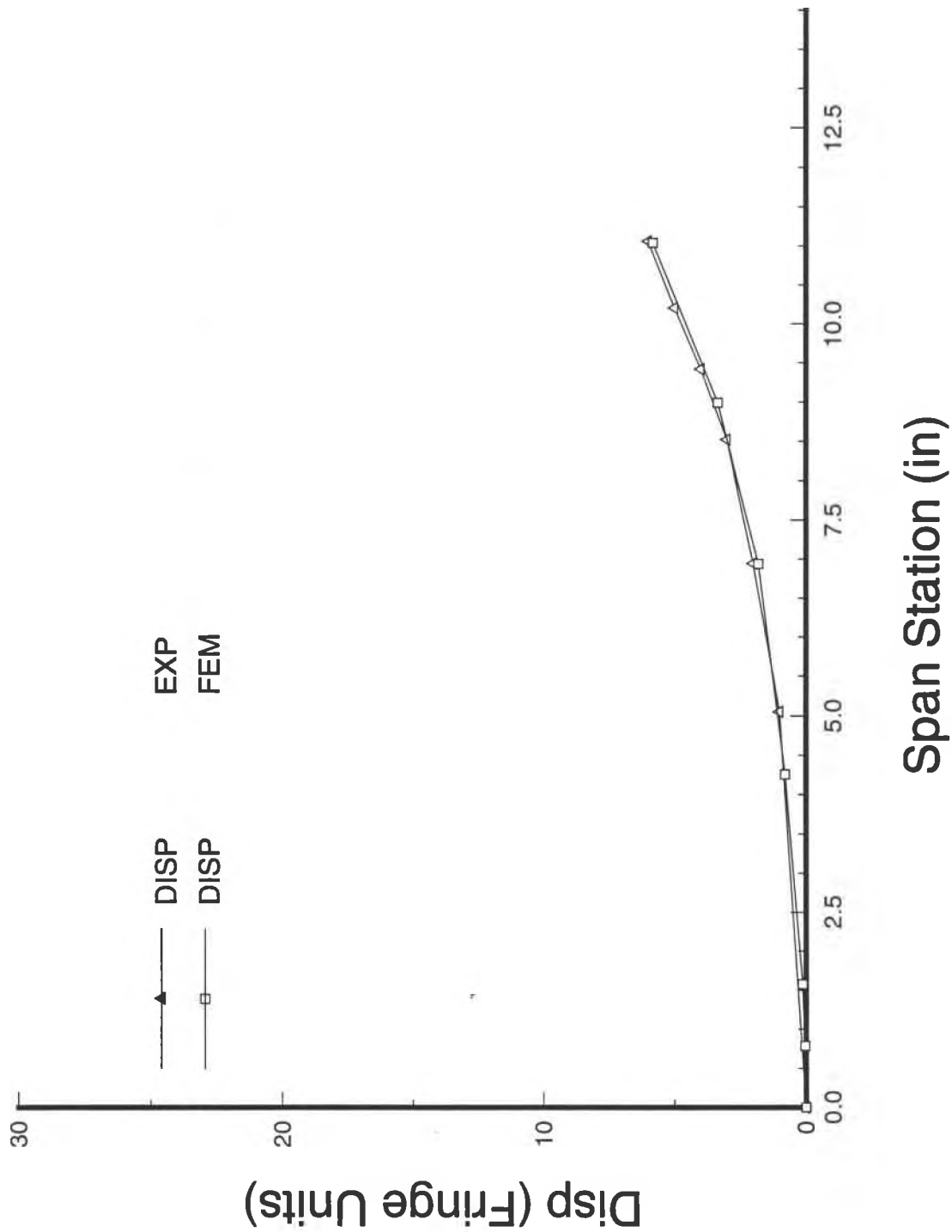


**Figure 44** - Deflections Along Spar 3 Due To A Deflection At Grid Pt 21

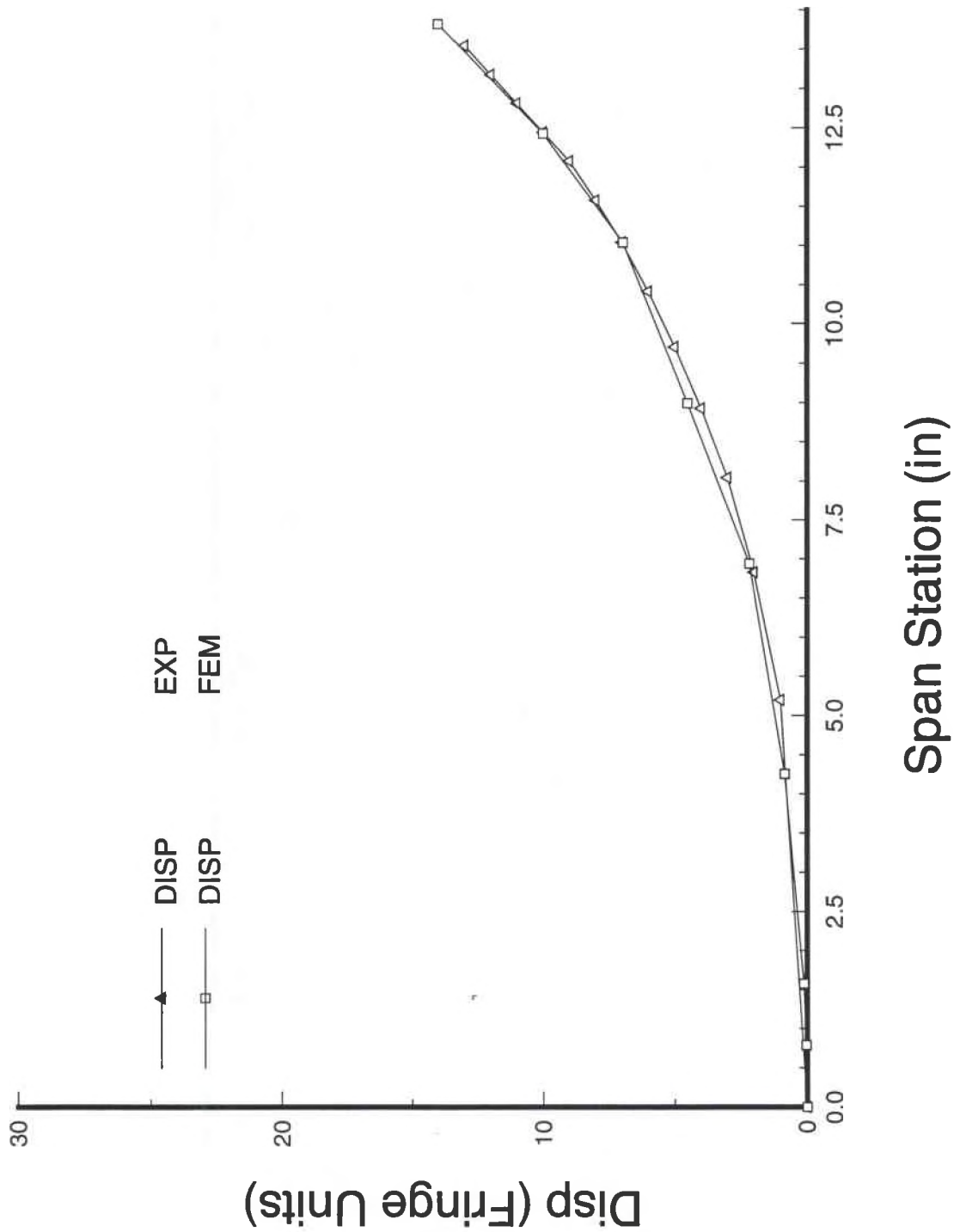


**Figure 45** - Deflections Along Spar 4 Due To A Deflection At Grid Pt 21

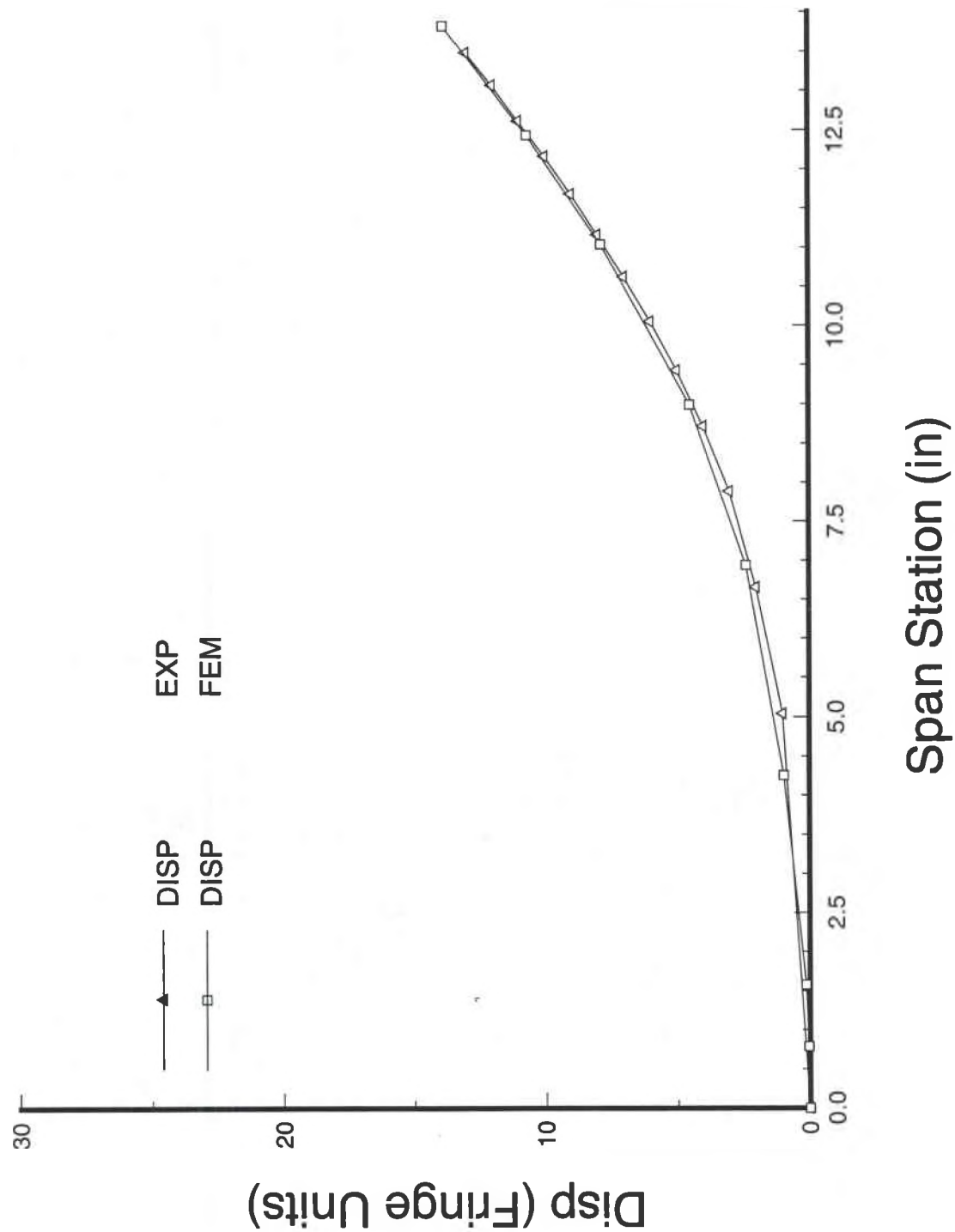


**Figure 46** - Deflections Along Spar 5 Due To A Deflection At Grid Pt 21

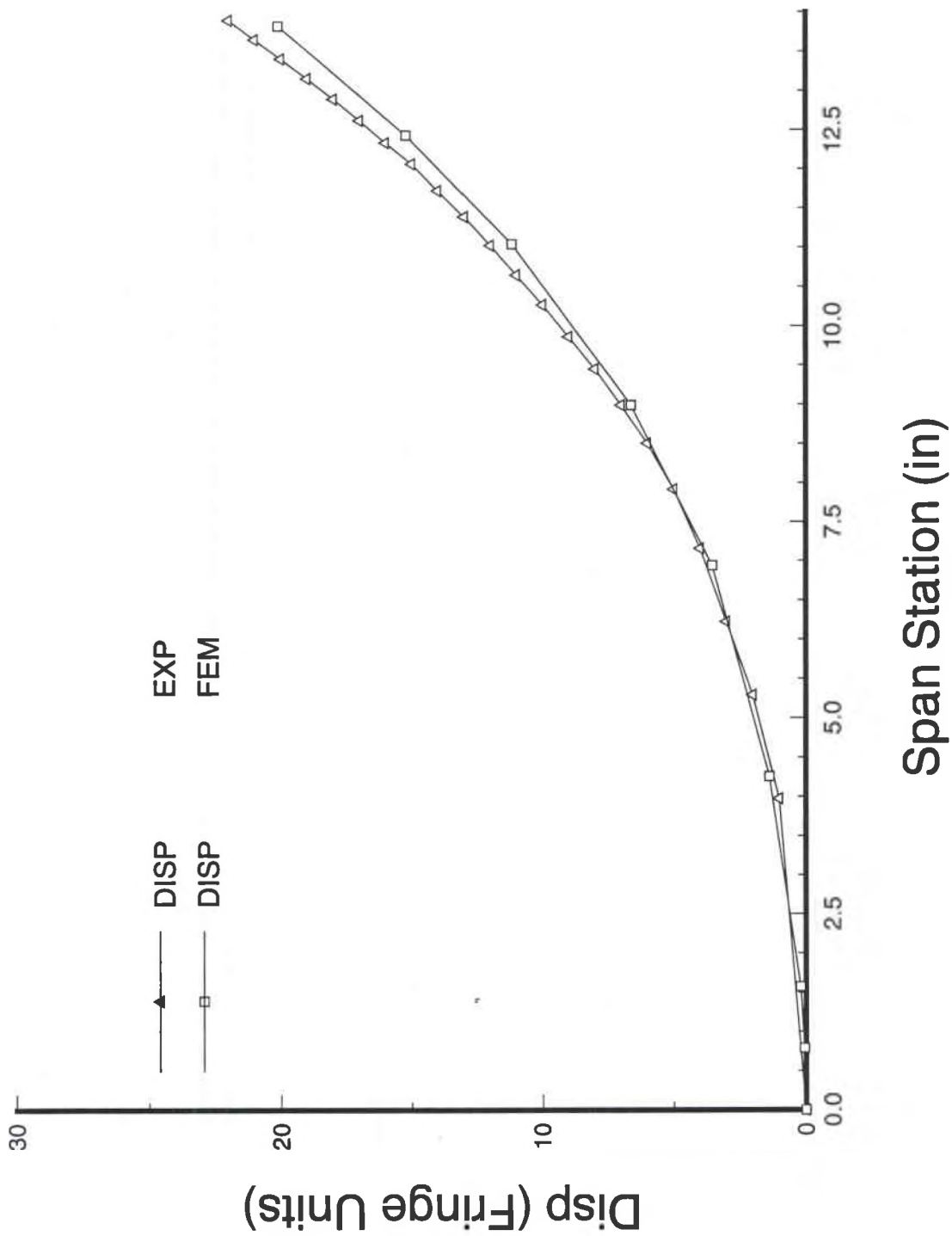


**Figure 47** - Deflections along Spar 4 Due To A Deflection At Pt 22

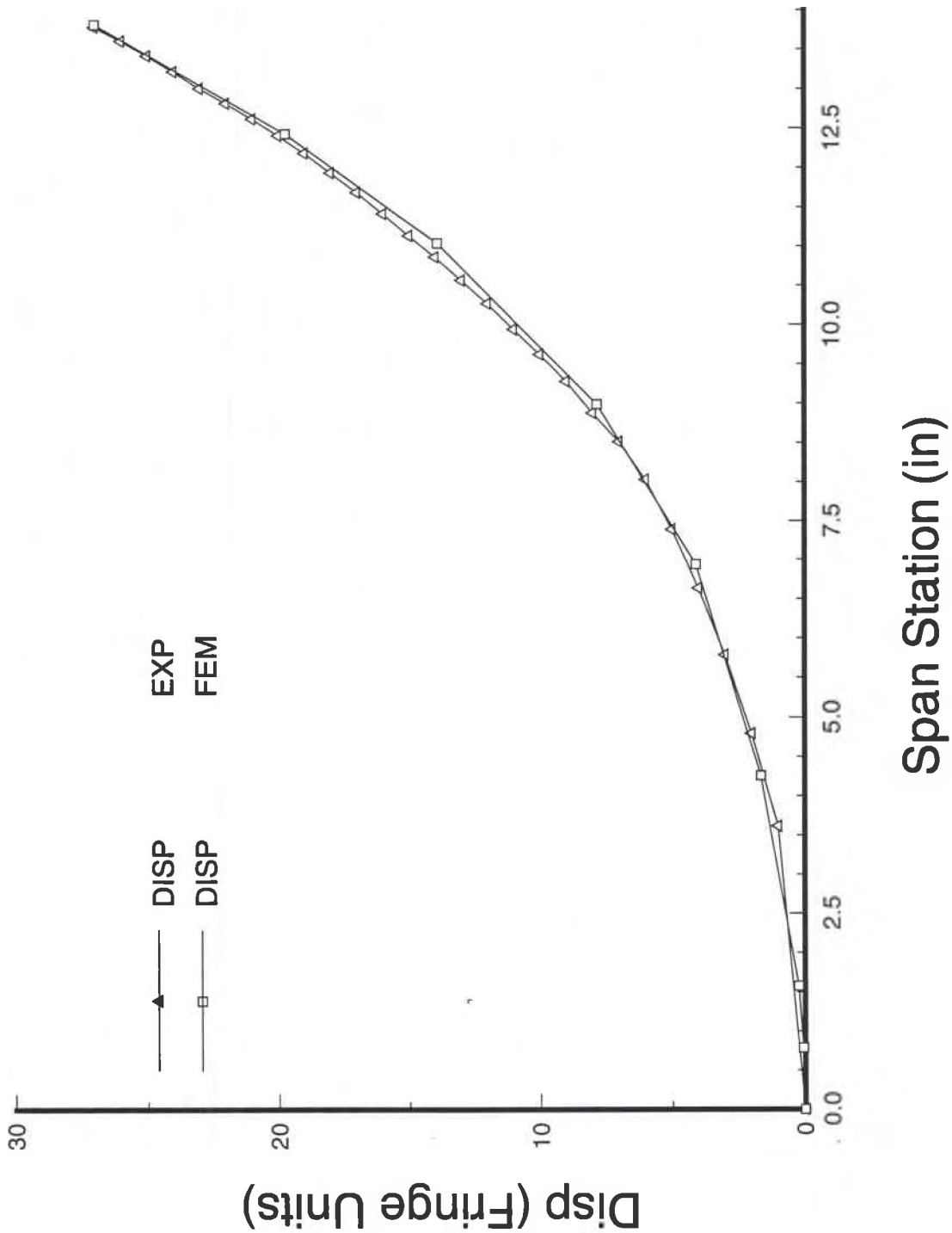


**Figure 48** - Deflections Along Spar 5 Due To A Deflection At Grid Pt 22

The purpose of static testing is to show that the stiffness of the real structure matches that predicted by the finite element model in spite of excess, material at the joints, manufacturing errors and whatever other problems that might crop up. The results presented above have all been normalized, so that the stiffness has only been shown to match to within some constant multiplication factor. It was hoped that the results of applying a known load would show that the experimental and analytical results matched without having to resort to normalizing the results. However, the results of these tests differ by what appear to be a constant multiplication factor. What follows is a description of how holographic data was interpreted and a brief sample of the experimental results.

The previous deflection data has all been due to a deflection applied at some point on the structure. A second set of deflection data was obtained, however, due to a known load applied at various points on the structure. Obtaining numerical results from these tests is slightly more complex than it was previously. In this case, the deflection data cannot be normalized for comparison with analytical data. Thus, a dimensional distance must be obtained for the deflection which results in a single fringe. This distance is a function of the wavelength of the illuminating beam and the geometry of the test setup. In order to get numerical results for comparison purposes, a correction must be made to the raw numerical data obtained from the scanned image.

The deflections induced are normal to the plane of the structure. However, fringe lines are formed due to deflections along the bisector of the angle formed by the object beam

as it is reflected off the structure. It is important to note that the angle made by the beam reflecting off the tip of the structure is not the same as that reflecting off the root. Therefore, the correction factor varies along the span of the wing.

If the angle formed by the object beam was zero, Each fringe would correspond to a 12.5 microinch deflection. The true deflection is 12.5 microinches divided by the cosine of the half angle made by the object beam reflecting off the structure. The difference in the object beam angle between the root and tip of the structure is small, so an average value of 14.5 deg was used, giving a half angle of 7.25 deg. The cosine of the half angle is .992, so there would be a negligible change in the deflection values. Thus, each fringe was assigned a 12.5 microinch displacement

The comparison between the analytical and experimental results was not as good as was hoped. There was a consistent difference between the two of about 25%. This difference was consistent in all the plots of displacement due to an applied load. Figure 50 plots displacement along spar 5 due to a load applied at grid point 22. This plot is representative of the results for the various load cases.

A significant amount of time was spent looking for an explanation for the difference in test data. Initially, the problem was to decide whether the difference was due to some error in test procedure or to increased stiffness of the test structure. Limited availability of the test facility prevented the static load test from being run again, but the test

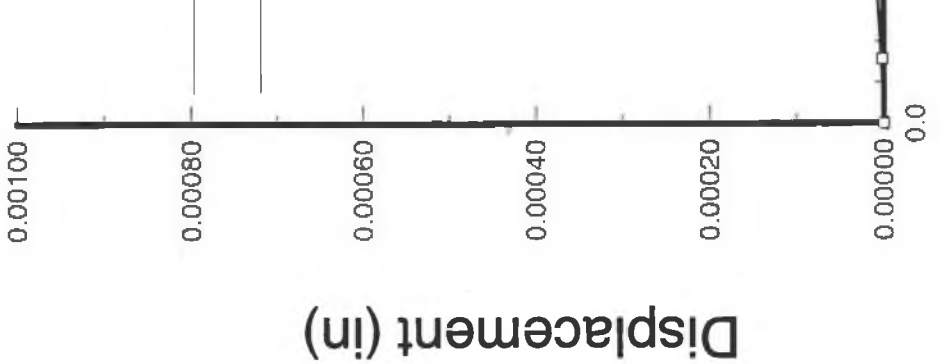


**Figure 49** - Displacement Along Spar 5 Due To A Load At Grid Pt 22

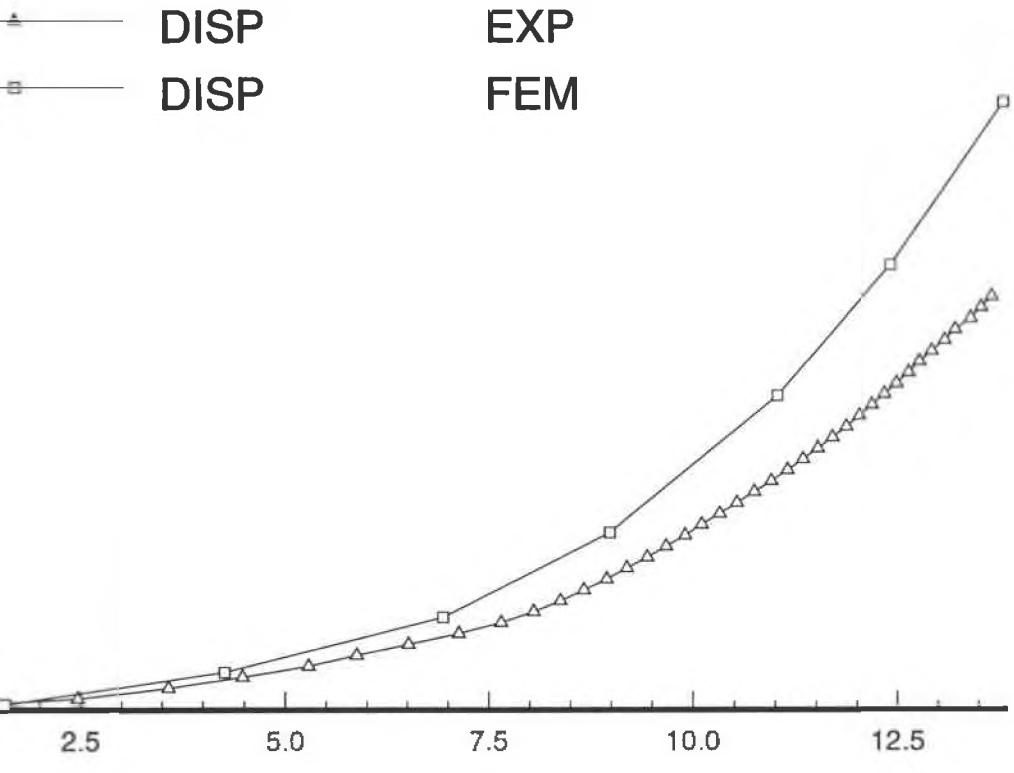
DISP EXP
DISP FEM
2.5
5.0
7.5
10.0
12.5
Span Station (in)

procedure was examined looking for some error in technique. The most apparent source of error was in the load application method

A simple test was performed to make sure the load was being applied to the structure correctly. A small static load was applied to a simple rectangular plate using the same string arrangement used in the second set of static tests on the wing. The rectangular plate was chosen since it is a very simple shape and modelling errors are not likely to be made. The plate was made of aluminum and was 5.00 inches long by 2.50 inches wide and .052 inches thick. The plate was cantilevered and the load was applied at the center of the tip. The load was provided by three small washers whose mass totalled .982 grams.

A simple finite element model was constructed to provide analytical data for correlation. The model had 10 elements arranged in a 5 x 2 element pattern. Analytical and experimental deflections along the centerline of the plate were plotted on the same axes for comparison. Figure 51 shows deflections due to the load from the washers.

The correlation between the experimental and analytical prediction is good, but not exact. The slight difference could easily result from a minor difference in the elastic modulus of the material or the thickness of the plate. The conclusion is that the load application method used for the second set of static test data on the wing works well enough that it is probably not the cause of the difference between analytical and experimental results.

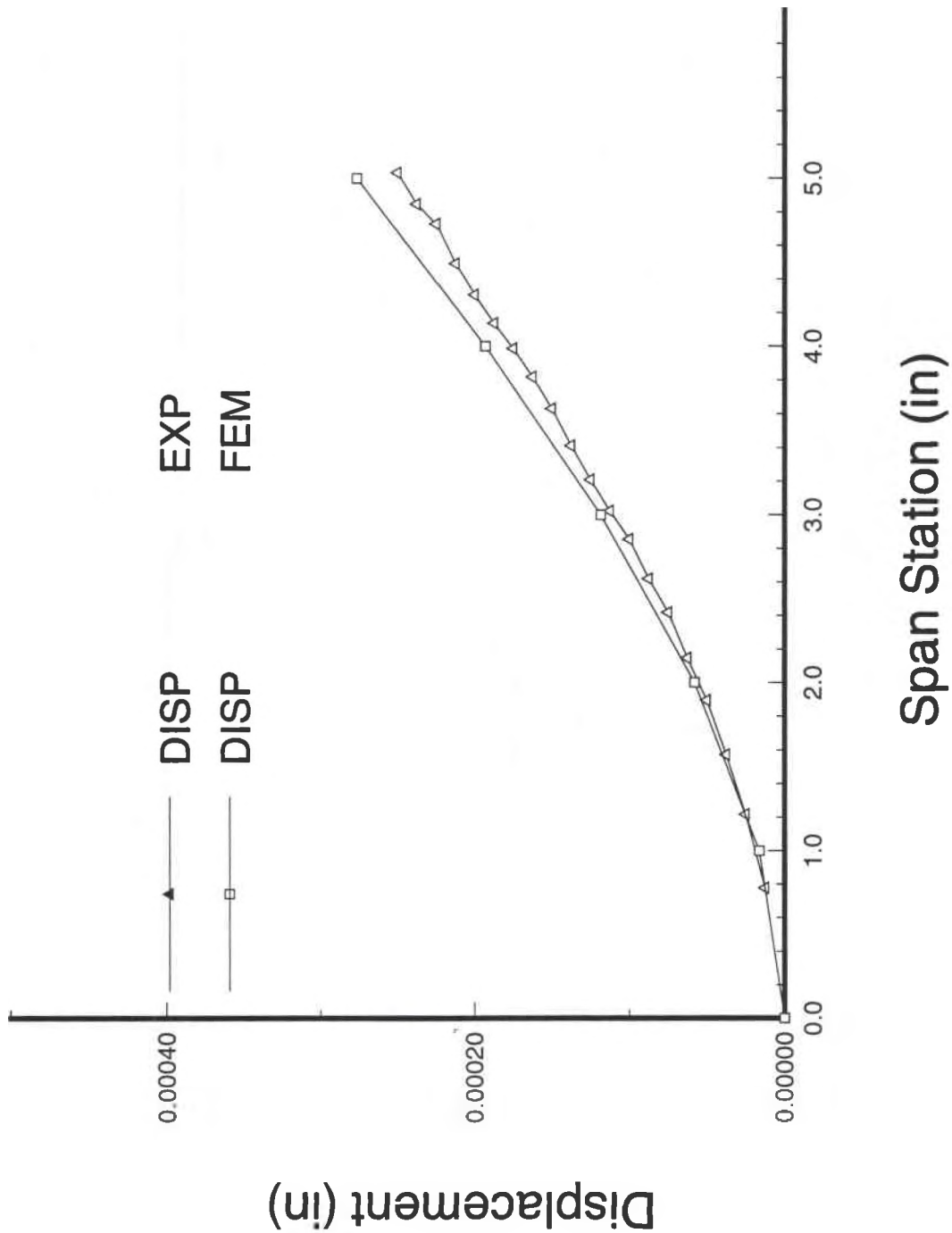


**Figure 50** - Example Static Deflections Of A Rectangular Plate

If the experimental technique was good, the measured flexibility matrix should be symmetric. A spot check was performed to see of this was the case. Two points were chosen, point 17 (about mid span along the trailing edge) and point 22 (trailing edge tip). A cubic spline fit of the experimental deformation data was made and the experimental deflections normalized for a unit load. Results using both experimental and analytical data are presented in Table 16. For these points, the measured flexibility coefficients are about as close as the calculated ones. Though, not conclusive, this is an indication that the experimental technique was good.

Table 16
Flexibility Coefficients For Points 17 and 20

| | Disp at 17 due to load at 22 | Disp at 22 due to load at 17 |
|---|---|---|
| Experimental | .00612 | .00601 |
| Calculated | .0078 | .00759 |

If the difference was not caused by experimental error, the next thing to be considered is modelling error. There are a limited number of sources of modelling error. A potentially significant one is joint stiffness. There is an excess of material around the joints. In some cases, the excess is great enough that the beams involved are effectively shortened. The stiffness of a beam is a cubic function of length, so a 7.7% decrease in length results in a 25% increase in stiffness. Several of the joints had enough excess material around them that the finite element representation was modified to include short rigid elements extending from the joint grid point to .25 inches from the grid point.

There was slight increase predicted stiffness, but not enough to account for the difference. Another modelling error considered was a difference between the actual and assumed values of the Elastic modulus of the steel. No sample coupons were machined from the material used to make the test structure, so the elastic modulus used was from a handbook. The elastic modulus of steel alloys does not vary greatly, though, and it seem very unlikely that a difference as large as this could be accounted for this way.

The finite element input file was checked by hand to make sure that the element sizes were input correctly and that moments of inertia were input correctly. There were a few minor differences, mostly due to round off, but nothing that would account for the differences observed. The next step was to perform modal tests on the structure. Excess stiffness in the structure would show up in the form of natural frequencies being higher than predicted.

## 5.3 Modal Testing

### 5.3.1 Modal Characteristics Of Wing Before Mass Balancing

The video holography system was used to measure the first three natural frequencies and the mode shapes of the wing before the concentrated masses were added at the grid points. The Frequencies are presented in Table 15. Also presented are frequencies predicted by a finite element model of the beam lattice structure. It should be noted that this model was slightly more refined than the one used for predicting static deflections. This was thought necessary because the cubic polynomial shape functions used for the individual beam elements in the finite element model are exact representations of a deformed beam, but only an approximation of the mode shape of a vibrating beam element (which, for a continuous beam, contains hyperbolic functions). The model was refined by roughly doubling the number of spanwise grid points. The rigid elements at some of the joints described earlier were retained.

Correlation between analysis and experiment was very good. This indicates that the stiffness of the test structure is close to that predicted by the finite element model. The next step was to add concentrated masses and perform another modal test.

Table 17
Measured Natural Frequencies of Wing Before Mass Balancing

| Mode | Experimental Frequency (hz) | Predicted Frequency (hz) | % Error |
|---|---|---|---|
| 1 | 77.0 | 79.6 | 3.2 |
| 2 | 227.9 | 226.6 | -.57 |
| 3 | 262.2 | 261.9 | -.11 |

A hologram is presented for only one mode shape. There is so little surface area on the structure to reflect light that it is very difficult to identify fringe lines from a dynamic test. Figure 51 shows a hologram showing a node line and fringes of the third mode shape since it was the clearest of the group. The white area near the root is a region where there is very little motion. The white area near the tip is the node line where it crosses some of the structure. The node line for this mode runs roughly parallel to the trailing edge from about the half span station outward. From the root to the half span station, it is roughly perpendicular to the root. The node line location compares well with the numerical prediction presented in Figure 22.

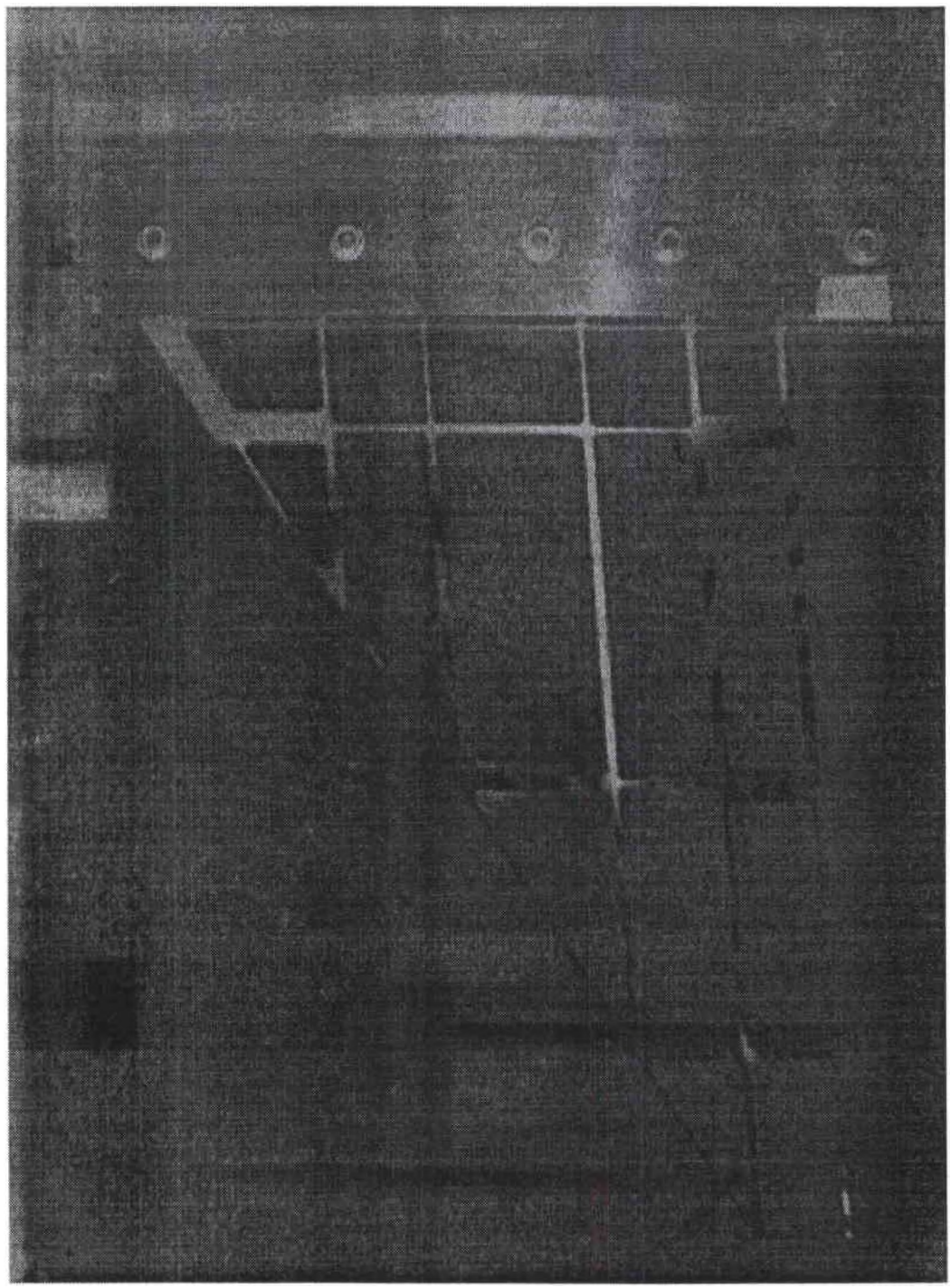

**Figure 51** - Third Normal Mode Before Mass Balancing

### 5.3.2 Modal Characteristics of Wing After Mass Balancing

A set of balancing weights was machined to match the weights presented in Table 10 and attached to the wing at the joints. The specified and actual weights are presented in Table 18. Modal testing was then done using the video holography system described earlier. The experimental and analytical natural frequencies are presented in Table 19.

Table 18
Specified and Actual Values of Balance Weights

| Number | Design Wt (gm) | Measured Wt (gm) |
|---|---|---|
| 1 | 1.730 | 1.70 |
| 2 | 17.231 | 17.05 |
| 3 | 17.104 | 17.05 |
| 4 | 17.527 | 17.32 |
| 5 | 18.193 | 17.95 |
| 6 | 19.383 | 19.15 |
| 7 | 14.530 | 14.24 |
| 8 | 18.158 | 17.94 |
| 9 | 21.835 | 21.67 |
| 10 | 26.527 | 26.28 |
| 11 | 26.440 | 26.24 |
| 12 | 20.119 | 19.94 |
| 13 | 22.307 | 22.19 |
| 14 | 22.500 | 22.43 |
| 15 | 21.660 | 21.46 |
| 16 | 21.274 | 21.09 |

Table 19
Natural Frequencies After Mass Balancing

| Mode | Experimental Frequencies | Computed Frequencies | % Difference |
|---|---|---|---|
| 1 | 39.54 | 37.87 | -.87 |
| 2 | 127.3 | 118.7 | -7.2 |
| 3 | 164.9 | 150.0 | -9.9 |

The frequencies in Table 19 are slightly different from those in Table 9. This is because slightly different finite element models were used. The analytical frequencies presented here were generated using the refined model with rigid joints. The frequencies in Table 9 were computed using a model which did not account for excess joint stiffness.

Agreement between test and analysis was not as good as it was before the masses were added. Agreement for the first mode was good, but it deteriorates as the frequencies get higher. Agreement for the higher modes not presented in the table was steadily worse as frequency increased.

The temptation is to conclude that the structure is not too stiff and that the finite element model is not refined enough. If this were true, however, one would expect the analytical frequencies to be higher than the experimental ones. The conclusion from this modal test is that either the stiffness of the structure is too high or the mass is too low. The only difference between the mass during this test and that during the previous modal test is the balance weights. It has already been shown that they match the design weights very closely, so they are probably not the cause of the difference.

The problem now is that there are four sets of data, two of which indicating the stiffness of the structure is as predicted and two which indicate the stiffness of the structure is too high. Leaving the problem at this stage is unacceptable; a more concrete explanation of the test results is necessary. Thus, an additional round of testing on simpler structures was undertaken.

## 5.4 Simplified Model Structure

### 5.4.1 Testing Simplified Truss Structures

It became apparent from the static and modal testing performed on the model structure that the increased stiffness was a real effect that was not being accounted for in the finite element model. A number of possible sources of error were considered with no obvious conclusion. Eventually, it seemed that the best course of action would be to fabricate some simpler structures and test them to try to isolate the error. Accordingly, two very similar beam structures were fabricated from aluminum. Both had the same geometry, the only difference being that one of them had varying element heights. A plan view is shown in Figure 53. It is important to note that the structure with varying element heights was machined so that one side was flat and the other was stepped. This was done

to see if the asymmetry about the midplane of the structure was the cause of the difference between analytical and experimental results.

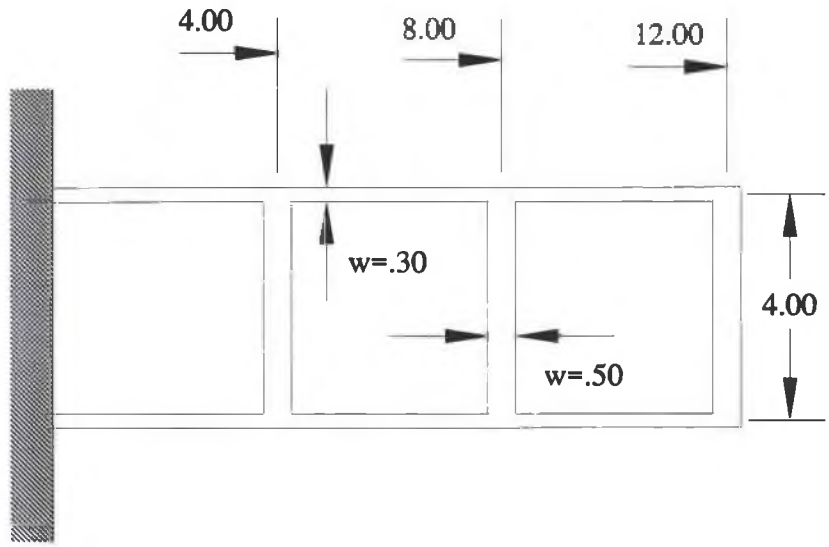


**Figure 52** - Layout of Three Bay Beam Structure

The design of the simpler test structures was intended to remove as many extraneous effect as possible and allow study of a single possible culprit. To observe the effect of varying element height, one structure has constant element height and the other does not. The comparison between analytical and experimental results for the two structures was intended to give an indication about whether modelling the different element heights is the problem.

To keep the geometry simple, there is no sweep and all elements are one of two widths. In addition, there are only nine elements in the structure. This was done to make modelling the structure as simple as possible, particularly if there was a need to use solid elements.

Modal and static testing were both performed using the video holography system. For expediency, mode shapes were obtained using the video system rather than a photographic system. One of the concerns in selecting the element widths was to make sure there was enough surface area that the relatively low resolution video system would yield good images. On the previous model structure, there was very little surface area and getting good fringe information, even when using photographic methods, proved to be a problem.

The object of testing these two structures was to make a comparison with analysis and find possible modelling errors. To do this, several different math models were developed. All used 6 DOF beam elements in increasingly refined meshes. The first used a single element for each bay. The second uses two elements per bay and the third uses four elements per bay. The three models are presented in Figures 54, 55 and 56.

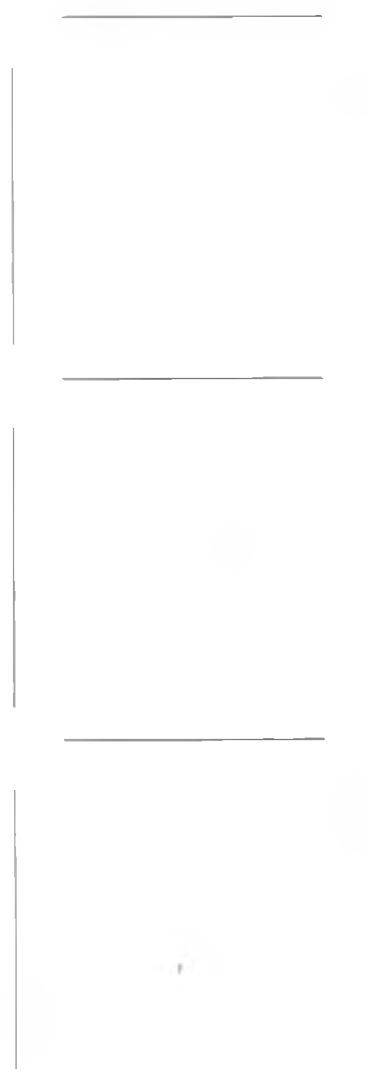

**Figure 53** - Single Element/Bay Finite Element Model

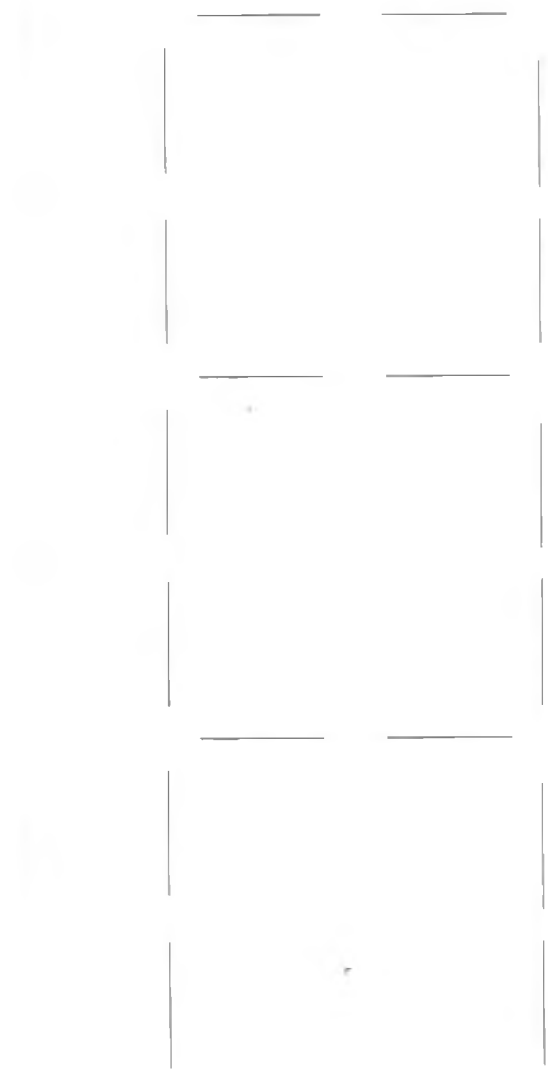

**Figure 54** - Two Element/Bay Finite Element Model

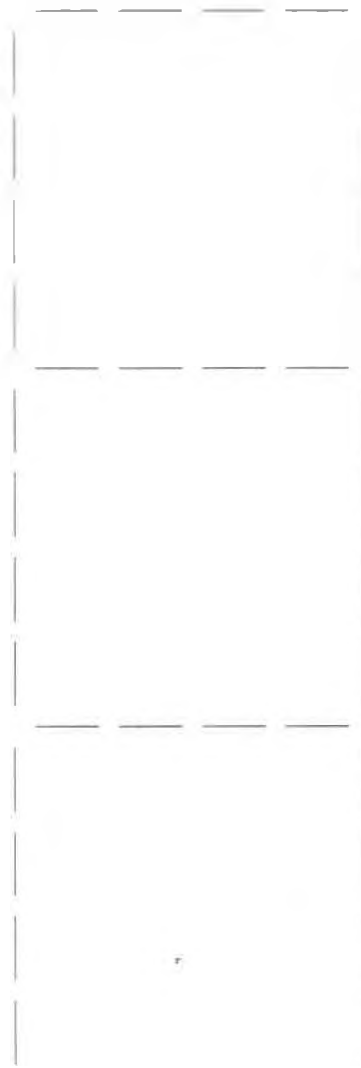

**Figure 55** - Four Element/Bay Finite Element Model

### 5.4.2 Static Testing of Ladder Structures

As with the wing model structure, the first step in testing the ladder structures was static testing. Static test procedures for the ladder structures were similar to those used for the wing model except that the video system replaced the photographic setup. The string and weight arrangement was used for load application. The load was applied at the center of the tip cross piece. This was done to keep the loading symmetric about the centerline axis of the structure, thus eliminating torsional loading. The weight used was a single small nut which weighed 3.0752 gm.

The first static test was performed on the even height structure. Figure 57 presents deflections along the upper beam due to a load applied at the tip as measured by experiment and calculated with the 4 element/bay finite element model. There is a slight difference between the two results, but the agreement is good. The likely reason for the slight difference is that the excess joint stiffness was not modelled in the finite element model.

The second static test was performed on the stepped structure. Figure 58 presents the deflections along the upper beam due to a load applied at the tip. Note that the difference between the analytical and experimental results is much more pronounced for this case than for the even height structure. The only difference between the two structures is the height of the elements and the fact that the second structure was not symmetric about the

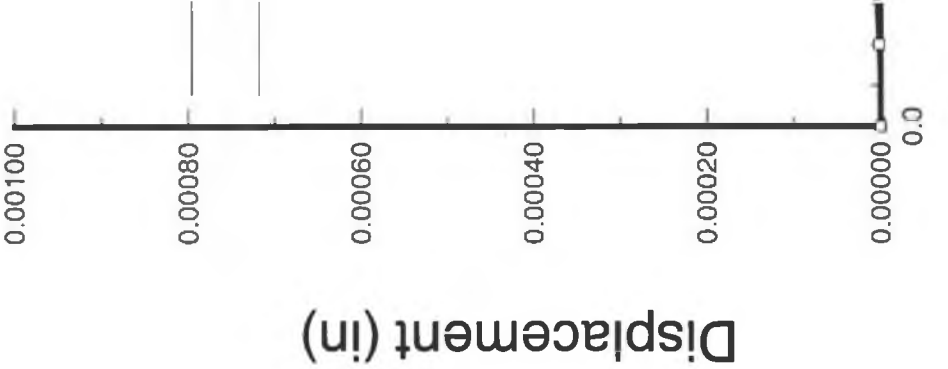


**Figure 56** - Deflections of Even Height Ladder Due to Tip Loading

DISP EXP

DISP FEM

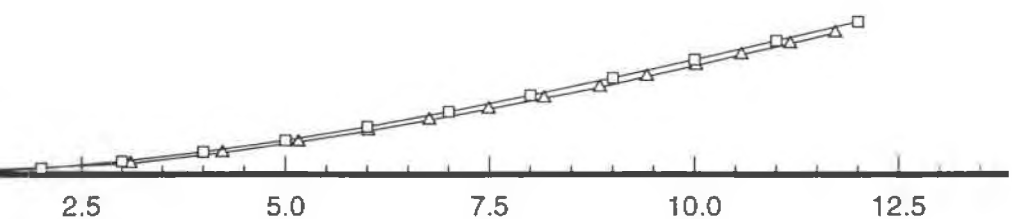


Span Station (in)

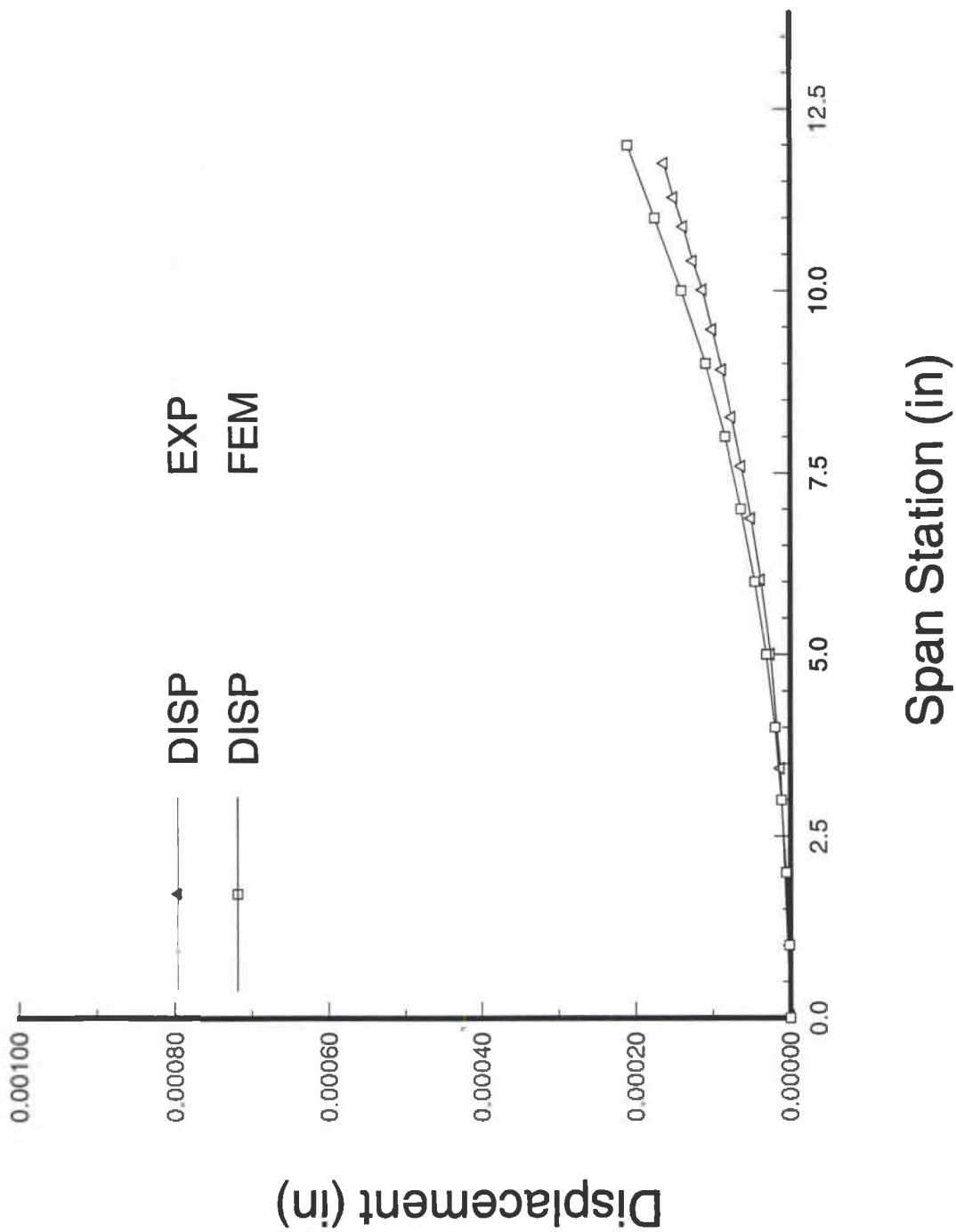


**Figure 57** - Deflections Due to Tip Loading of Stepped Ladder Structure

midplane. This is a strong indication that similar asymmetry in the wing model structure was the cause of the increased stiffness recorded during static testing.

### 5.4.3 Modal Testing of Ladder Structures

Procedures for modal testing were similar to those used for the wing model except that the video system replaced the photographic system. Acoustic excitation was used for both structures. Table 20 presents the experimental and analytical natural frequencies for the even height structure. Analytical results are presented for the three different finite element models discussed above. The percent difference column presents differences between experiment and analysis using the 4 element/bay model.

Table 20
Natural Frequencies For Constant Height Structure
Finite Element Results

| Mode | Exp | 1 Element | 2 Elements | 4 Elements | % Difference |
|---|---|---|---|---|---|
| 1 (1B) | 49.3 | 49.65 | 49.38 | 49.58 | -.58 |
| 2 (1T) | 221.8 | 217.5 | 203.2 | 213.6 | 3.7 |
| 3 (2B) | 309.7 | 308.2 | 304.4 | 306.9 | .90 |
| 4 (1T2B) | 731.7 | 716.5 | 658.0 | 698.4 | 4.6 |
| 5 (3B) | 825.7 | 820.7 | 812.8 | 813.0 | 1.5 |

Correlation between analysis and experiment is good. It is noteworthy, however, that correlation is much better for the bending modes than for modes which have a significant

torsional component. It is assumed that this difference is due the approximation used for the torsional moment of inertia for the individual beam elements. The approximation was necessary because there is no closed form expression.

Natural frequencies for the stepped height structure are presented in Table 21. Since run times are short, only the 4 element/bay finite element model was used for these comparisons. Two different runs were made. The first modelled the varying element cross-sections but assumed that the structure was symmetric about the midplane. The second used offsets for the beam elements to model the asymmetry of having a step on one side but not on the other. The natural frequencies for the offset model are the same as those for the model without offsets.

Table 21
Natural Frequencies For Stepped Height Structure

| Mode | Exp | FEM (4 Elements) | % Difference |
|---|---|---|---|
| 1 (1B) | 65.3 | 65.20 | .15 |
| 2 (1T) | 253.8 | 241.7 | 4.8 |
| 3 (2B) | 259.4 | 253.0 | 2.5 |
| 4 (1T2B) | 609.1 | 574.1 | 5.7 |
| 5 (3B) | 654.7 | 644.3 | 1.6 |

It is interesting to note that the correlation between analysis and experiment for the stepped ladder structure is basically as good as it was for the even height structure. At first glance, one would expect that the frequencies for the stepped structure would be higher than analysis by a larger percentage than for the even height structure. The fact that this is not true indicates that in addition to the stiffness effect that is not being

adequately modelled, there is a compensating error in the mass modelling. The modal testing was repeated after tightening the bolts in the clamping fixture to make sure that the boundary conditions were as close to cantilevered as possible. The natural frequency data proved to be very repeatable with differences between tests being less than 1%.

In an effort to double check the results of modelling the structures with beam elements, the even height structure was also modelled using solid elements. Several different models were generated using increasingly refined meshes to check for convergence. The most refined model was very large, having about 2500 grid points. In all cases, however, the modal results from the solid element models were unsatisfactory. Even for the most refined model, the fundamental natural frequency differed from that of the beam models by about 40%. Even larger models are possible, but would require excessive computer time for a limited benefit.

Chapter VI

## Summary and Conclusions

It has been shown, both numerically and experimentally, that mathematical optimization techniques can be successfully employed in designing aeroelastically scaled wind tunnel model structures. After a survey of system identification methods, a set of requirements for a new method applicable to model design was determined. A number of optimization-based model identification methods were then developed and evaluated using a low aspect ratio fighter wing model as a test case. The identification procedures have been developed to make as few assumptions as possible, thus preserving generality. Finally, extensions have been made to the passive structural design methods to include simple feedback control systems and several possible solution methods suggested.

The methods developed here address the requirements of a useful, general identification method in the following ways:

-Complete stiffness and modal information from the full scale structure is not required

-Methods are applicable to any linear structural model

-The model structural representation may have any number of degrees of freedom

-An accurate initial design is not required

-System matrices are physically meaningful

-System matrices are symmetric

-Computed model mode shapes are orthogonal

-The methods generate enough information to fabricate the model structure

-Generality is preserved so that new optimization routines can be easily substituted

-All design variables are physically meaningful parameters

-Both passive and active elements may be included in the model design

The design of the passive structure was separated into two discrete steps. In the first phase, elements are sized so that the stiffness of the structure matches some desired value. In the second, concentrated masses are sized so that the resulting system has the desired frequencies and mode shapes. Several different approaches were used for the stiffness design and most of them worked at one time or another. Method four gave the best results. It consistently converged to designs which had lower error function than the other methods. Method five proved to be unacceptable. It did not consistently converge to a usable answer and consistently gave designs with higher error function than the other methods.

Both constrained and unconstrained optimization methods were evaluated for stiffness design of the passive model. The methods which used unconstrained minimization

techniques appeared to show quick initial convergence and were relatively insensitive to the initial design. Alternatively, the methods which included constraints seemed to converge to a better overall design more consistently. The approach which seemed to work the best was to use unconstrained minimization techniques initially and then use the resulting design as input for one of the constrained techniques.

Convergence was typically fairly quick at first, but slowed down greatly as the objective function neared the final value. It was common to take a few hundred analyses and a few dozen gradient calculations to reach a final design. This performance would not be acceptable in a production environment where a large number of designs were needed. However, the model design process is one in which each job is unique, and the extra CPU time needed for convergence is not considered a problem.

Mass design of the passive structure proved to be less difficult than did stiffness design. Two separate methods were developed and evaluated. The original mass design method matched only frequencies, using unconstrained minimization and a squared error function based on natural frequencies as an objective function. The rationale was that if the stiffness characteristics are correct and the natural frequencies are correct, the mass must be correct. This was unsatisfactory since the natural frequencies were not sensitive to the masses on the inboard part of the structure. By matching only natural frequencies, it was possible to match the desired number of natural frequencies closely, but have the wrong total mass. The mode shapes were qualitatively similar, but the node lines were not

located accurately. The result was that the computed flutter results were not close to the desired results.

The successful method used a constrained minimization method (Interior Penalty Function) with an objective function made of a squared error function based on the eigenvectors. Squared frequency error and total structural mass were used to make up a set of constraints. Convergence was not always possible if the initial design was far from the final design. In practice, the initial design was changed by hand until the fundamental frequency was in the neighborhood of the desired value. The result was then used as the input for the mass design program.

A 1/10 scale structural model was built and tested to validate the new design methods. There are some uncertainties involved in the step from the finite element model of the scaled structure to the actual test article. Testing of a sample structure showed that the assumptions made in the mathematical modelling were not unreasonable. Two series of static tests were performed to measure the stiffness of the structure. The first measured the deflections of the structure due to applied displacements and showed the stiffness to be correct to within a constant multiplier. That is, when the two curves were normalized to tip displacements of 1.00, the displacement curves were almost identical.

The second set of tests measured the displacements due to an applied load. The correlation between the results of this test and the analytical prediction were not very

good; there was constant difference between the two of about 25%. The difference was shown to result from differences between the finite element model of the scaled structure and that which was fabricated.

To identify the cause of the difference between experimental and numerical displacement predictions, two simple plane frame structure were fabricated. One had constant height elements. The other had varying element heights with one side of the structure being stepped and the other being flat. Experimentally derived displacement data agreed well with numerical predictions for the constant thickness frame and differed significantly for the stepped thickness frame. Since, the two specimens were identical but for the thickness differences, it was determined that elastic offset was not being modelled correctly.

Two sets of dynamic tests were performed. The first determined the natural frequencies of the bare wing structure without mass balance weights and the second determined the natural frequencies after the weights had been added. The experimentally determined frequencies of the bare structure agreed very well with analysis, particularly after the rigid joints were added to the finite element model. Results from the modal tests matched numerical predictions more closely before the tuning masses were added than after. Table 16 shows that the largest difference between test and analysis before the masses were added was about 3%. After they were added, the maximum difference increased to about 10%.

## 6.1 Possibilities For Further Work

The methods developed here worked well on the test case. There are issues which should be addressed. These include:

-Convergence is too slow. This is tolerable for a specialized application like model design, but not for a truly general method

-Repeated roots are not accounted for yet

-Mode switching may be a problem is the initial design is far from the final design

-The equations of motion must be partitioned to allow for free-free boundary conditions

-Stress constraints were not addressed

Methods of addressing mode switching have been proposed and shown to alleviate some convergence problems. The problem of repeated roots has also been addressed. Citations in the literature were presented earlier. The problem of stress constraints is not as straightforward as it may initially appear.

A model with the correct mass and stiffness properties which will reach yield stresses during the course of a wind tunnel test is not of much use. Adding stress constraints to the design problem must be done carefully, however, because of the obvious relationship between displacements and stresses. If stress constraints were to be added to the design process, it is quite likely that some shape optimization capabilities must be included as

well. The only way to decrease stresses which maintaining the desired stiffness properties is to vary the geometry of the structure.

The last section in almost any research report suggests follow-on work and this one is no different. In the course of doing this work, some obvious extensions have become apparent. The first is a more systematic examination of the modelling problems encountered with beam lattice structures such as the one used in this effort. A comparison of different finite element modelling techniques and an examination of the effects of joint stiffness would be good areas of concentration. Beam structures are used extensively for low speed models, but can be deceptively difficult to analyze correctly.

A problem which was addressed in only a cursory way is that of choosing which of the available grid points are necessary to successfully design the model structure. A small subset was used for this effort and was chosen using a largely intuitive process. It may be possible to conduct an analysis to show whether the desired stiffness properties could be modelled using the chosen structural geometry.

For any complete model design, it is necessary to examine the effect of adding an aerodynamic covering to the structure. This might consist of balsa or foam glued to the metal structure and sanded to the correct aerodynamic shape. This relatively soft material could then be skinned with some covering ranging from a flexible model airplane covering (like Monokote) to something more structurally significant like fiberglass. In

any case, the aerodynamic covering will have an effect on the mass and stiffness properties of the complete wing and should be taken into account in the design process. It has been assumed here that the aerodynamic covering is light and flexible compared to the rest of the structure, but it would be helpful if some provision were made for cases in which this is not true.

A problem which emerged was that the beam structures used in this effort might not always be light enough for a given stiffness. This is obvious from the discussion of scaling laws. An effort was made to design the structure of an aeroelastic model of the NASP wing made it more clear. The scaling laws required that the final model be very stiff and very light. It was found that a structure made of beams could not meet both constraints. Accordingly, it would be useful if this method were extended to some type of structure which is lighter for a given stiffness than a beam structure. The two obvious choices are a conventional built up structure and a composite sandwich structure

Two different approaches appear possible. In the first approach, the structure is assumed to form the aerodynamic envelope (stressed-skin structure) and the skin thickness could be varied to change stiffness characteristics. In the second approach, the skin thickness is assumed to be constant and the wing thickness (distance between top and bottom skins) at various points on the wing is used for the design variables. This might make fabrication easier, but would require and aerodynamic covering over the structure.

Another intriguing possibility is that of introducing shape optimization into the design process. The methods presented here do not alter the basic structural configuration proposed by the designer. While this is usually a guess and is almost certainly not the optimum configuration, no method has been developed for altering it in any rational way. Since the model is based on the discretized representation of the full size structure, the shape optimization process would have to make use of the discrete grid points available and model grid points could not be treated as continuous variables.

An alternative approach is to use a surface fitting technique to eliminate the dependency on scaling down the full size structure grid point locations. If this were the case, the grid point locations of the scaled model representation could be treated as continuous variables.

The subject of complex eigenvalues and eigenvectors was not treated rigorously in this work, but is another source of follow on work. Any real structure has damping associated with it, even though it may be small. The ability to model such damping in a methodical way is of benefit. The addition of velocity feedback terms to the control system adds apparent damping. It is reasonable to expect full scale structures involving active structural elements to have complex response properties which would have to be duplicated by the aeroelastically scaled model.

Concentrated masses were modelled by adding the mass values to the diagonal elements of the mass matrix. The mass balancing process would be more flexible, however, if a method were developed to change the non-diagonal elements. In physical terms, this means adding a balancing weight which changes the effective mass properties at two grid points.

## References


1. Bisplinghoff, R.L., Ashley, H. and Halfman, R.L.; "Aeroelasticity"; Addison-Wesley; 1955.

2. Wasserman, L.; "Flutter Model Design", undated, no reference number

3. Rogers, W.A., Braymen, W.W. and Murphy, A.C., Graham, D.H. and Love, M.H.;" Validation of Aeroelastic Tailoring by Static Aeroelastic and Flutter Tests, Volume I - Model Design and Fabrication"; AFWAL-TR-81-3160; February 1982.

4. Pendleton,E.W., Lee, M.R. and Wasserman, L.; "A Low Speed Flexible Model Simulating an F-16 Derivative Design"; WRDC-TR-90-3038; January 1991.

5. Keller, C.L.; "Methods For Determining Modal Parameters and Mass, Stiffness and Damping Matrices"; AFFDL-TR-78-59; June 1978.

6. Keller, C.L.; "Determination of Complex Characteristic Values and Vectors From Sinusoidal Excitations at Near Resonance Frequencies"; AFWAL-TR-80-3136; June 1981.

7. Ibrahim, R.S. and Saafan, A.A.; "Correlation of Analysis and Test in Modelling of Structures Assessment and Review"; nth IMAC (1986 or later); pp 1651-1660.

8. Berman, Alex and Flannely, William G.;" Theory of Incomplete Models of Dynamic Structures"; AIAA Journal; Vol 9, No 8, August 1971; pp 1481-1487.

9. Greville, T.N.E; "The Pseudoinverse of a Rectangular or Singular Matrix and its Application to the Solution of Systems of Linear Equations"; SIAM Review; Vol 1, No 1, January 1959.

10. Albert, Arthur; "An Introduction and Beginner's Guide to Matrix Pseudo-Inverses"; ARCON-Advanced Research Consultants; Lexington MA, July 1964.

11. Pilkey, W.D. and Cohen, R., editors; "System Identification of Vibrating Structures"; American Society of Mechanical Engineers, 1972.

12. Gravitz, S.I., "An analytical Procedure for Orthogonalization of Experimentally Measured Modes"; Journal of the Aerospace Sciences; Vol 25, Nov 1958, pp 721-722.

13. Rodden, W.P.; "A Method For Deriving Structural Influence Coefficients From Ground Vibration Tests"; AIAA Journal; Vol 5, No 5, May 1967; pp 991-1000.

14. Baruch, Menahem and Bar Itzhack, Itzhack Y.; "Optimal Weighted Orthogonalization of Measured Modes"; AIAA Journal; Vol 16, No. 4, April 1978, pp 346-351.

15. Baruch, Menahem; "Optimization Procedure to Correct Stiffness and Flexibility Matrices Using Vibration Tests"; AIAA Journal, Vol 16, No 11, November 1978, pp 1208-1210.

16. Wei, Fu-Shang; "Stiffness Matrix Correction From Incomplete Modal Data"; AIAA Journal; Vol 18, No 10, October 1980, pp 1274-1275.

17. Berman, Alex; "Mass Matrix Correction Using an Incomplete Set of Measured Modes"; AIAA Journal, Vol 17, No 10, October 1979, pp 1147-1148.

18. Berman, A. and Nagy, E.J.; "Improvement of a Large Analytical Model Using Test Data"; AIAA Journal; Vol 21, No. 8, August 1983, pp 1168-1173.

19. Guyan, R.J.; "Reduction of Mass and Stiffness Matrices"; AIAA Journal, Vol 3, No 2, p380, February 1965.

20. Kabe, Alvar M.; "Stiffness Matrix Adjustment Using Mode Data"; AIAA Journal, Vol 23, September 1985, pp 1431-1436.

21. Caesar, Bernd; "Updating System Matrices Using Modal Test Data"; Proceedings, nth IMAC (1986 or later) ; pp 453-459.

22. Liping, H., Kecheng, C. and Zhandi, X.; "Method for Modifying Structural Dynamic Model by Means of Incomplete Complex Modes Identified From Experimental Data"; Proceedings, 4th International Modal Analysis Conference, Los Angeles, CA, 1986, pp 434-437.

23. Coppolino, R.N. and Stroud, R.C.; "A Global Technique for Estimation of Modal Parameters From Measured Data"; Proceedings, 4th International Modal Analysis Conference, Los Angeles, CA, 1986, pp 674-681.

24. Ojalvo, I.U.; "Contrasts in Two Classes of Structural Dynamic Correlation Procedures"; Proceedings, 4th International Modal Analysis Conference, Los Angeles, CA, 1986, pp 81-87.

25. Collins, J.D., Hart, G.C., Hasselman, T.K. and Kennedy, B.; "Statistical Identification of Structures"; AIAA Journal; Vol 12, No 2, February 1974, pp 185-190.

26. Dobson, B.J.; "Modification of Finite Element Models Using Experimental Modal Analysis"; Proceedings, Second International Modal Analysis Conference, Vol B, Orlando FL, 1984.

27. Berman, Alex; "System Identification of Structural Dynamic Models - Theoretical and Practical Bounds"; Proceedings, 25th AIAA Structural Dynamics and Materials Conference; Palm Springs, CA; AIAA Paper 84-0929, May 1984.

28. Sidhu, J. and Ewins, D.J.; "Correlation of Finite Element and Modal Test Studies of a Practical Structure"; Proceedings, 2nd International Modal Analysis Conference, Orlando, FL, pp 756-762, 1984.

29. Gysin, H.P.; "Critical Application of the Error Matrix Method for Localization of Finite Element Modelling Inaccuracies"; Proceedings, 4th International Modal Analysis Conference, Los Angeles, CA, 1986, pp1339-1343.

30. Steinwender, F. and Nordman, R.; "Parameter Adjustment of a Finite Element Model by Means of Measured Natural Frequencies"; Proceedings, 4th International Modal Analysis Conference, Los Angeles, CA, 1986, pp 795-801.

31. Ojalvo, I.U. and Pilon, D.; "Diagnostics for Geometrically Locating Structural Math Model Errors From Modal Test Data"; Proceedings, 29th AIAA structures, Dynamics and Materials Conference, Orlando, FL, Feb 1988, pp 1174-1186 (AIAA paper 88-2385).

32. Ojalvo, I.U., Ting, T., Pilon, D. and Twomey, William; "Practical Suggestions for Modifying Math Models to Correlate With Actual Modal Test Results"; Proceedings, 7th SEM International Modal Analysis Conference, Las Vegas, NV, 1989, pp 347-354.

33. Ojalvo, I.U. and Ting, T.; "An Interpretation and Solution of Ill-Conditioned Linear Algebraic Conditions"; Proceedings, Second NASA/Air Force Symposium on Multidisciplinary Analysis and Optimization, Hampton, VA; Sept 1988.

34. Wei, Max L. and Janter, Theo; "Optimization of Mathematical Model Via Selected Physical Parameters"; Proceedings, 6th SEM International Modal Analysis Conference, Kissimee, FL, 1988, pp 73-79.

35. Ewing, M.S. and Venkayya, V.B.; "Structural Identification Using Mathematical Optimization Techniques"; Proceedings, 32nd AIAA Structural Dynamics and Materials Conference; Baltimore, MD; April 1991; AIAA Paper 91-1135.

36. Ewing, M.S. and Kolonay,R.M.; "Dynamic Structural Model Modification Using Mathematical Optimization Techniques"; Proceedings, Computer Aided Optimum Design of Structures 91, Boston, MA, pp 285-295.

37. Gibson, Warren C.; "ASTROS-ID: Software For System Identification Using Mathematical Programming"; WL-TR-92-3100; September 1992.

38. Hunt, D. and Blelloch, P.A.; "Direct Correlation of Test-Analysis Cross-Orthogonality"; presented at Aerospace Flutter and Dynamics Council Meeting, Dayton, OH, 16 October, 1992.

39. West, Walter M.; "Illustration of the Use of Modal Assurance Criterion to Detect Structural Changes in an Orbiter Specimen"; Proceedings, 4th International Modal Analysis Conference, Los Angeles, CA, 1986, pp 1-6.

40. Alemang, R.J. and Brown, D.L.; "A Correlation Coefficient for Modal Vector Analysis"; Proceedings, 1st International Modal Analysis Conference, Nov 1982.

41. Pappa, R.S. and Ibrahim, S.R.; "A parametric Study of the Ibrahim Time Domain Modal Identification Algorithm"; The Shock and Vibration Bulletin, Vol 51, No 3 pp 43-51, 1981.

42. Badenhausen, K.; "Time Domain Identification of Incomplete Physical System Matrices Using a Condensed Estimation Equation"; Proceedings, 4th International Modal Analysis Conference, Los Angeles, CA, 1986, pp 402-408.

43. Batill, S.M. and Hollkamp, J.J.; "Time Series Modelling For Structural Response Prediction"; AFWAL-TR-88-3114; November 1988.

44. Hollkamp, J.J. and Batill, S.M.; "Automated Parameter Identification and Order Reduction for Discrete Time Series Models"; AIAA Journal; Vol 29, No 1, January 1991, pp 96-102.

45. Zavodney, L.D. and Hollkamp, J.J.; "Experimental Identification of Internally Resonant Nonlinear Systems Possessing Quadratic Nonlinearity"; Proceedings, 32nd AIAA/ASME/ASCE/AHS/ASC Structures, Structural Dynamics and Materials Conference, Baltimore, MD, April 1991, AIAA 91-1226.

46. Zavodney, L.D.; "The Identification of Nonlinearity in Structural System: Theory, Simulation and Experiment"; Applied Mechanics Review; Vol 44, No 10, Part 2, October 1991.

47. Hollkamp, J.J. and Batill, S.M.; "Structural Identification Using Order Overspecified Time Series Models"; Journal of Dynamic Systems, Measurement and Control; Vol 114, March 1992, pp 27-33.

48. Hollkamp, J.J.; "Multiple-Input Multiple-Output Time Series Models From Short Data Records"; To Appear in the Journal of Guidance, Control and Dynamics.

49. McIntosh, S.C. and Eastep, F.E.; "Design of Minimum Mass Structures With Specified Stiffness Properties"

50. McCullers, L.A. and Lynch, R.W.; "Dynamics of Advanced Filamentary Composite Structures, Volume II - Aeroelastic Synthesis Procedure Development"; AFFDL-TR-73-111; Sept 1974.

51. Wilkinson, K., Markowitz, J., Lerner, E., Chipman, R., George, D., et al.; "An Automated Procedure for Flutter and Strength Analysis and Optimization of Aerospace Vehicle Structures, Volume I - Theory and Application"; AFFDL-TR-75-137; December 1975.

52. Johnson, E.H. and Venkayya, V.B.;" Automated Structural Optimization System (ASTROS), Volume I - Theoretical Manual"; AFWAL-TR-88-3028; December 1988.

53. Honlinger, H., Mussman, D., Manser, R. and Huttsell, L.J.; "Development and Flight Test of an Active Flutter Suppression System For The F-4F With Stores - Parts I-III"; AFWAL-TR-82-3040; September 1982.

54. Sensburg, O., Honlinger, H., Noll, T.E. and Huttsell, L.J.; "Active Flutter Suppression On An F-4F Aircraft"; Journal Of Aircraft; Vol 19, No 5, May 1982, pp 354-359.

55. Hwang, C. and Johnson, E.H.; "Test Demonstration Of Digital Adaptive Control Of Wing/Store Flutter - Parts I and II"; AFWAL-TR-82-3044; July 1982.

56. Winther, B.A., Cowan, D.L. and Joshi, D.S.; "Adaptive Flutter Suppression System Design And Simulation"; AFWAL-TR-86-3020; May 1986.

57. Peloubet, R.P., Bolding, R.M. and Penning, K.B.; "Adaptive Flutter Suppression Wind Tunnel Demonstration"; AFWAL-TR-3053; October 1987.

58. Johnson, E.H., Hwang, C., Joshi, D.S., Harvey, C.A., Huttsell, L.J. and Farmer, M.G.; "Adaptive Flutter Suppression - Analysis and Test"; Proceedings, AGARD 55th Structures and Materials Panel Meeting, AGARD-R-703, September 1982.

59. French, R.M.; "An Application of Structural Optimization in Wind Tunnel Model Design"; AIAA 90-0956; Presented at 1990 SDM Conference; April 1990.

60. French, R.M. and Kolonay, R.M.; "An Application of Compound Scaling to Aeroelastic Model Design"; Presented at Third Air Force/NASA Symposium on Recent Advances in Multidisciplinary Analysis and Optimization; Sept 1990.

61. French, R.M. and Kolonay, R.M.; "A Demonstration of Structural Optimization Applied to Wind Tunnel Model Design"; Journal of Aircraft; Vol 29, No 5, September-October 1992, pp 966-968.

62. Vanderplaats, G.N.; "ADS - A FORTRAN Program For Automated Design Synthesis"; NASA CR 172460; Oct 1984.

63. Venkayya, V.B.; "A Generalized Compound Scaling Algorithm For Mathematical Optimization"; WL-TR-92-xxxx; To Be Published.

64. Venkayya, V.B., Tischler, V.A., Kolonay, R.M. and Canfield, R.A.; "A Generalized Optimality Criteria for Mathematical Optimization"; AIAA 90-1192; April 1990.

65. Vanderplaats, G.N.; "An Efficient Feasible Directions Algorithm For Design Synthesis"; AIAA Journal, Vol 22, No 11, Oct 1984, pp 1633-1640.

66. Vanderplaats,G.N.; "Numerical Optimization Techniques for Engineering Design"; McGraw-Hill; 1984.

67. Moore, G.J.; "MSC/NASTRAN V67 Design Sensitivity And Optimization User's Guide", The MacNeal-Schwendler Corporation, 1992.

68. Cassis, J.H. and Schmidt, L.A.; "On The Implementation Of The Extended Interior Penalty Function"; International Journal Of Numerical Methods In Engineering, Vol 10, No 1, 1976, pp3-23.

69. Haftka, R.T. and Stearns, J.H.;"Applications Of A Quadratic Extended Interior Penalty Function For Structural Optimization"; AIAA Journal, Vol 14, June 1976, pp 718-724.

70. Nelson, R.B.; "Simplified Calculation of Eigenvector Derivatives"; AIAA Journal, Vol 14, No 9, September 1976, pp1201-1205.

71. Venkayya, V.B.; "Aerospace Structures Design on Computers"; WRDC-TR-89-3045; March 1989.

72. Ojalvo, I.U.; "Efficient Computation of Mode Shape Derivatives for Large Dynamic Systems"; AIAA Journal, Vol 25, No 9; October 1987; pp 1386-1390.

73. More, J.J, Garbow, B.S., Hillstrom, K.E.; "User's Guide to MINPACK 1"; Argonne National Laboratory Publication ANL-80-74, 1980.

74. Smith, H.M., "Principles of Holography", Wiley-Interscience, New York, 1969.

75. Abramson, N., "The Making and Evaluation of Holograms", Academic Press, London, 1981.

76. Kobayashi, A.S. ed, "Handbook on Experimental Mechanics", Prentice-Hall, Englewood Cliffs NJ, 1987.

77. Lokberg, Ole, "Electronic Speckle Pattern Interferometry", Physics Technology, Vol 11, 1980, pp16-22.

78. Lokberg, O.J., Malmo, J.T and Strand, A.; "TV Holography - A Tool For Vibration Measurements", Noise and Vibration Control Worldwide, October 1987, pp286-289.

## Appendix A

Analytical Model Improvement Method Example Problem

The AMI update procedure mentioned previously is representative of many parametric update schemes and is presented here in more detail. The update process uses a Lagrange multiplier optimization approach to minimize error functions which express some measure of difference between measured and analytical matrices. Variables in the optimization problem are the individual elements of the analytical mass and stiffness matrices. It is assumed that there are n degrees of freedom in the analytical model and m degrees of freedom in measured data where m < n.

The basic relationships satisfied during the update process are the modal orthogonality conditions and the eigenvalue equation (for clarity, notation here follows that of the authors)

$$\{\Phi\}^T[M]\{\Phi\} = [I] \tag{43}$$

$$[K][\Phi] = [M][\Phi][\Omega]^2 \tag{44}$$

where [Φ] is an nxm matrix derived in part from test data and [Ω] is an mxm diagonal matrix of measured eigenvalues. [M] and [K] are mass and stiffness matrices of order

n. The first step is to partition the eigenvalue equation written using analytically derived mass and stiffness matrices

$$[M_A][\Phi] - [K_A][\Phi][\Omega]^2 = 0 \tag{45}$$

so that degrees of freedom for which mode shape data was measured are grouped together

$$\left[\begin{bmatrix} K_1 & K_2 \\ K_1^T & K_4 \end{bmatrix} - \omega^2 \begin{bmatrix} M_1 & M_2 \\ M_2^T & M_4 \end{bmatrix}\right] \begin{Bmatrix} \phi_{1_i} \\ \phi_{2_i} \end{Bmatrix} = 0 \tag{46}$$

where i represents the $i^{th}$ measured mode. Solving for the unknown terms $\phi_2$ in terms of the known terms $\phi_1$ results in either of the following equivalent expressions

$$\phi_{2_i} = -[K_2 - \omega_i^2 M_2]^{-1} [K_1 - \omega_i^2 M_1] \phi_{1_i} \tag{47}$$

$$\phi_{2_i} = -[K_4 - \omega_i^2 M_4]^{-1} [K_2^T - \omega_i^2 M_2] \phi_{1_i} \tag{48}$$

At this point, the first m eigenvectors are now of order n, the same order as the analytical model. It is important to remember, though, that analytical mass and stiffness matrices are used to complete the eigenvectors. Thus, if the analytical model is not a reasonably accurate representation of actual structure, the corrected eigenvalues will be suspect.

The next step in the AMI procedure is to correct the analytical mass matrix. The basic idea is to establish some desired property of the corrected mass matrix and find a feasible solution which minimizes some measure of the change between the analytical and

corrected matrices. The mass matrix property which must be satisfied is the eigenvector orthogonality condition

$$[\Phi]^T[M][\Phi] = [I] \tag{49}$$

The error function to be minimized is

$$\varepsilon = \| [M_A]^{-1/2}\left([M]-[M_A]\right)[M_A]^{-1/2} \| \tag{50}$$

Where the double line indicates the sum of the squares of the matrix elements. The orthogonality condition is used to write $m^2$ equality constraints and the method of Lagrange multipliers used to minimize the error function defined in Equation 131. The Lagrange function is written as

$$\Psi = \varepsilon + \sum_{i=1}^{m}\sum_{j=1}^{m} \lambda_{ij}\left([\Phi]^T[M][\Phi]-[I]\right)_{ij} \tag{51}$$

The minimum of the Lagrange function is determined by setting the gradient of $\Psi$ equal to zero where the gradient is written as

$$\left\{\begin{array}{c} \frac{\partial \Psi}{\partial m_{11}} \\ \vdots \\ \frac{\partial \Psi}{\partial m_{ij}} \\ \vdots \\ \frac{\partial \Psi}{\partial m_{nn}} \\ \frac{\partial \Psi}{\partial \lambda_{11}} \\ \vdots \\ \frac{\partial \Psi}{\partial \lambda_{ij}} \\ \vdots \\ \frac{\partial \Psi}{\partial \lambda_{mm}} \end{array}\right\} = 0 \qquad \textbf{(52)}$$

The gradient forms a system of $n^2+m^2$ equations and $n^2+m^2$ unknowns which is then solved for the unknown values of $m_{11}...m_{nn}$ and $\lambda_{11}...\lambda_{mm}$.

The resulting expression for the corrected mass matrix is

$$M = M_a + M_a \Phi m_a^{-1}(I - m_a) m_a^{-1} \Phi^T M_a \qquad \textbf{(53)}$$

Once the mass matrix has been corrected, the stiffness matrix is addressed. The three constraint equations (in matrix form) are

$$[K][\Phi] - [M][\Phi][\Omega]^2 = 0 \qquad \textbf{(54)}$$

$$[\Phi]^T[K][\Phi] - [\Omega]^2 = 0 \qquad \textbf{(55)}$$

Equations 135 and 136 are simply expressions of the eigenvalue equation and equation

$$[K]-[K]^T=0 \tag{56}$$

137 requires that the updated stiffness matrix is symmetric. As with the mass matrix, an error function to be minimized is defined as

$$\varepsilon = \|[M]^{-1/2}([K]-[K_a])[M]^{-1/2}\| \tag{57}$$

The Lagrange function is

$$\begin{aligned}\Psi = \varepsilon &+ \sum_{i=1}^{n}\sum_{j=1}^{m}\Lambda_{1_{ij}}\left([K][\Phi]-[M][\Phi][\Omega]^2\right)_{ij} \\ &+ \sum_{i=1}^{m}\sum_{j=1}^{m}\Lambda_{2_{ij}}\left([\Phi]^T[K][\Phi]-[\Omega]^2\right)_{ij} \\ &+ \sum_{i=1}^{n}\sum_{j=1}^{n}\Lambda_{3_{ij}}\left([K]-[K]^T\right)_{ij}\end{aligned} \tag{58}$$

As before, the gradient of the Lagrange function is set zero and solved for the unknown terms of the stiffness matrix and the multipliers. The corrected stiffness matrix is

$$[K] = [K_a] + ([\Delta]+[\Delta]^T) \tag{59}$$

Where $\Delta$ is

$$[\Delta] = \frac{1}{2}[M][\Phi]\left([\Phi]^T[K_a][\Phi] + [\Omega]^2\right)[\Phi]^T[M] - [K_a][\Phi][\Phi]^T[M] \tag{60}$$

To demonstrate the method, two example problems are presented. In the first, a simple cantilevered beam was modelled using three 4-DOF beam elements as shown in Figure 59.

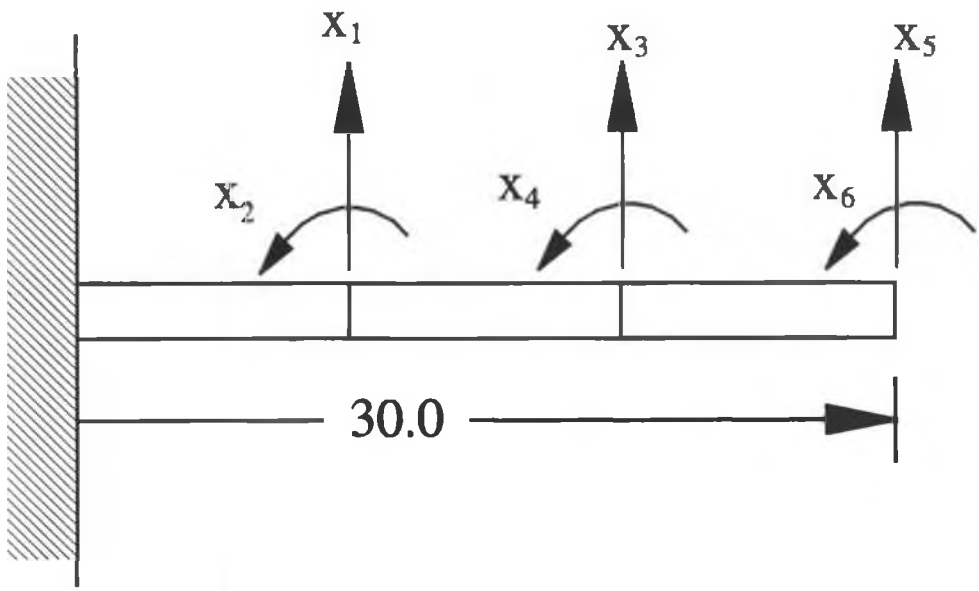


**Figure 58**- Beam Model From Example Problem

The beam was assumed to be made of aluminum with $E=10^7$ and $\rho=.101$ lb/in$^3$. All three elements were assumed to be of square cross section with b=h=.20 in. A complete set of eigenvalues and eigenvectors were calculated for this model and used as if the comprised a set of experimental data. Since experimental data almost never contains as many degrees of freedom as the analytical model, it was assumed that only the displacement degrees of freedom of the first three modes were available to update an analytical model. An analytical model was then constructed with the element sizes deliberately incorrect. The widths of the elements were not modified, but the heights, in order from root outward, were .20, .18 and .16 inches. The natural frequencies for the

model assumed as experimental data and the model to be corrected are presented in table 22.

Table 22

Natural Frequencies For Nominal and Perturbed Analytical Models

| Mode | Original(Hz) | Perturbed(Hz) |
|---|---|---|
| 1 | 7.0193 | 7.4943 |
| 2 | 44.1291 | 41.0749 |
| 3 | 124.6929 | 111.087 |

The first step of the AMI procedure is to calculate eigenvectors of order n for each of the measured modes. These were then compared with those from the original model and the results presented in Table 23. It is important to recall that both sets of eigenvectors are normalized with respect to the mass matrices, not the largest term in the eigenvector.

Table 23
Eigenvector Summary From Beam Example

| Mode | Correct Eigenvector | AMI Predicted Eigenvector | Ratio Correct/AMI |
|---|---|---|---|
| 1 | 18.6896 | 18.6896 | 1.000 |
| | 3.40405 | 3.4466 | .9876 |
| | 61.7517 | 61.7517 | 1.000 |
| | 4.92612 | 4.8319 | 1.1095 |
| | 112.904 | 112.904 | 1.000 |
| | 5.18044 | 5.2052 | .9952 |
| 2 | 66.9963 | 66.9963 | 1.000 |
| | 6.67676 | 6.6798 | .9995 |
| | 48.0954 | 48.0954 | 1.000 |
| | -11.2042 | -11.9759 | .9356 |
| | -113.578 | -113.578 | 1.000 |
| | -18.1156 | -15.3859 | 1.1774 |
| 3 | 84.3938 | 84.3938 | 1.000 |
| | -6.28365 | -16.0236 | .3921 |
| | -74.4174 | -74.4174 | 1.000 |
| | -4.79638 | -2.9368 | 1.6332 |
| | 113.425 | 113.425 | 1.000 |
| | 30.0529 | 2.3257 | 12.9219 |

It is apparent that the approximation used to complete the eigenvectors becomes less accurate at higher modes. This is not surprising, since a model that is only approximately accurate can often match the first couple of natural frequencies and mode shapes while failing for higher modes.

The example worked above may have been somewhat skewed by comparing one set of finite element results to another. Since the analytical solution for cantilevered beam natural frequencies and modes shapes are relatively simple, a set of 'experimental' data

was generated using exact expressions. The analytical frequencies and modal displacements the grid points are presented in Table 24.

Table 24
Analytical Frequencies And Partial Mode Shapes For Beam Example

| Mode | Freq (Hz) | Disp at Grid Points |
|---|---|---|
| 1 | 7.01857 | .33107 |
| | | 1.09388 |
| | | 2.000 |
| 2 | 43.98465 | 1.17928 |
| | | 0.84541 |
| | | -2.000 |
| 3 | 123.1583 | 1.44376 |
| | | -1.2873 |
| | | 2.000 |

Table 25 presents the analytically predicted eigenvectors along with those predicted using AMI and incomplete analytical information. Normalization was done with respect to the largest element of each eigenvector.

Table 25
Analytical and AMI Predicted Eigenvectors

| Mode | Analytical | AMI Predicted | Ratio Exp/AMI |
|---|---|---|---|
| 1 | .16554 | .16554 | 1.000 |
| | .03015 | .03053 | .98755 |
| | .54694 | .54694 | 1.000 |
| | .04363 | .0428 | 1.0194 |
| | 1.000 | 1.000 | 1.000 |
| | .04588 | .0461 | .9952 |
| 2 | -.58964 | -.58964 | 1.000 |
| | -.05875 | -.05925 | .9911 |
| | -.42271 | -.42271 | 1.000 |
| | .09869 | .10579 | .9329 |
| | 1.000 | 1.000 | 1.000 |
| | .15936 | .13520 | 1.1787 |
| 3 | .72188 | .72188 | 1.000 |
| | -.05672 | -.11975 | .4737 |
| | -.64366 | -.64366 | 1.000 |
| | -.03903 | -.03202 | 1.2189 |
| | 1.000 | 1.000 | 1.000 |
| | .26162 | .05462 | 4.7898 |

By definition in the derivation, the first m eigenvalues calculated using analytical system matrices corrected with AMI will match the experimental values. The quality of the expanded eigenvectors is a function of how well the analytical model matches represents the real structure. If the initial model is reasonably accurate, the first m eigenvectors should also be useful for other analyses.

A critical measure of the value of an update scheme is whether the stiffness matrix can be used to calculate displacements which are at least as accurate as those generated by

the analytical model before correction. Ideally, the displacements calculated using the corrected stiffness matrix will match experimental data better than those using the original analytical one. Table 26 shows a comparison of displacement vectors calculated using the exact analytical solution, the 'exact' finite element model, the perturbed finite element model and the stiffness matrices corrected using the analytical solution and the unperturbed finite element model. Displacements are calculated using unit vertical loads at the tip.

Table 26
A Comparison of Calculated Displacements

| DOF | Exact | Initial FEM | Pert. FEM | Corrected (Exact Data) | Corrected (FEM Data Mass Nrm) | Corrected (FEM Data Max Nrm) |
|---|---|---|---|---|---|---|
| 1 | 1.000 | 1.000 | 1.000 | -.00133 | 1.000 | -.0014 |
| 2 | .1875 | .1875 | .1875 | .00149 | .1887 | .0015 |
| 3 | 3.500 | 3.500 | 3.732 | .0009374 | 3.4992 | -.0001252 |
| 4 | .300 | .300 | .3418 | -.00291 | .2945 | -.0031 |
| 5 | 6.75 | 6.75 | 7.638 | .0191 | 6.760 | .0181 |
| 6 | .3375 | .3375 | .4151 | .00958 | .3350 | .0097 |

Using the AMI scheme, the stiffness matrix is only meaningful on its own if eigenvectors are orthonormalized using an analytical mass matrix. In a test situation, the only available mass matrix is that from the uncorrected analytical model.

## Appendix B

Experimental Methods

Two separate sets of tests were performed on the sample model structure, a stiffness test and a modal test. Holographic techniques were used for each test; conventional photographic holography was used for the stiffness testing and some modal testing, while video holography and a laser vibrometer were used for the remainder of the modal testing. This section describes the testing methods used. Before describing the methods used, a brief description of the holographic process is helpful.

Holography is similar to photography in that both methods are used to store an image of some object. They vary significantly in how this is done and in what information is stored. A photograph stores a two-dimensional image of the object. Holography stores information which can be used to recreate the beam of light reflected from the object[74]. This beam has a three-dimensional character. Thus, a hologram appears to be a three-dimensional image of the object.

A hologram can be created using the coherent light beam produced by a laser. The beam is split into two beams, an object beam and a reference beam. The reference beam is

trained directly on a photographic plate while the object beam is reflected off the subject onto the photographic plate. If the object beam strikes the recording medium at an angle to the reference beam, interference fringes are recorded on the plate. Figure 60 shows object and reference beams striking a photographic plate. The recorded image can be reconstructed by illuminating the developed photographic plate with a beam similar to the original reference beam. The interference pattern on the plate diffracts the light of the illuminating beam as if it came from the object. Thus, an observer looking at the plate from the other side sees an image of the original object. Figure 61 shows the reconstruction process.

By making two exposures on the same hologram plate, the holographic process described above can be used as an interferometric process[75,76]. Figure 62 shows the layout of a typical double exposure holography experiment. The following is a description of how stiffness testing is performed using double exposure holography. During the first exposure, hologram fringes are recorded on the photographic plate. After the first exposure has been made, either a known load is applied or a deflection enforced at some point on the model. Then a second exposure is made without changing anything in the experimental setup. The second exposure makes a second set of fringes over the first set. If the fringe locations don't move between exposures, existing fringes are simply reinforced. If the fringe locations did move between exposures, however, an interference pattern results.

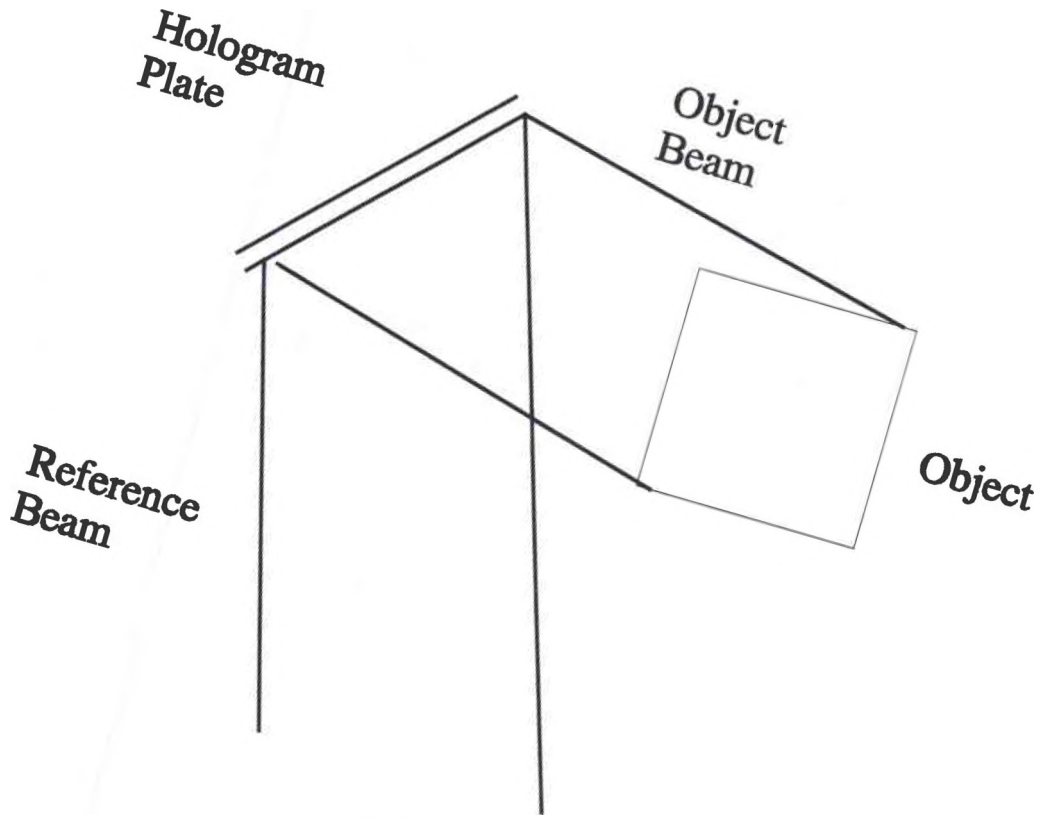


**Figure 59** - Exposure Of A Holographic Plate

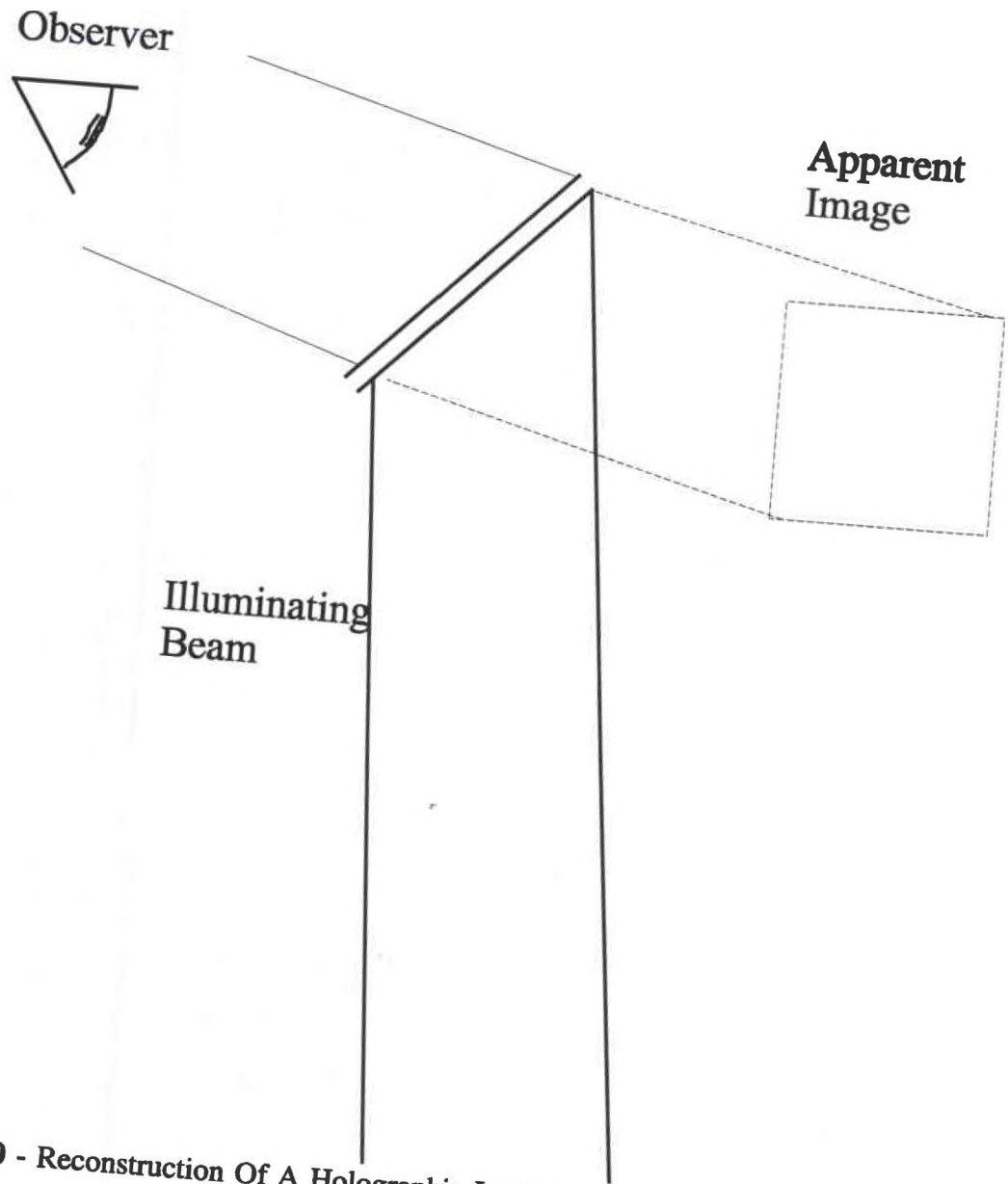


**Figure 60** - Reconstruction Of A Holographic Image

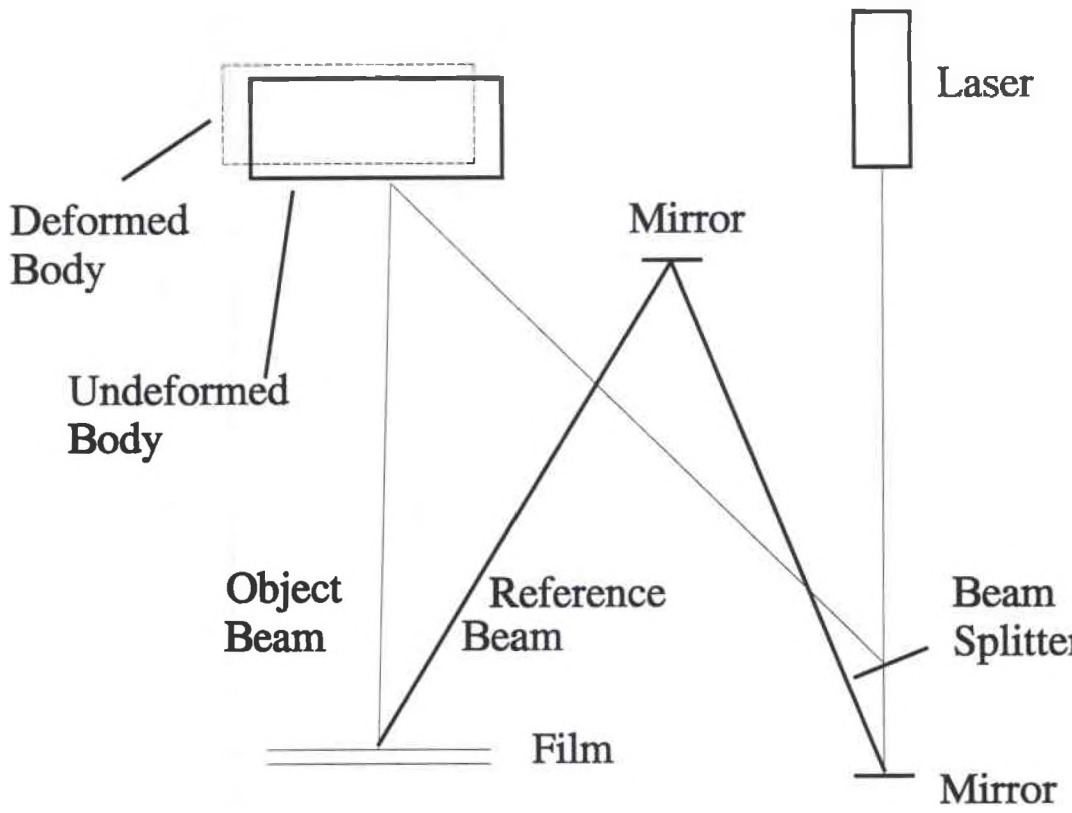


**Figure 61** - Typical Experimental Setup For Double Exposure Holography

The fringes on the plate will move by one fringe separation if the path length for the light transmitted from the laser to the hologram plate via the object is changed by one whole wavelength or some multiple of a whole wavelength. All parts of the object will appear bright during reconstruction if the path length is unchanged or changed by a whole number of wavelengths. Thus all parts of the object that are unchanged or that move by a whole number of wavelengths appear bright. Those parts that move by a half wavelength or an odd number of half wavelengths appear dark during reconstruction. Figure 63 Presents a typical image showing fringes due to deflection of the structure.

The holographic method used for static testing is a variation called image plane holography. It differs from the process described above in that a lens is inserted between the object and the holographic plate to focus the object beam. The effect is that the resulting hologram can be reconstructed with white light rather than with laser light. Photographic holography was used for both static and modal tests. Determination of natural frequencies was done using electronic speckle pattern interferometry (ESPI)[77,78]. ESPI is a video-based system which function much like a photographic system, but provides immediate results. A drawing of the basic system components is presented in Figure 64.

A speckle pattern is an unavoidable feature of laser light reflected off an object. many objects, even those appearing to be quite smooth, appear rough when viewed using a distance scale on the order of a wavelength of light. Coherent light reflected off such an

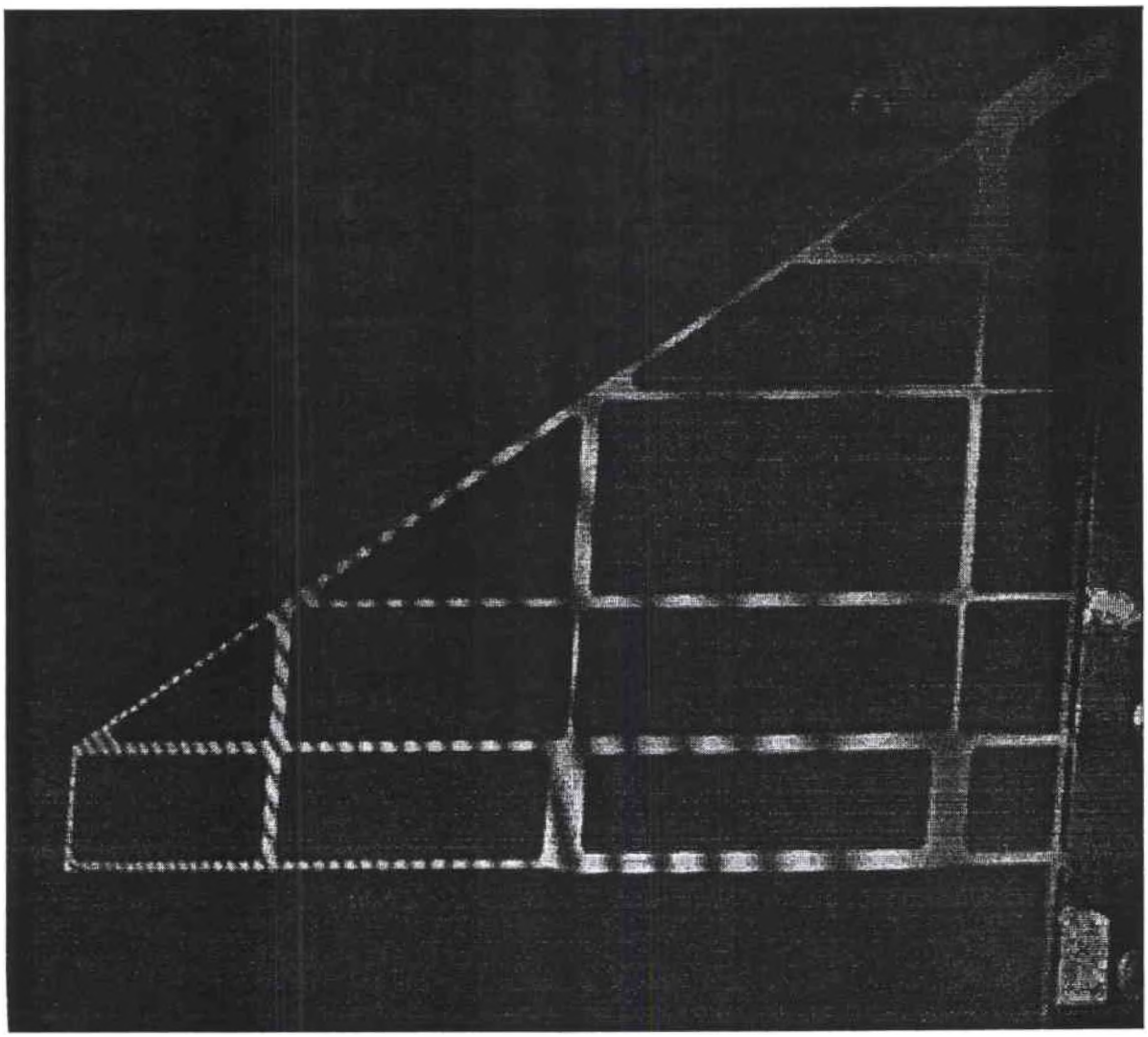

**Figure 62** - Typical Holographic Image With Deflection Fringes (wing11.tif)

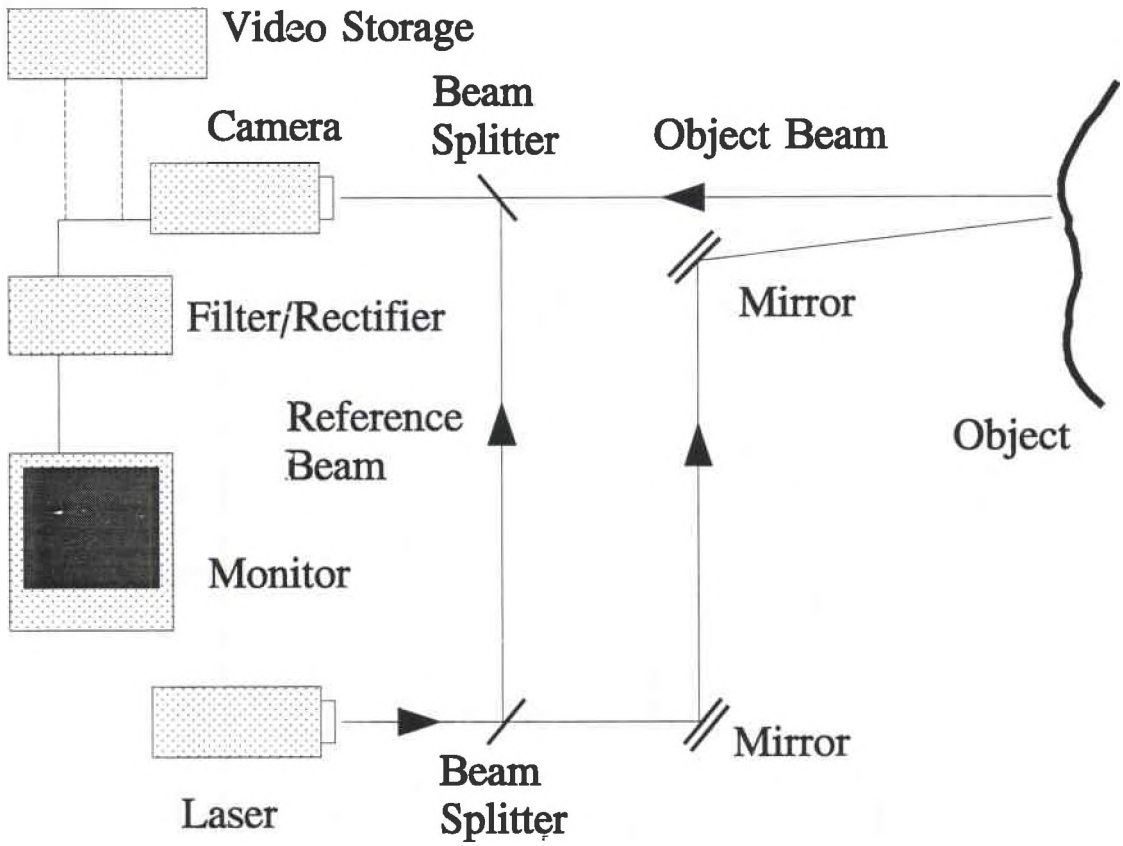


**Figure 63** - Basic Components Of The ESPI System (After Lokberg)

object is not reflected uniformly, but rather at many discrete angles. This results in a reflected image that has small dark and light patches often referred to as speckles. Speckles reduce the resolution of holographic images, but can be used to gather information about the specimen.

The basics of the system are much like those of the photographic system. A coherent beam generated by a laser is split into an object and a reference beam and information which results from combining the two beams is used to form a fringe pattern. A key difference is that a photographic plate stores the interference pattern which reproduces the image and ESPI uses a video camera to record only the image itself. Thus, photographic holography can be used to reproduce a three-dimensional image and ESPI can only reproduce a two-dimensional image.

The resolution of the system is limited by the resolution of the camera and is typically much lower than that of the photographic system. It is common for ESPI systems to have resolution 100 times less than photographic systems. The comparative convenience of the system more than outweighs this limitation for most applications, though.

Like the photographic system, two images are needed to form a hologram. The way this is done depends on whether the system is being used to measure static deformations of deformations of a vibrating system. If the system is static, and undeformed image of the object must be stored. This is typically done with a solid state device which stores the

image digitally. An image of the undeformed object is stored and takes the place of the first image taken in a double exposure photographic process. The completed video image is formed when a deformation is induced. The image of the deformed object is combined with the stored image of the undeformed object to create the interference pattern that maps out deformations over the object.

If the object is vibrating, a stored image is not required. The video system which was used refreshes the image about 25 times a second and so, has an exposure time of about 1/25 second. The image formed is essentially a time average of the image taken over 1/25 second.

The signal generated by the video camera is not useful until it is electronically processed as shown in Figure 65. The image captured by the camera can be thought of as a light intensity distribution which is a function of spatial variables x and y. As the camera scans, it converts the spatial image, I(x,y), into a time varying signal, S(t). The signal from the camera is then passed through a high-pass filter to remove the DC component. The next step is to pass the signal through a full wave rectifier. From the rectifier, the signal is sent to the monitor where the object appears covered with bright and dark fringes as with conventional holography.

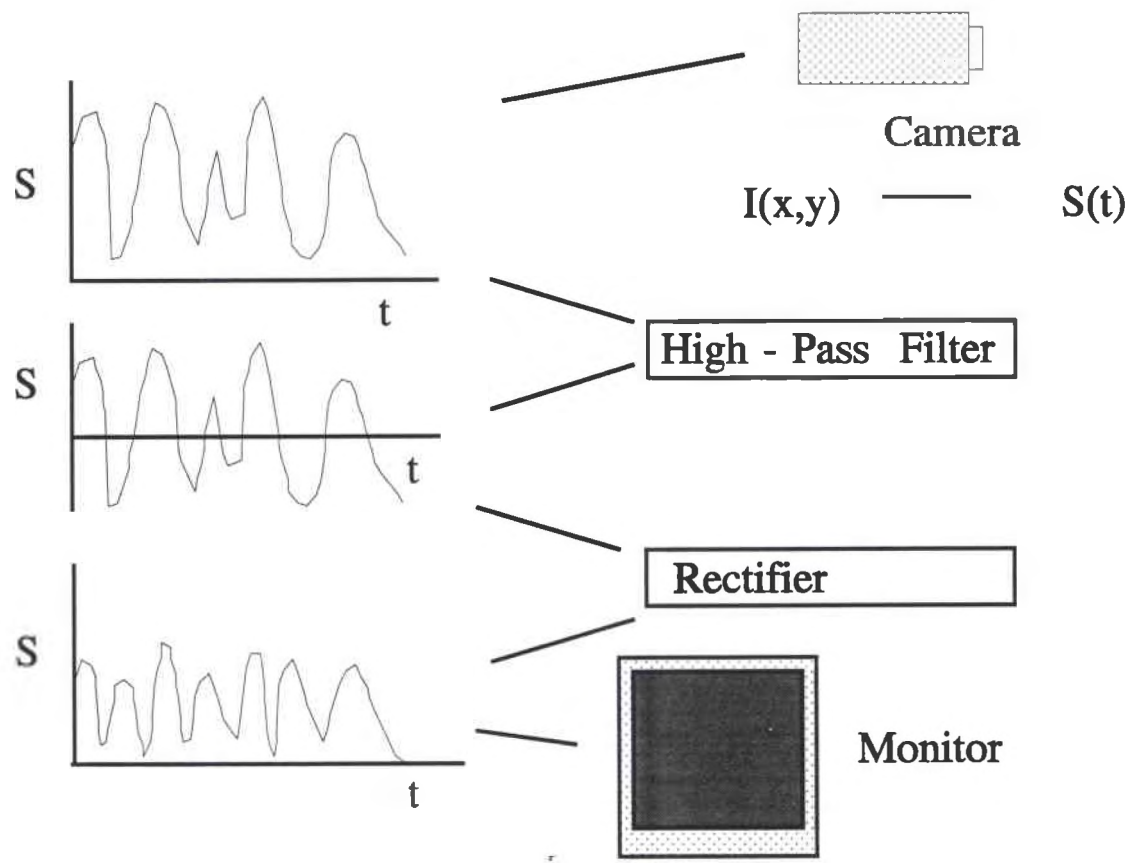


**Figure 64** - ESPI Signal Processing (After Lokberg)